Jeffrey Alan Searcy

2006

Report Documentation Page

Form Approved
OMB No. 0704-0188

1. REPORT DATE	2. REPORT TYPE	3. DATES COVERED
01 JUL 2006	**N/A**	**-**

4. TITLE AND SUBTITLE	5a. CONTRACT NUMBER
The Effects of Spanwise Structures and Unsteady Forcing of Vortex Generators on a Shock-Induced Separated Flow Using Planar Laser Scattering	5b. GRANT NUMBER
	5c. PROGRAM ELEMENT NUMBER
6. AUTHOR(S)	5d. PROJECT NUMBER
	5e. TASK NUMBER
	5f. WORK UNIT NUMBER
7. PERFORMING ORGANIZATION NAME(S) AND ADDRESS(ES) **The University of Texas at Austin**	8. PERFORMING ORGANIZATION REPORT NUMBER
9. SPONSORING/MONITORING AGENCY NAME(S) AND ADDRESS(ES) **AFIT/CIA, Bldg 125 2950 P Street WPAFB, OH 45433**	10. SPONSOR/MONITOR'S ACRONYM(S)
	11. SPONSOR/MONITOR'S REPORT NUMBER(S)

12. DISTRIBUTION/AVAILABILITY STATEMENT
Approved for public release, distribution unlimited

13. SUPPLEMENTARY NOTES
The original document contains color images.

14. ABSTRACT

15. SUBJECT TERMS

16. SECURITY CLASSIFICATION OF:			17. LIMITATION OF ABSTRACT	18. NUMBER OF PAGES	19a. NAME OF RESPONSIBLE PERSON
a. REPORT	b. ABSTRACT	c. THIS PAGE			
unclassified	**unclassified**	**unclassified**	**UU**	**121**	

Standard Form 298 (Rev. 8-98)
Prescribed by ANSI Std Z39-18

The Effects of Spanwise Structures and Unsteady Forcing of Vortex Generators on a Shock-Induced Separated Flow Using Planar Laser Scattering

by

Jeffrey Alan Searcy, B. S.

Thesis

Presented to the Faculty of the Graduate School of

The University of Texas at Austin

in Partial Fulfillment

of the Requirements

for the Degree of

Master of Science in Engineering

The University of Texas at Austin

May 2006

The Effects of Spanwise Structures and Unsteady Forcing of Vortex Generators on a Shock-Induced Separated Flow Using Planar Laser Scattering

Approved by
Supervising Committee:

_____

_____

For my grandfather

Acknowledgements

I would like to thank my advisors, Dr. David S. Dolling and Dr. Noel T. Clemens, for their guidance and support. Both showed unbelievable patience with a fledgling graduate student and provided a wealth of knowledge and advice in the course of my time at UT. I would additionally like to thank Eddie Zihlman for all his help while working at Pickle Research Campus. Similar gratitude is due to Travis Crooks, David Gray and Joe Edgar for all their help in machining many, many parts for my wind tunnel tests, and Frank Wise for his help in getting our motor working. Without Donna Soward and Tina Woods I would still be lost in bureaucratic red tape.

Many thanks are also owed to all of my fellow graduate students and post-doctoral fellow who worked at the lab and were in the fluid dynamics group: Paul Belden, Pablo Bueno, Mirko Gamba, Bharathram Ganapathisubramani, Krishna Lakshminarasimhan, Zach Murphree, Venkat Narayanaswamy, Justin Wagner and Steven Yeldell. Only with their help in courses and at the lab was I able to finish.

Finally, my special thanks are due to my wife. Without her love and support I would be lost. My special thanks also go to all of my family, especially my parents. They have always driven me to achieve my best and provided love and support when it was most needed.

I join my advisors in gratefully acknowledging the Air Force Office of Scientific Research for their support of this research under grant FA9550-04-1-0387.

May 2006

The Effects of Spanwise Structures and Unsteady Forcing of Vortex Generators on a Shock-Induced Separated Flow Using Planar Laser Scattering

Jeffrey Alan Searcy, M.S.E.

The University of Texas at Austin, 2006

Supervisor: David S. Dolling

Through the use of planar laser scattering, the effects of vortex generators (VGs) on the separation shock in an unswept compression ramp interaction have been investigated in a Mach 2 and Mach 5 wind tunnel. Additionally, the undisturbed Mach 5 boundary layer was examined for the existence of long strips of uniform momentum fluid. These strips were previously identified in a Mach 2 boundary layer but had not been observed at Mach 5. The effects of the strips on the Mach 5 compression ramp interaction were also investigated. The counter-rotating vane-type VGs used in this study moved the shock downstream and reduced the separation region at both Mach 2 and Mach 5; however, at Mach 5 the control was sporadic and did not move the shock beyond the extent of the intermittent region. The reduced effectiveness at Mach 5 may be a result of the VGs rising to a significantly lower

scaled height. This was necessary because the VGs resulted in large-scale separation when inserted farther into the boundary layer. Plan view PLS imaging in the streamwise-spanwise plane showed the VGs created a highly three-dimensional separation region in both the Mach 2 and Mach 5 interactions.

Plan view PLS results of the undisturbed Mach 5 boundary layer showed the existence of large-scale strips of uniform momentum similar to those previously found at Mach 2. Taylor's hypothesis was used to construct an instantaneous image of a long portion of the boundary layer and the strip structures were observed to be on the order of 40 boundary layer thicknesses in length. When the effects of these strips were examined on the shock induced separated flow, average images showed that a separation region that extended upstream was preceded by a low-speed strip in the corresponding upstream boundary layer. Regions where the separated flow was in a more downstream location were preceded by high-speed strips in the corresponding upstream boundary layer. These results agree with a recent quantitative study at Mach 2 which showed a correlation between the approximate separation location and the average velocity of the corresponding upstream boundary layer. While only qualitative in nature, the results at Mach 5 seem to agree with recent speculation that these strips may provide a turbulent mechanism of sufficient length which is capable of producing the low frequency oscillations in shock wave / turbulent boundary layer interactions.

Table of Contents

List of Figures

Nomenclature

e	vortex generator chord length
h	vortex generator height
M_∞	freestream Mach number
P_o	total pressure
Re	freestream Reynolds number
Re_x	Reynolds number based on distance from plate leading edge
Re_θ	Reynolds number based on the momentum deficit thickness
T_o	total temperature
U_∞	freestream velocity
X	streamwise coordinate
Y	wall-normal coordinate
Z	spanwise coordinate
z	vortex generator height
β	vortex generator sweep angle
δ^*	boundary layer displacement thickness
δ	mean undisturbed turbulent boundary layer velocity thickness
γ	shock foot intermittency

Abbreviations

CMOS	complementary metal oxide semiconductor
PIV	particle image velocimetry
PLS	planar laser scattering
SRS	Stanford Research Systems
SWTBLI	shock wave / turbulent boundary layer interaction
VG	vortex generator

Chapter 1

Introduction

Unsteady shock wave/turbulent boundary layer interactions (SWTBLIs) have been a constant research topic spanning the past 50 years. The deleterious effects of such interactions have been well documented and include high heat fluxes, fluctuating pressure loads, as well as implications for inlet unstart. These effects create difficulties in the aerothermodynamic design of both supersonic and hypersonic vehicles. Figure 1 presents several areas of concern on a typical hypersonic vehicle.

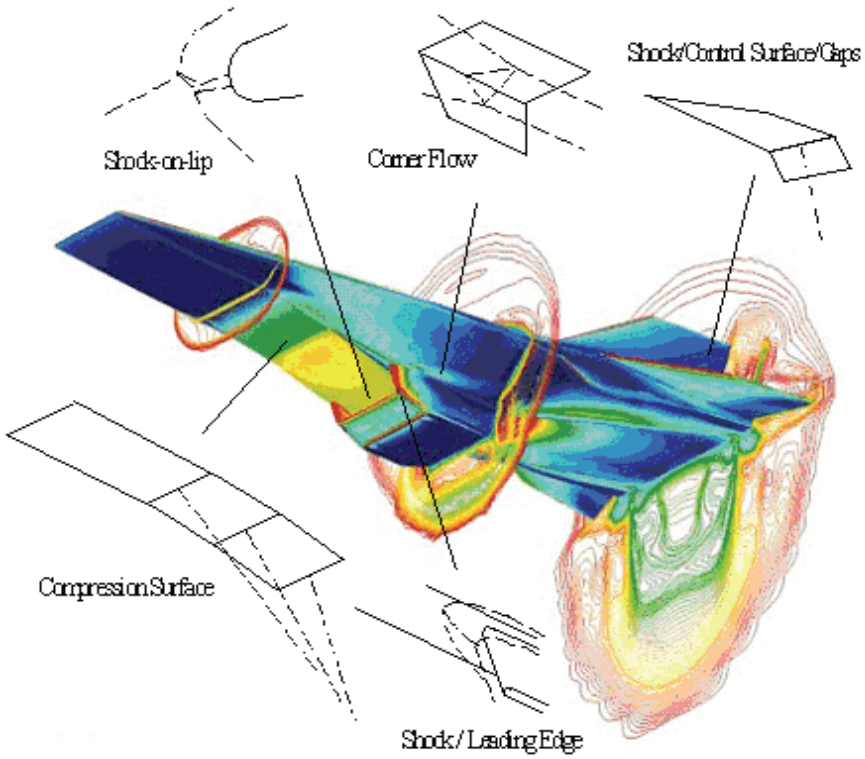

Figure 1. Illustration of areas on a hypersonic vehicle where SWBLIs are of importance. X-43 image courtesy NASA, adapted from Jackson, L. R. et al. 1987

The high heat fluxes are important in the design of thermal protection systems while fluctuating pressure loads can lead to material fatigue. Inlet unstart is an emerging concern with the recent work on hypersonic airbreathing propulsion. An important aspect of these interactions, and a possible cause of the unsteadiness, concerns the separation region that forms downstream of the initial shock. Much work over the past few decades has been carried out in an effort to better understand and control the interaction. However, many of the fundamental aspects of SWTBLIs are still not understood. This has resulted in difficulties in developing physics-based control strategies to suppress the effects.

SWTBLIs change the structure of the shockwave from that predicted by inviscid theory. Figure 2 shows a diagram of the characteristic flowfield in a SWTBLI.

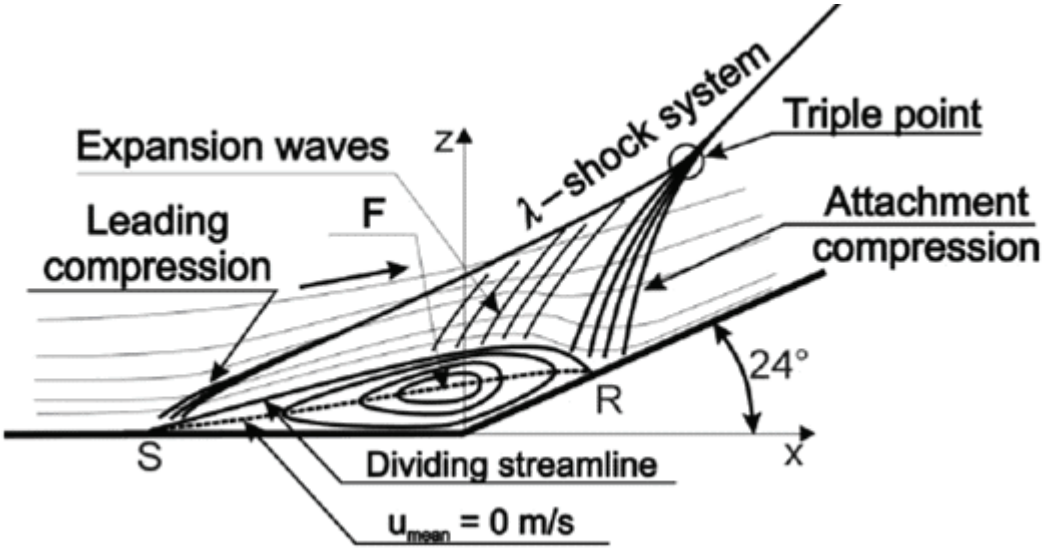

Figure 2. Schematic diagram of global flowfield structure of unswept compression ramp generated SWTBLI. Reproduced from Müller, et al. [2001], with permission from Elsevier.

In an inviscid flow the shock forms at the corner of the ramp and extends outward at the angle calculated from the incoming Mach number and the deflection angle of the ramp. In viscous flows a boundary layer develops and if the shock is of sufficient strength the boundary layer can separate. If the flow separates the resultant shock is 3-D as observed in figure 2. The "separation shock" extends upstream of the corner of the ramp and forms in front of the separation region. The location where this shock impinges on the surface is the "shock foot". The separation region formed downstream is a recirculation region that contains very low momentum fluid and reverse flow. The flow expands as it passes over the separation region and compression waves form as the flow reattaches downstream of the separation region. These compression waves coalesce and meet the separation shock at the triple point. At this point the shock returns to the inviscid shock angle. This flowfield structure is referred to as a lamda shock system, owing to the similarity of the shape to the Greek letter λ.

Recent studies concerning SWTBLIs have focused on the unsteady nature of the separation shock and the separation region. Dolling and Murphy [1983] used fast-response pressure transducers to study a Mach 3 SWTBLI generated by a 24º unswept compression ramp. To measure the unsteadiness of the shock foot, they defined the intermittency factor, γ, as the fraction of time that the shock foot remained upstream of a given transducer. The intermittent region was defined as the region in which the shock foot oscillates, bounded by an intermittency of 0.0 upstream of the shock foot and 1.0 downstream of the shock. Erengil and Dolling [1991] used similar wall

pressure measurements underneath the intermittent region in a Mach 5 SWTBLI and found two significant peaks in the pressure power spectra for different transducer locations. Typical power spectra measured at different points under the intermittent region are given in figure 3.

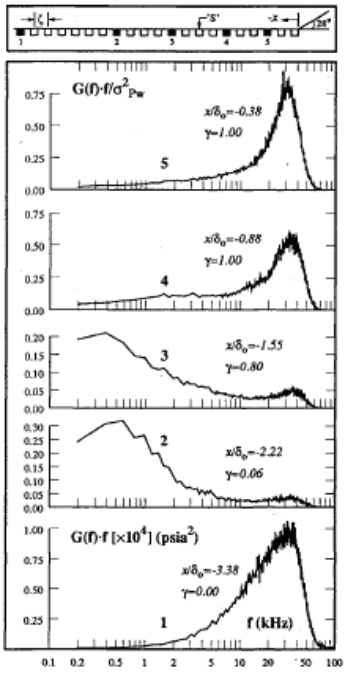

Figure 3. Pressure power spectra taken by wall-mounted pressure transducers underneath the intermittent region of a Mach 5 SWTBLI. Reproduced from Erengil and Dolling [1991], with permission from AIAA.

These results showed a peak around 40-50 kHz for transducer locations 1, 4 and 5 which were outside the intermittent region and a significant peak below 1 kHz for transducers 2 and 3 which were inside the intermittent region. Additionally the high frequency peak was observed inside the intermittent region but was dominated by the low frequency peak. Erengil and Dolling [1991] suggested that turbulent structures on the order of one boundary layer thickness (δ) could cause the high

frequency oscillations. The cause of the low frequency oscillation was unknown, however, and is still a reason of investigation today. Much of the recent work has been dedicated to investigating the cause of the low frequency oscillations observed in SWTBLIs. There is growing evidence that the low frequency unsteadiness of the separation shock and separation region is related to the upstream turbulent boundary layer, however this relation is not yet fully understood.

McClure [1992] studied SWTBLIs in Mach 5 flow using fast-response pressure transducers to measure the shock foot location and a Pitot probe to simultaneously measure the velocity of the upstream boundary layer. His results showed that lower than average and higher than average Pitot pressures in the upstream boundary layer corresponded to upstream and downstream shock foot locations, respectively. Ünalmis and Dolling [1998] used a similar setup to McClure, but used a triple tip Pitot probe oriented in the spanwise direction and showed a correlation between the scale of the separated flow and the spanwise variations of velocity. The authors of that study suggested there may be a spanwise vortical structure in the upstream boundary layer, and that the vortex structure may be a possible cause of the low frequency unsteadiness of the separation region.

PIV studies of a Mach 5 SWTBLI by Beresh [1999] showed a correlation between velocity fluctuations in the lower part of the upstream boundary layer and the separation shock motion. A more full velocity profile corresponded to a downstream shock location, while a less full velocity profile corresponded to an upstream shock location. Figure 4 shows an illustration of this correlation.

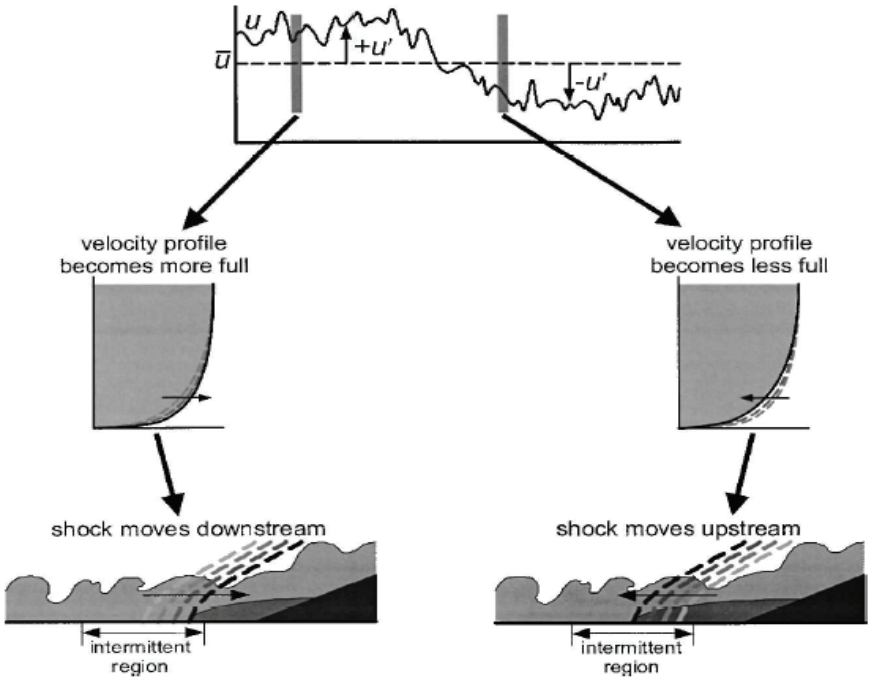

Figure 4. Schematic of the observed relationship between upstream boundary layer and the location and scale of the separation region. Reproduced from Beresh et al. [2002], with permission from AIAA.

Hou et al. [2003] used PIV in a Mach 2 SWTBLI to show that an upstream shock location corresponded to a thicker boundary layer and a downstream shock location corresponded to a thinner boundary layer. This led to speculation that a low frequency change in the boundary layer thickness could cause the low frequency oscillation of the shock.

These models seem to indicate a relationship between the upstream boundary layer and the unsteadiness of the shock. Turbulent mechanisms of a large enough scale capable of producing these effects had not previously been identified in supersonic boundary layers. The scale required to produce the low frequency

oscillations observed would have to be at least an order of magnitude larger than the boundary layer thickness. Recent studies by Ganapathisubramani et al. [2006] have shown coherent regions of uniform momentum fluid as long as 40δ exist in a Mach 2 boundary layer. Additionally, the low-speed and high-speed regions of these structures, referred to as "strips", have been correlated to the upstream or downstream location of the separation region, respectively. Ganapathisubramani et al. speculate that these structures are of a large enough scale that they are capable of producing the low frequency oscillations in SWTBLIs.

The results of these studies showed that it may be possible to control the unsteady nature of the interaction by introducing positive velocity fluctuations upstream of a SWTBLI. The specific mechanism of streamwise vortices, which produce positive velocity fluctuations on the downward sweep and negative fluctuations on the upward sweep, have been shown to be effective in controlling the interaction. Barter [1995] showed passive control with stationary Wheeler doublet vortex generators and boundary layer separators. The Wheeler doublets reduced the maximum upstream separation shock location by 60%. Additionally, Bueno et al. [2006] have shown that streamwise vortices induced by pulsed injection jets have moved a shock to a more downstream location.

These results provide motivation for the current study, which has several main objectives and examines both the naturally occurring SWTBLI and the interaction generated by inserting VGs into the boundary layer.

The specific goals of this study were to:

1) Study the effect of unsteady insertion of VGs on a Mach 2 SWTBLI
2) Study the effect of unsteady insertion of VGs on a Mach 5 SWTBLI
3) Examine the Mach 5 turbulent boundary layer for existence of uniform momentum strips
4) Study the effect of the strips on the Mach 5 SWTBLI

Chapter 2

Literature Review

2.1 UNSTEADINESS OF SWTBLIS

Over 50 years of SWTBLIs research on many different geometry types, including 2-D ramps and 3-D blunt bodies, have shown the unsteady nature of the interaction, irrespective of the facility or model used in testing. This unsteady effect seems to be an inherent quality of SWTBLIs. Much of the data gathered in the early years of testing utilized pitot pressure and wall pressure measurements. The advancement in laser and imaging technology over the recent years has introduced new laser diagnostic techniques. The non-intrusive nature of these techniques and the ability to image large regions of the entire flowfield have allowed more insight into the underlying physics of SWTBLIs in recent years.

As illustrated in figure 3 in Chapter 1, the results of previous studies (Erengil and Dolling [1991]) have shown two distinct frequency ranges dominate the pressure power spectra in SWTBLIs. Dolling and Brusniak [1989] found the dominant frequency of motion in the intermittent region was in the range of 0.4 kHz to 2 kHz. Erengil and Dolling [1991] attribute the high frequency components, from about 10-50 kHz, to boundary layer turbulence with structures on the order 1δ. These results

were not able to allow inferences into the low frequency motion of the shock, and this topic has been of primary importance in the most recent studies.

McClure [1992] studied SWTBLIs generated by a compression ramp in Mach 5 flow using fast-response pressure transducers to measure the shock foot location and a Pitot probe to simultaneously measure the velocity of the upstream boundary layer. The data showed that lower than average and higher than average Pitot pressures in the upstream boundary layer corresponded to upstream and downstream shock foot locations, respectively. This variation in Pitot pressure may be a result of the boundary layer becoming thick and thin. McClure found that the time scales of the variations in the pitot pressure were long enough that 20-40 turbulent structures of a streamwise extent of one or two boundary layer thicknesses would pass by. This evidence suggested that there may be some low frequency component within the boundary layer, but that it was unrelated to the passage of turbulent structures as there was no model of turbulent structures that long at that time. Ünalmis and Dolling [1998] studied SWTBLIs generated by a blunt fin in Mach 5 flow using fast-response pressure transducers and a triple tip Pitot probe, oriented in the spanwise direction, to measure the spanwise variation in velocity of the upstream boundary layer. The data showed a correlation between the scale of the separated flow and the spanwise variations of velocity in the upstream boundary layer. The authors of that study suggested that the low frequency variation of Pitot pressure indicated a spanwise vortical structure in the upstream boundary layer, and that the vortex structure may be a possible cause of the low frequency unsteadiness of the separation region.

Chan [1996] used planar laser scattering (PLS) from a condensed alcohol fog in a Mach 5 SWTBLI and, despite significant scatter, demonstrated that the mean boundary layer thickness as determined by the PLS images varied similarly to the pitot pressure measurements of the boundary layer thickness. His work, however, did not show a thickening and thinning of the boundary layer corresponding to an upstream and downstream position of the shock. This motivated the work of Beresh [1999] who completed a PIV study of the Mach 5 SWTBLI. The data of that study also did not show a thickening and thinning of the boundary layer. This work seemed to contradict the previous work of McClure [1992] that the variations in Pitot pressure were caused by a thickening and thinning of the boundary layer. This suggested some other mechanism may be responsible for the low frequency oscillation, more like the notion of a spanwise vortical structure proposed by Ünalmis and Dolling [1998]. Beresh's study did, however, show another correlation between the upstream boundary layer and the shock location. When the upstream boundary layer data was conditioned on the upstream or downstream shock foot motion, it was determined that the upstream case had a less full velocity profile and the downstream case had a more full velocity profile. An illustration of this can be found in figure 4 in Chapter 1. This result would suggest that negative velocity fluctuations in the lower part of the upstream boundary layer correspond to an upstream shock motion, while positive velocity fluctuations correspond to a downstream shock motion. When the velocity profile becomes more full, it becomes less prone to separation causing the separation region to become smaller and the shock to move downstream.

Hou et al. [2004] confirmed this relationship for SWTBLIs generated by blunt fins. Hou [2003] expanded on these results and completed a PIV investigation of the Mach 2 SWTBLI generated by a compression ramp. Additionally, he noted that a thicker and thinner boundary layer did correspond to an upstream and downstream shock foot location. Bueno et al. [2005] confirmed these results on a SWTBLI generated by a blunt fin in Mach 2 flow through direct visualization using PLS. Clearly, there was a distinct thickening and thinning of the boundary layer corresponding to the shock motion at Mach 2, while previous studies showed that this relationship did not exist at Mach 5.

The conclusion that was commonly drawn in many of the aforementioned studies was that the separation shock foot had a low frequency oscillation, but turbulent mechanisms did not seem to be able to explain the source. Typical turbulent structures were believed to be of scale δ, and the low frequency oscillations observed would require turbulent structures that are more than an order of magnitude larger than δ. However, recent studies have shown the possible existence of turbulent structures that are long enough to result in the low frequency oscillations. PIV investigations by Tomkins and Adrian [2003] and Ganapathisubramani et al. [2003a,b and 2005] of incompressible turbulent boundary layers have shown the existence of long coherent regions of streamwise velocity fluctuations that extended up to 2δ in the streamwise direction. Hotwire studies by Hutchins [2004] seemed to indicate these long regions of uniform momentum extended up to 20δ. There have been few studies similar to these in supersonic boundary layers. Samimy et al. [1994] found

evidence of long streamwise structures in a Mach 3 turbulent boundary layer with instantaneous visualization experiments at boundary layer heights of 0.49δ and 0.65δ. More work in the supersonic regime has recently been accomplished. Ganapathisubramani et al. [2006a] completed a wide field PIV study in streamwise-spanwise planes in a Mach 2 turbulent boundary layer and found similar high-speed and low-speed regions that extended up to 8δ in length. The authors of that paper speculated that since these structures were so long, approaching an order of magnitude larger than δ, these low frequency structures could explain the low frequency oscillations of the shock foot and separation region.

Ganapathisubramani et al. [2006b] extended that work to study the influence of these structures, referred to as strips, on a Mach 2 SWTBLI. A 20º compression ramp was used to generate the interaction, and PLS and PIV data were obtained to examine the streamwise-spanwise structure of the flow. Several important implications on the unsteadiness of the SWTBLI were found. First, the PLS images were acquired at a high repetition rate of 10 kHz. Because the flow did not convect entirely out of the field of view in the time between frames, Taylor's hypothesis was used to reconstruct the instantaneous spatial structure in the upstream boundary layer. When this was accomplished, the structures were observed to extend up to about 40δ in length. This length scale tends to confirm that these structures could cause the low frequency oscillation. The second implication of that study was that the strips seemed to correspond to the separation region. In spanwise locations where there were low-speed strips immediately upstream of the separated flow, the separation region was

observed to extend upstream, and likewise in spanwise regions of high-speed strips the separation region was observed to extend downstream. PIV data showed a correlation between the upstream point of the separation region at a given spanwise location and the average velocity over 9δ of the upstream boundary layer at the same spanwise location. These results supported the notion that the strips are responsible for the low frequency oscillation of the separated flow.

The low-speed and high-speed strips may correspond to a turbulent mechanism that is analogous to the very-large scale motion (VLSM) model proposed by Kim and Adrian [1999] in incompressible flow. The authors of that paper proposed that the very long regions of uniform low-speed and high-speed flow were formed by groups of hairpin packets, found by Ganapathisubramani et al. [2003a,b] and Adrian et al. [2000], traveling in succession at the same streamwise velocity. The hairpin packet model suggests that the region of flow between the legs of the vortices possesses negative streamwise velocity fluctuations. These negative velocity fluctuations are most likely the result of the hairpin nature of the vortices, which is associated with rotation in an upstream direction on the inside the legs of the hairpin. Similarly the flow on the outside of the hairpin experiences positive streamwise velocity fluctuations as a result of the vortices rotating in a downstream direction on the outside of the hairpins. Adrian et al. [2000] hypothesized that the packets could contain a group of up to 10 individual hairpin vortices convecting downstream in a coherent manner. These structures were hypothesized to extend up to 2δ. However, hotwire measurements by Kim and Adrian [1999] and Hutchins et al. [2004] found

regions of uniform momentum extending up to 15δ. Therefore the hairpin packet model was used by Kim and Adrian to construct the VLSM model in which groups of hairpin packets are formed to create a larger-scale structure. Figure 5 below illustrates the VLSM model of Kim and Adrian.

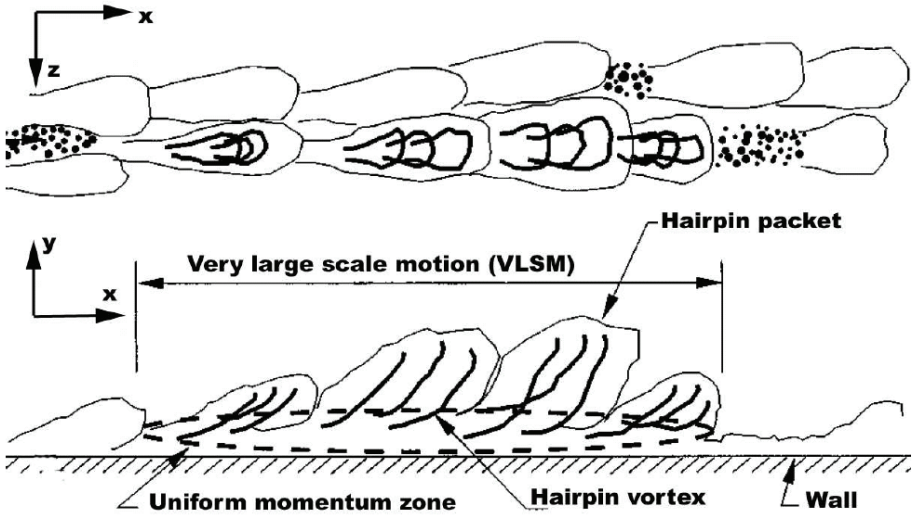

Figure 5. Very Large Scale Motion model proposed by Kim and Adrian [1999]. Reproduced from Kim and Adrian [1999], with permission from American Institute of Physics, Physics of Fluids.

Ganapathisubramani et al. [2006b] found that the uniform regions of low-speed and high-speed flow observed in the Mach 2 boundary layer were remarkably similar to the pattern suggested by the VLSM model of Kim and Adrian. The authors of that paper suggest that the VLSM model could be used to understand the instantaneous flow patterns of long regions of low-speed and high-speed flow.

In earlier work, Ünalmis and Dolling [1998] inferred a stationary streamwise vortical structure was present in the upstream boundary layer and they suggested that

Görtler vortices, which may be wind tunnel dependent, may be responsible for these structures. These vortices form in the boundary layer as a result of the expansion through the nozzle. If Görtler vortices are responsible, then the low frequency unsteadiness observed in SWTBLIs may just be an artifact of wind tunnel testing and may not be encountered in actual flight. While the cause of these strucutres is unknown, Ganapathisubramani et al. [2006b] suggested that these structures may not be a result of Görtler vortices, owing to varying vorticity signatures that were not primarily streamwise.

The results of the last study by Ganapathisubramani et al. [2006b] served as the primary motivation for objectives three and four of the present study. This study seeks to "expand the envelope" to the high supersonic regime, approaching the hypersonic regime.

2.1 VORTEX GENERATORS

Lin [2002] made a review of passive low profile VGs applied to subsonic and low-supersonic boundary layer separation control. Lin found that low profile VGs, defined as having a height that is greater than 0.1δ, but less than 0.5δ, have been shown to be successful at reducing boundary layer separation and are far more efficient than standard VGs with a height of approximately 1δ. The effectiveness of low profile VGs compared to standard VGs stems from the full nature of turbulent boundary layer velocity profiles. Lin [1999] observed that there is a point where

further increases in VG height yield minimal boundary layer momentum gains, but can induce significant drag due to strong 3D effects. Compared to VGs that induce spanwise vortices, VGs that induce streamwise vortices have been shown to give boundary layers greater resistance to separation. Figure 6 illustrates the effectiveness of several categories of VGs.

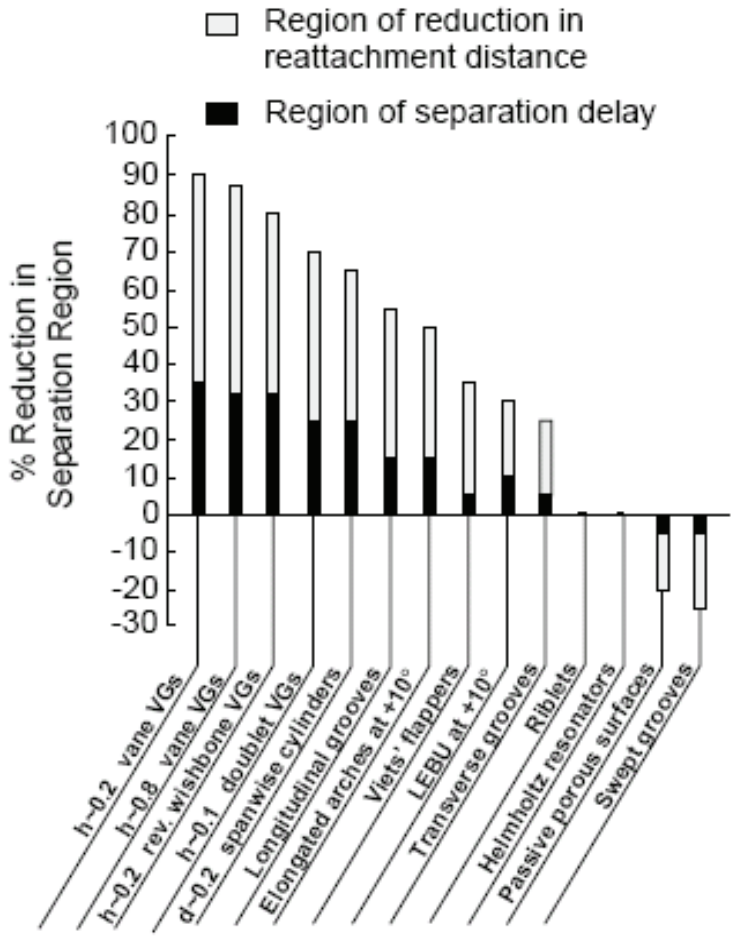

Figure 6. Summary of control effectiveness of various devices. Reproduced from Lin [2002], with permission from Elsevier.

The low profile VGs, no matter their type, clearly demonstrated the greatest effects in reducing the separation region, while the vane type VGs showed the best results of the low profile VGs.

Figure 7 shows several different types of VGs, including counter-rotating vane VGs and Wheeler doublets, and defines their associated measurement parameters.

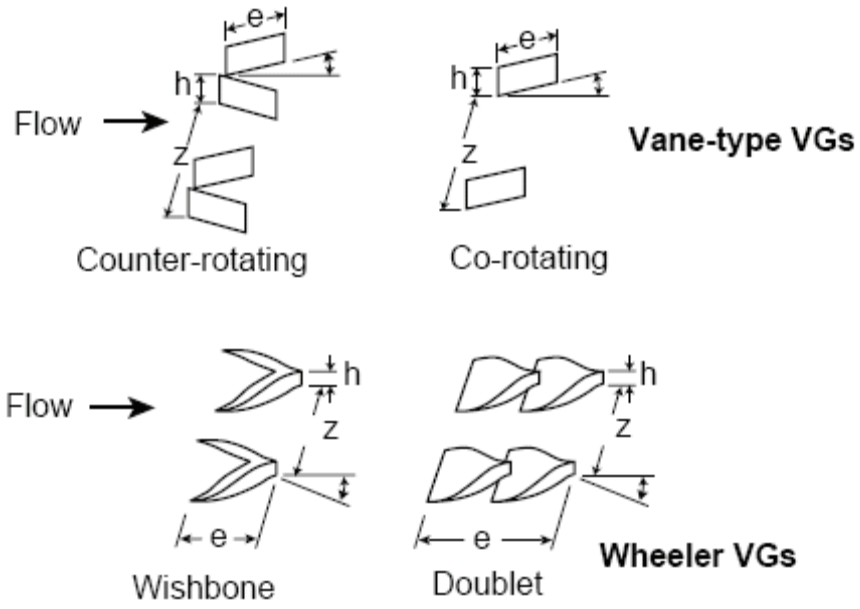

Figure 7. VG geometries and device parameters. Reproduced from Lin [2002], with permission from Elsevier.

Previous work by Barter et al. [1995], focused on passive control of separated SWTBLIs using Wheeler Doublets similar to those shown in figure 7. Using doublets with heights of 0.33δ, Barter was able to simultaneously reduce the intermittent region and maximum upstream separation shock location of a Mach 5 SWTBLI by

60%. Although Wheeler doublets have proven to be useful in separation reduction, vane type VGs may prove to be just as effective, if not more effective. Lin et al. [2002] report in subsonic studies, vane-type VGs at equal heights tend to be more effective while producing less drag than wishbone VGs having similar geometry to Wheeler doublets. Ashill et al. [2001] provides some inferences into the reasons for the greater effectiveness of vane type VGs. Downstream vortex strength decay was studied for various VGs, and compared to the forward wedge, backwards wedge and joined vane, counter-rotating vanes spaced by 1h and 2h proved to produce streamwise vortices that were more resistant to decay with downstream distance. Ashill et al. [2001], attributed the greater downstream vortex decay of the forward wedge and joined vane to interference of the streamwise counter-rotating vortex pairs that were created. This was most likely caused because the devices were placed too close together. Wheeler doublets have a similar geometry to forward-wedge VGs, implying counter-rotating VGs may produce more decay resistant streamwise vortices than Wheeler doublets.

In addition to being more effective, vane-type VGs provide practical engineering advantages for active control systems. The fact that vane type VGs are thin allows them to be raised and lowered through slots as opposed to large holes or cavities that would be required for wedge and Wheeler type VGs. For these reasons, low profile counter-rotating vane VGs were used in this study.

Chapter 3

Experimental Program

This chapter outlines the facilities, individual components, and experimental techniques used to complete testing.

3.1 WIND TUNNEL FACILITY

All experimental testing was conducted in the supersonic blowdown wind tunnel facility at the J.J. Pickle Research Campus of The University of Texas at Austin. Testing was accomplished at Mach 2 and at Mach 5, and each case utilized the same major facility with some variation in specific components. In both cases the wind tunnel was supplied with approximately 140 ft^3 (4 m^3) of air by a Worthington HB4 four-stage compressor. The air was stored in external tanks at a pressure of about 2550 psia. A 1.5 *in* Dahl valve controlled by a Moore 352 controller regulated the flow of air from the storage tanks to the stagnation chamber so that a constant stagnation chamber pressure was maintained. The pressure in the stagnation chamber was measured by a Setra model 204 transducer with a range from zero to 500 psia. For testing at Mach 5, the air passed through two banks of 420 kW nichrome wire resistive heaters to increase the total temperature of the air before it entered the nozzle. The heaters were controlled by a Love Controls 1543 controller and the temperature was monitored by a K-type thermocouple. The stagnation pressure and

temperature for Mach 5 testing were P_0 = 360 ± 5 psia and T_0 = 640 ± 10 ºR, respectively. The stagnation conditions for Mach 2 testing were P_0 = 41 ± 1 psia and T_0 = 525 ± 10 ºR.

Two different nozzles were used to achieve the different Mach numbers, and each case had a slightly different test section. The Mach 2 constant-area test section measured 6 *in* wide by 6.3 *in* high and had a length of 30 *in*. Freestream conditions were: Mach number, M_∞ = 2, unit Reynolds number, Re_∞ = 3.3 x 10^7 m^{-1}, and velocity, U_∞ = 500 m/s. Typical boundary layer properties just upstream of the interaction were: 99% velocity thickness, δ = 12.7 mm (0.5 *in*), momentum thickness, θ = 0.9 mm (0.035 *in*), displacement thickness, δ^* = 2.54 mm (0.1 *in*), and Re_θ = 35,000. The Mach 5 constant-area test section measured 6 *in* wide by 7 *in* high and had a length of 27 *in*. This produced freestream conditions of: M_∞ = 4.95, Re_∞ = 49.5 x 10^6 m^{-1}, and U_∞ = 770 m/s. Typical boundary layer properties were: δ = 19 mm (0.75 *in*), momentum thickness, θ = 0.76 mm (0.030 *in*), displacement thickness, δ^* = 9.1 mm (0.36 *in*), and Re_θ = 3.9 x 10^4. In both cases the incoming boundary layer underwent natural transition and developed under approximately adiabatic wall temperature conditions.

For both cases the same side walls were used, each of which was fitted with a fused silica window. The windows measured 6 *in* wide by 2 *in* high by 0.75 *in* thick. A fused silica window measuring 8 *in* long by 2.5 *in* wide by 0.75 *in* thick was fitted to a plug which was mounted in a hole cut out of the ceiling of each test section.

These windows allowed optical access into the tunnel for a laser sheet as the PLS illumination and for imaging purposes, and combined to provide several different fields of view.

3.2 TEST ARTICLES

Experimental models were placed in the test section by mounting them to a floor-plug which is bolted into a large rectangular hole in the floor of each test section. The main floor-plug can have additional holes in it to allow multiple components to be used in the same experiment, as was the case for this experiment. This set of experiments used a compression ramp to generate the shock for the SWTBLI. At Mach 2 a full span, 20º, 2-D unswept compression ramp was used and at Mach 5 a full span, 28º, 2-D unswept compression ramp was used. Both ramps measured 1 *in* high and were mounted to the same base plug, which had two rails on it that fit into slots in the bottom of each ramp. This allowed the ramp to be translated along the streamwise direction of the tunnel by sliding it along the rails.

3.2.1 Vortex Generators

Many types and geometries of vortex generators were considered for use in this project and an overview can be found in section 2.2. The following section discusses the VGs that were implemented for this testing.

3.2.1.1 Vortex Generator Design

The vane-type VGs used for testing were a low-profile type ($0.1 \leq h/\delta \leq 0.5$) and consisted of two pairs of counter-swept vanes that produced two pairs of counter-rotating vortices. These VGs were chosen because previous studies, outlined by Lin [2002] have shown that the vortices generated decay relatively slowly as they convect downstream. The relevant dimensions for the VGs were: z = 1.52 *in* (38.73 mm), e = 1.5 *in* (38.10 mm), and h = 0.21 *in* (5.33 mm). The sweep angle with respect to the freestream was $\beta = \pm 14^{\circ}$, and the leading edge gap of the counter-rotating vanes was 0.3 *in* (7.57 mm) or 1.43h. The reader is referred to section 2.2, figure 6 for definitions of the above dimensions. Note that the VGs were not rectangular in cross section shape, as in Figure 7, but rather formed a right triangle with the hypotenuse originating at h = 0 at the leading edge and extending to the full height at the trailing edge. This was done to create a more streamlined supersonic geometry. This VG design was tested at both Mach 2 and Mach 5 to compare and contrast results from a consistent setup. The VGs were placed at a relatively close location to the ramp of 3 *in* (76 mm), which was 6 δ and 4 δ for Mach 2 and Mach 5 testing, respectively. While not optimal, this location was used because of space constraints within the wind tunnel. Future work should include optimal design for each Mach number as well as placement at a more optimal upstream location. Figure 8 shows the VGs in a full up position in relation to the location of the compression ramp within in the test section.

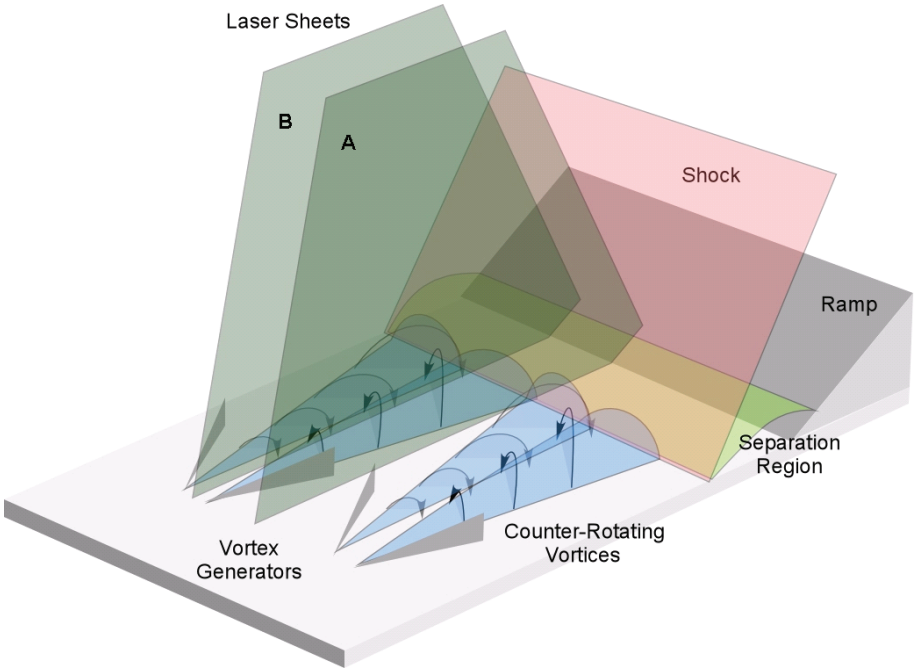

Figure 8. Schematic of VG experimental setup showing laser sheet locations of PLS imaging and illustration of rotation of vortices.

Figure 8 also shows the location of the laser sheets used in testing and the vortices that are formed by the VGs. The arrows on the vortex structures indicate the direction of rotation for that vortex. The area between the two pairs of VGs experiences an upwash, as the vortices on either side have an upward direction of motion. Laser sheet A corresponds to this upwash region. The area within each individual pair of VGs experiences a downwash due to the downward direction of rotation of the vortices on either side. Laser sheet B corresponds to this downwash location.

This study looked at the unsteady forcing of the VGs as a prelude to future active control schemes. Therefore the VGs were designed to come out of slots in the floor that were only slightly larger than the VGs themselves. In this manner the VGs

could be completely retracted from the flow or inserted into the flow to some height. One limitation of this design pertained to the necessity to keep the VG assembly sealed from the air outside the tunnel. To solve this problem a cavity was created inside the floor-plug for the VGs with slots being the only opening to the tunnel. The VGs were mounted to a bar that was contained within the cavity and the bar was attaching to the shaker device with a bellows keeping the inside of the cavity sealed from the outside air. This design created a space constraint inside the cavity that limited the height of the VGs. If the VGs were too tall they would protrude out of the slotted surface into the tunnel even when the bar was completely retracted. Therefore the actual height of the VGs was approximately 0.24 *in*, which allowed enough space for the VGs to be completely retracted from the flow, but remain inside the cavity.

3.2.1.2 Vortex Generator Driving Mechanism

Although passive VGs have been previously studied in this facility [Barter 1995], the current study evaluated the effects of unsteady forcing of the VGs to demonstrate possibilities for an "active" control system. Therefore the VGs were pulsed up and down through slots in the test section floor at a constant rate of 50 Hz. This frequency was necessitated by the response of the driving mechanism, which was an AGAC Derritron model AV50 shaker. A Stanford Research Systems DG535 pulse delay generator sent a square wave signal to an MB Electronics 125 VA model 2120MB amplifier and then to the shaker. A bellows was attached to the driving rod

and to the test section floor for sealing purposes. Figure 9 shows the components of the VG setup.

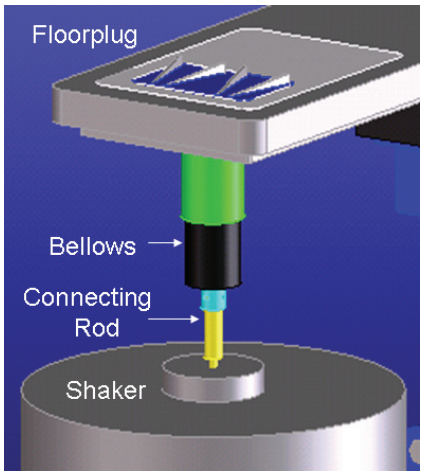

Figure 9. Schematic of VGs showing shaker, connecting rod, and bellows mounted underneath wind tunnel floor.

3.3 PLANAR LASER SCATTERING

This experiment utilized planar laser scattering (PLS) as the method to visualize the flowfield. This technique has been used extensively in previous and current studies at this facility for imaging SWTBLIs. In this technique the flow is seeded with a liquid aerosol of a relatively large droplet size (100 μm) upstream of the stagnation chamber [Clemens and Mungal 1991]. The droplets evaporate and then re-condense into a fine fog (0.2 μm) [Clemens and Mungal 1991] as the vapor-laden flow travels through the nozzle, due to the isentropic cooling experienced as the flow expands. The fog creates an excellent medium for Mie/Rayleigh scattering measurements [Chan 1996]. A planar image is formed as the light from an incident

laser sheet is scattered from the fog particles. The droplets are sensitive to static temperature, as high temperatures cause the fog to evaporate and emit lower signal or no signal at all. This method can show the interface of the boundary layer and the freestream, since the fog in the warm boundary layer fluid evaporates, and this leads to lower signals as compared to the freestream. Additionally, the shockwaves can be visualized since the density increase across the shock results in higher droplet concentration and a higher signal [Chan 1996]. The high signal may not remain, however, owing to the temperature increase across the shock, which causes evaporation and lower signal. This process is not instantaneous so for strong shocks there is a noticeable increase and then decrease in signal across the shock.

The ability to image these different aspects of the flow, including the boundary layer interface and the separation shock requires a vapor pressure of the fog sufficiently high that the fog will remain through the boundary layer and across the shock. This is driven by the pressure of the seeding system which is discussed in section 3.3.1 below.

The implementation of the PLS technique in this facility involved a diode-pumped, Nd:YLF laser (Coherent Evolution-90) as the source of illumination. The laser used intra-cavity harmonic generation to produce an output wavelength of 527 nm. The laser was externally triggered at 10 kHz by a Stanford Research Systems DG535 pulse delay generator and the settings of the laser were optimized to produce approximately 90 W of power. The temperature of the LBO frequency-doubling crystal was optimized to 315 ºF, and the pulse width was set at 200 ns. The 90 W of

power corresponded to approximately 9 mJ per pulse at the repetition rate of 10 kHz. The beam was highly multi-modal with $M^2 \approx 30$, so the optical path length of the beam was minimized to reduce the divergence of the beam. Additionally, by using a half-wave plate the polarization of the laser was oriented so that it was perpendicular to the scattering plane. This was accomplished to maximize the scattering signal from the fog particles, since they are sufficiently fine to be in the Rayleigh scattering regime.

To image the scattered light from the condensed fog, a single high-framing rate CMOS camera (Photron FASTCAM-Ultima APX) was externally triggered at 10 kHz by the same SRS DG535 pulse delay generator used to trigger the laser. For Mach 2 testing the camera was fitted with a Canon 50 mm focal length lens operated at f/1.2. Mach 5 testing was accomplished with a Nikon MicroNikkor 50 mm lens with an aperture setting of f/1.4. The shutter of the camera was set at 1/250,000 second to minimize the background illumination from ambient light. When operating at 10 kHz, the resolution of the camera was restricted to a maximum of 512 pixels x 256 pixels. For this framing rate and resolution the camera could capture and store 16,384 images, or 1.6384 s of data.

A Thorlabs PDA 55 fast photodiode was used to measure the laser pulse and was connected to a Tektronix TDS 520C digital oscilloscope. The camera shutter was also monitored by the oscilloscope and the delay from the SRS corresponding to the shutter was set so that the laser pulse coincided with the center of the camera shutter being open.

3.3.1 Seeding System

The seeding system for testing at Mach 2 varied slightly from Mach 5. For Mach 2 testing, the fog was generated by seeding the flow with acetone droplets through the use of two atomizing nozzles (Spraying Systems LN3). Because the two heater banks were not required for Mach 2 testing, the acetone was injected into the supply piping approximately 20 feet upstream of the stagnation chamber. The particle-laden flow traveled through approximately 17 feet of 4 *in* diameter pipe before undergoing a large expansion into the 12 *in* diameter plenum section. By injecting this far upstream, the acetone droplets had sufficient time to evaporate and mix. A stainless steel reservoir held approximately 2 ft^3 of liquid acetone and was pressurized to 300 psia by a cylinder of compressed nitrogen.

Ethanol was used to generate the fog at Mach 5 and because heaters are used for Mach 5 testing, the ethanol was injected directly into the plenum using three atomizing nozzles (Spraying Systems LN3). The same stainless steel reservoir was used and was pressurized by the compressed nitrogen cylinder. For Mach 5 testing the reservoir was pressurized to 600 psia to increase the fog density.

3.3.2 Optical Setup

PLS was implemented in two different image planes. The first plane imaged the streamwise-transverse (wall-normal) plane, which will be referred to as "side view" PLS. The other plane that was imaged was the streamwise-spanwise plane,

which will be referred to as “plan view” PLS. Each image plane required a different optical setup, found in the following sections.

3.3.2.1 Side View PLS Optical Setup

The setup for side view imaging is shown in figure 10.

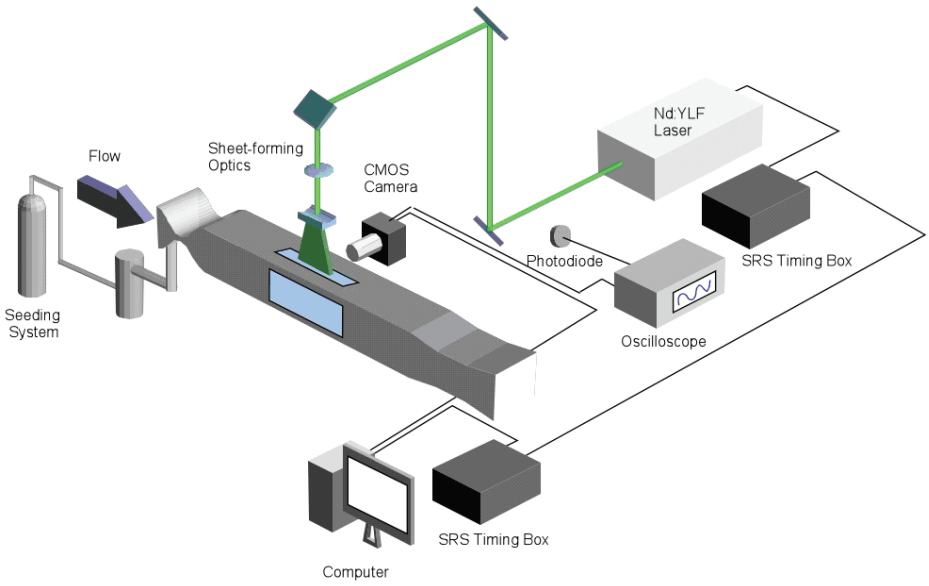

Figure 10. Optical setup employed for side view PLS imaging.

For side view imaging of the SWTBLI, the laser was focused by a 500 mm spherical lens, at the center of the imaging field of view. A planar-concave cylindrical lens with a -100 mm focal length was used to create the laser sheet. The cylindrical lens was translated vertically so that the resultant sheet filled the required field of view. These optics were mounted on translation stages attached to a vertical

rail above the tunnel. The camera was mounted on an x-y translation stage and to a "tilt" stage to facilitate viewing the appropriate field of view.

3.3.2.2 Plan View PLS Optical Setup

The setup for plan view imaging is shown in figure 11.

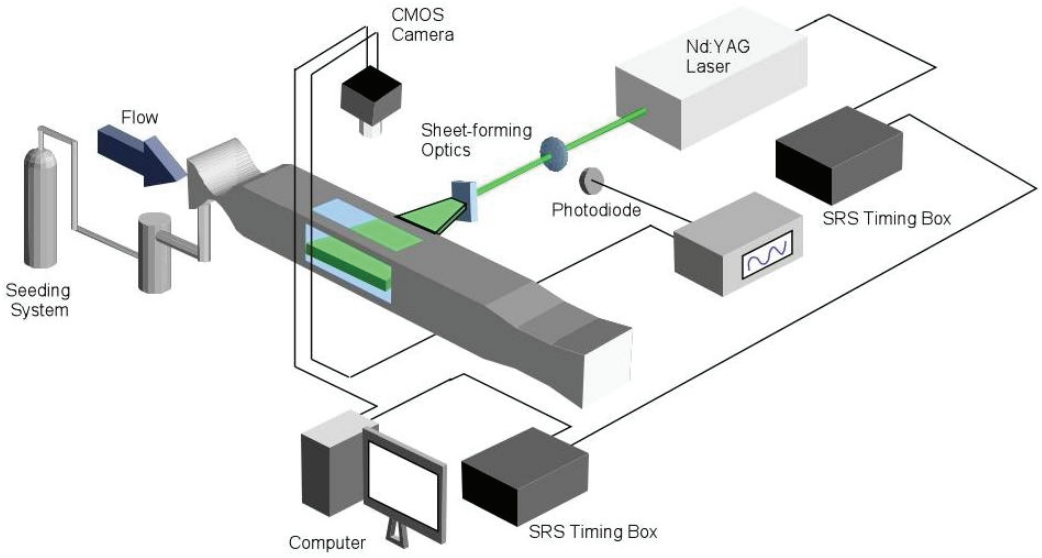

Figure 11. Optical setup employed for plan view PLS imaging.

For plan view imaging of the SWTBLI, the laser sheet was formed in the same manner as described in section 3.3.2.1. In this configuration, the optics were mounted on a horizontal rail attached to a stage that enabled vertical translation of the entire setup. This facilitated moving the laser sheet to various heights above the tunnel floor. The camera was mounted on a rail above the tunnel.

3.3.3 PLS Image Analysis

The PLS images were acquired using the Photron Fastcam Viewer software that came with the APX camera. The data was downloaded to a personal computer and sets of images were saved in ".RAWW" format. These files were then processed using an image-processing MATLAB program. Some filtering of the images was accomplished by using a median filter over a three pixel by three pixel kernal. Additionally, the images were contrast stretched to maximize the dynamic range of the output device. Of the 16,384 images captured per run, approximately 1000 images were downloaded and processed. A sequence of several hundred successive images could then be used to create a movie showing the unsteadiness of the interaction.

Chapter 4

Results

There were three main aspects of the current experiment. First, the effect of unsteady actuation of the VGs was studied on a SWTBLI generated by a 20º compression ramp in a Mach 2 freestream flow. PLS was used to capture side view and plan view images at a rate of 10 kHz. The next aspect of testing involved studying the effect of the same VGs on a SWTBLI generated by a 28º compression ramp in a Mach 5 freestream flow. PLS was again used to capture side view and plan view images. Finally, PLS was used to capture plan view images at several locations within the Mach 5 boundary layer to determine if the same coherent spanwise structure previously shown in a Mach 2 boundary layer also existed at Mach 5. The experiments showed the existence of a large-scale spanwise structure within the boundary layer, so PLS was utilized to study the effect of this spanwise structure on the Mach 5 SWTBLI. Results from these experiments will be presented in this order, and a discussion of the results as they relate to one another will follow.

All results presented in this chapter use the same coordinate system: x, y, and z are the streamwise, wall-normal, and spanwise directions respectively. The coordinates are normalized by δ. The origin in the streamwise direction ($x/\delta = 0$) is located at the corner of the ramp. Negative coordinates correspond to streamwise locations upstream of the ramp. The origin in the spanwise direction ($z/\delta = 0$) is

along the centerline of the test section, which corresponds to the centerline of the VGs for the VG results. In all images the flow is from left to right.

4.1 EFFECTS OF UNSTEADY ACTUATION OF VGS ON MACH 2 SWTBLI

4.1.1 Undisturbed Mach 2 SWBLI

Before determining the effect of the VGs on the SWTBLI, it was first necessary to document the undisturbed SWTBLI to determine the range of the intermittent region and compare to previous results. Figure 12 shows 10-frame average side view PLS images of the baseline interaction.

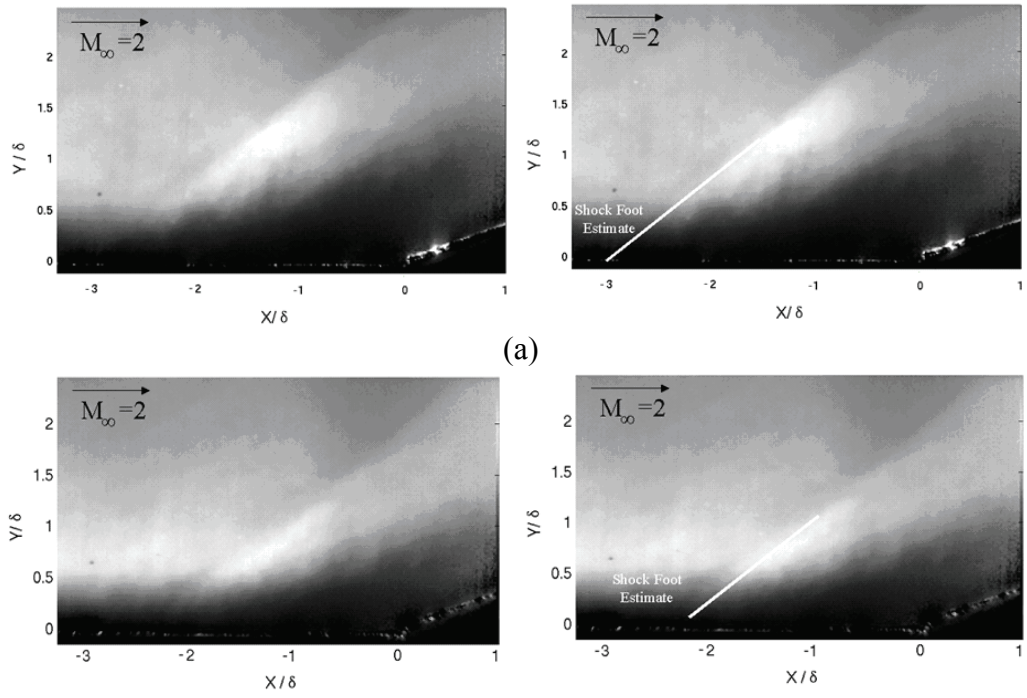

Figure 12. 10 frame averaged PLS images of Mach 2 undisturbed boundary layer. Figure (a) shock upstream, figure (b) shock downstream. The right images are identical to the left images with the addition of a shock foot estimate line.

Figure 12 (a) shows the upstream location of the shock while figure 12 (b) shows the downstream location of the shock. Each average image was computed by locally averaging 10 consecutive instantaneous images in time. This acts as a low-pass filter where the high-frequency motion is blurred, leaving only motions that occur at frequencies less than 1 kHz. In this manner the images show the extent of the intermittent range due to the low-frequency component and not just the effect of a single turbulent structure. In figures 12(a) and 12(b) the right images are identical to the left images but with the addition of a line representing an estimate of the shock foot location. While in actuality the separation shock is curved through the extreme lower part of the boundary layer, the estimates of these lines prove to correspond well with the measured intermittent range of Hou [2003]. This method was utilized to determine an estimate of the shock foot location for all side view results presented in this chapter, but the line is not shown in order to preserve the clarity of the images.

4.1.2 PLS Imaging Results of Unsteady Actuation of VGs on Mach 2 SWTBLI

The next step of the experiment was to study the effect of the VGs on the SWTBLI. The VGs were oscillated at 50 Hz and were raised to a height of 0.24 *in* (0.48 δ). By acquiring images at 10 kHz, the low frequency oscillation of the separation shock was "time-resolved". Additionally, the motion of the interaction was time-resolved as it responded to the VGs being pulsed at 50 Hz. Therefore, a major component of analyzing the data was observing the movies of a sequence of several hundred images. Through these locally-averaged images the low-frequency

oscillations could be easily observed and the periodic effects of the VGs were readily apparent. Readers must note that these "PLS movies" revealed important information on the interaction dynamics when viewed as a movie, which cannot be represented in a sequence of still images.

4.1.2.1 PLS Imaging Results in the Upwash Region of the Vortices

The first images taken in the experiment were side view images with the laser sheet location at the center of the test section (z = 0). This corresponded to the imaging plane being in the center of the counter-rotating VG pairs. This sheet location was in the "upwash" region between the counter-rotating vortices created by the two center VGs. Figure 13 shows the effect of the VGs at this sheet location, with (a) being the flowfield when the VGs were down and (b) when the VGs were up.

The upwash region tends to have the effect of bringing low momentum fluid from the lower part of the boundary layer into the upper part of the boundary layer. This can be analogous to the turbulent mechanism of an "ejection", which is detrimental to the overall boundary layer momentum. The effect of the VGs in the upwash region was most likely to induce momentum losses creating a less full velocity profile, which as Beresh et al. [2002] observed causes the shock to move upstream. The observed effect of the VGs does not energize the boundary layer in this case and, in fact, creates an overall negative velocity fluctuation which was most likely the cause of the separation shock moving further upstream.

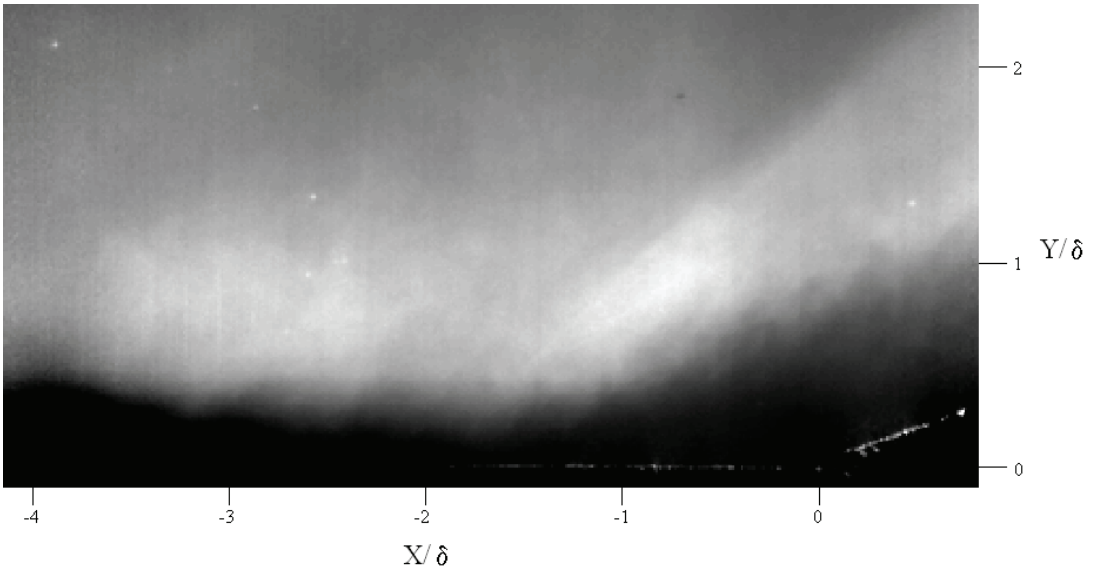

(a)

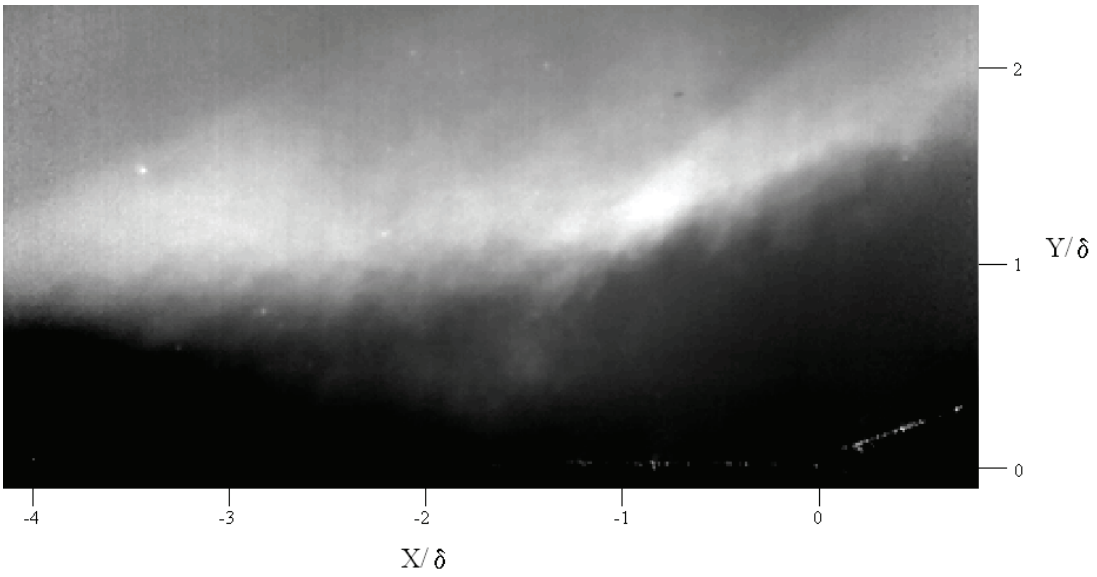

(b)

Figure 13. 10-frame averaged PLS images showing the VGs effect in the upwash region in Mach 2 flow with VGs down (a) and VGs up at height of 0.48δ (b).

Additionally, figure 13 (b) shows a second shock upstream of the separation shock. This shock is generated by the VGs when they are injected into the boundary layer and may have a significant influence on the flowfield. This shock was seen in Mach 5 testing and is further examined in section 4.2.2.

4.1.2.2 PLS Imaging Results in the Downwash Region of the Vortices

To investigate the possible positive influence of the VGs, the next step in the experiment was to image at a spanwise location corresponding to the "downwash" region between two outer counter-rotating vortices. The downwash region should bring high momentum fluid from the upper part of the boundary layer into the lower part of the boundary layer. The reader is directed to figure 8 in section 3.2.1.1 which illustrates the direction of rotation of vortices from their associated VG and also shows the laser sheet locations in the upwash region and downwash region.

Figure 14 shows the effect of the VGs in the downwash region, with (a) showing the flowfield when the VGs were down and (b) when the VGs were up.

As expected, the effect of the VGs in the downwash region was to move the shock to a further downstream location. The VGs actually moved the shock to a location further downstream than the extent of the intermittent region. Using the shock foot estimate described in the baseline results, it is estimated that the shock moved to -1.5δ when the VGs were up. This is a marked changed from the intermittent region of -2δ to -3δ of the baseline case. The effect of the VGs resulted

in the furthest upstream location of the shock decreasing 50% when the VGs were up. Additionally, the shock remained in a relatively constant location when the VGs were fully up, reducing the scale of the intermittent region.

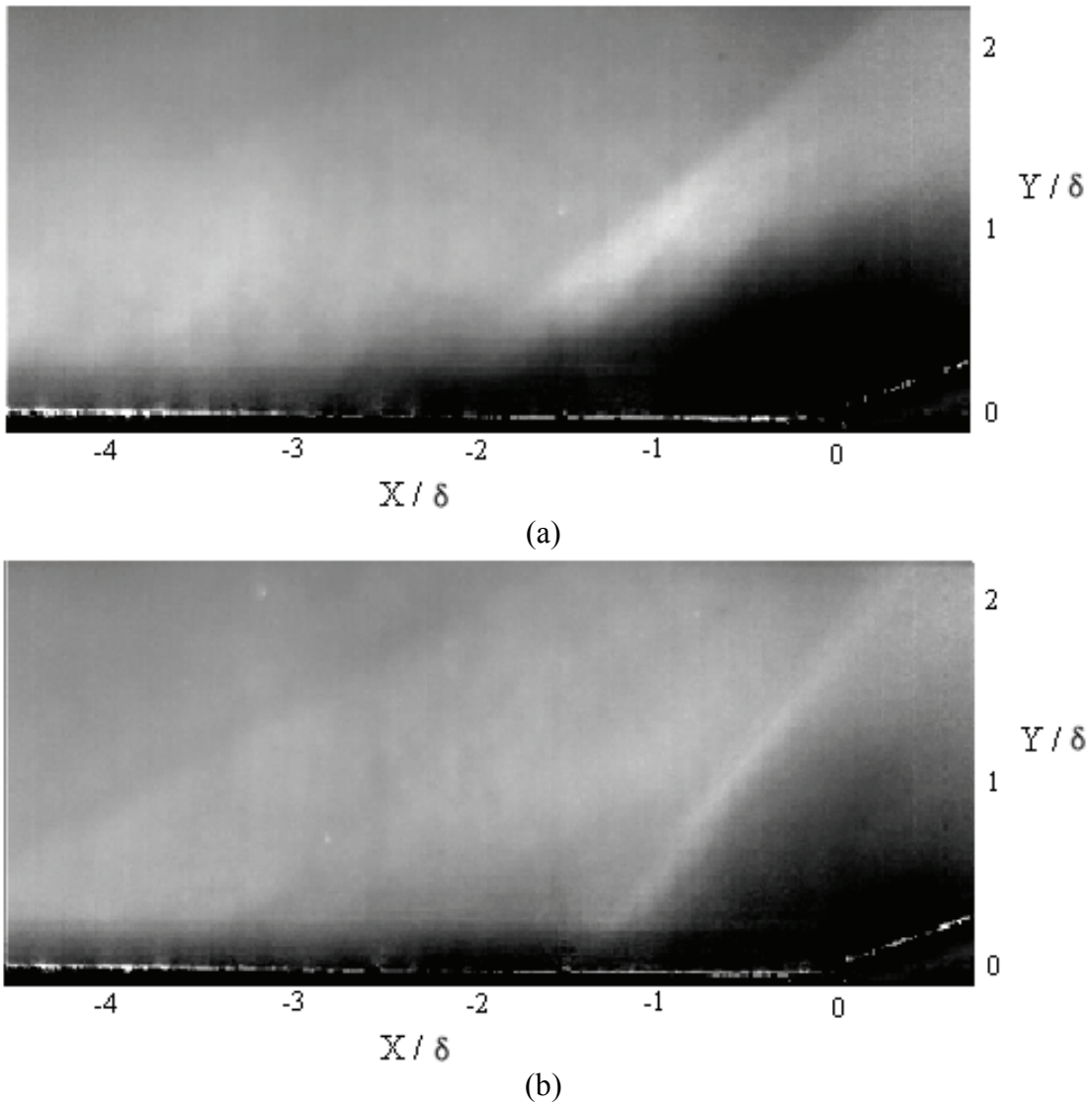

Figure 14. 10 Frame Averaged PLS Images of VGs effect in the downwash region in Mach 2 flow with VGs down (a) and VGs up at height of 0.48δ (b).

It is also clear in these figures that the angle of the separation shock increased when the VGs were up. It is estimated that the shock angle in figure 14 increased from approximately 39º without VGs to 51º with VGs, which is very close to the inviscid angle of 53.4º. A possible cause is that the downwash induces a downward component of velocity which results in the velocity vectors no longer being parallel to the floor. If the velocity vectors point slightly downward, then the ramp deflection and the separation region would appear greater compared to when the flow is horizontal. If this were the case, then for a given incoming Mach number the shock angle would increase because of the increased deflection angle. This is likely the reason that the shock angle increases in the downwash region when the VGs are up.

4.1.2.3 Planview PLS Imaging Results

One important observation that was made regarding the effect of the VGs involved the resulting highly 3-D behavior of the separation shock as it responded to the upwash and downwash regions created by the counter-rotating vortices. To evaluate this effect, plan view PLS was used to image the spanwise structure of the interaction. Figures 15 and 16 show plan view PLS images at heights of 0.12δ and 0.5δ within the boundary layer, respectively. In both figures (a) shows the flowfield when the VGs were fully down and (b) when the VGs were fully up.

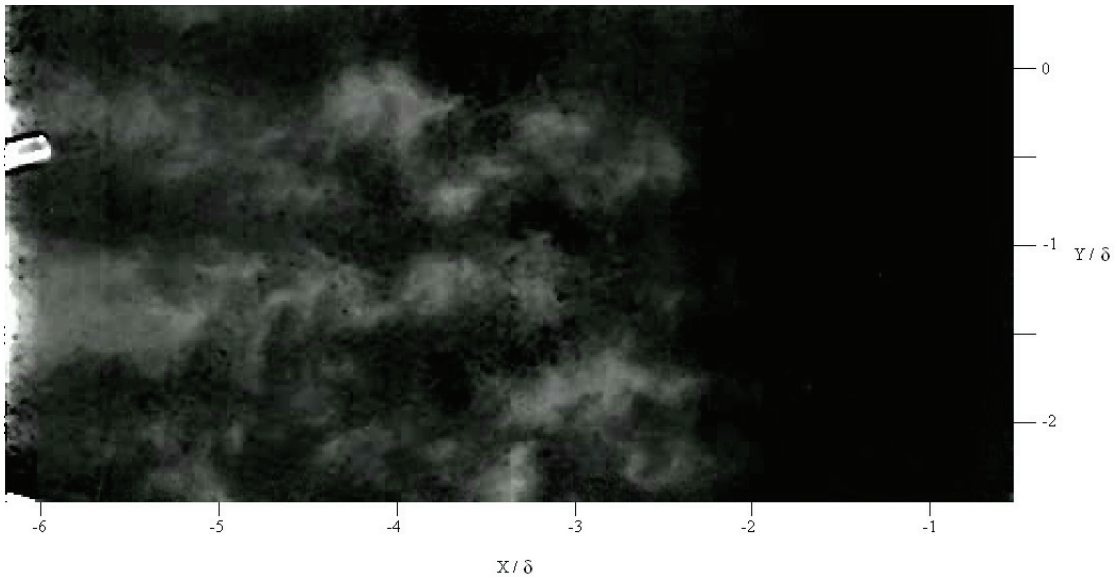

(a)

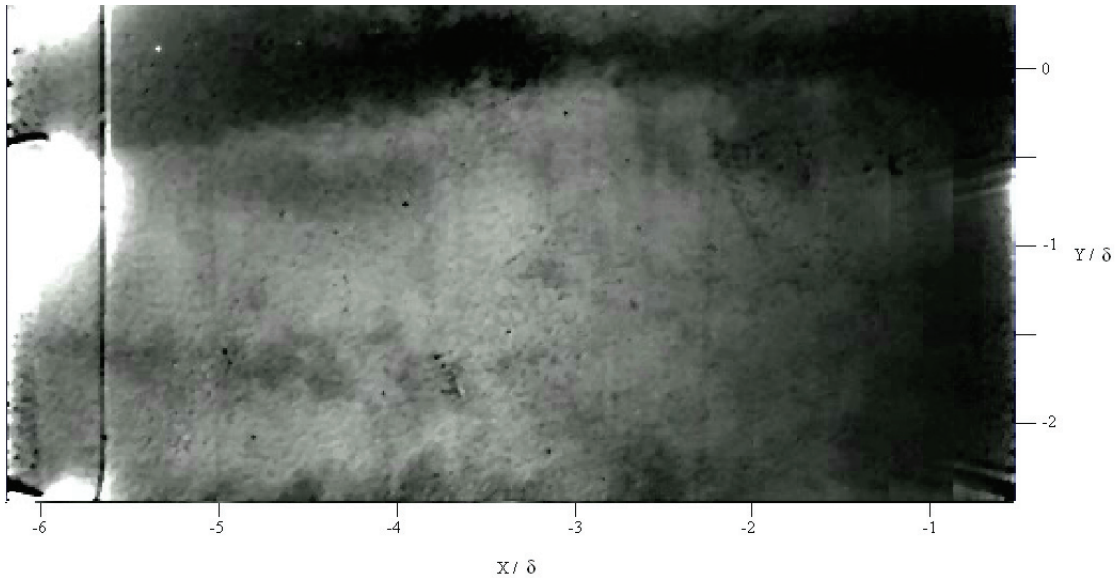

(b)

Figure 15. Instantaneous plan view PLS images at a height of 0.12δ showing the 3-D effect of the VGs on the Mach 2 separation region with VGs down (a) and VGs up at height of 0.48δ (b).

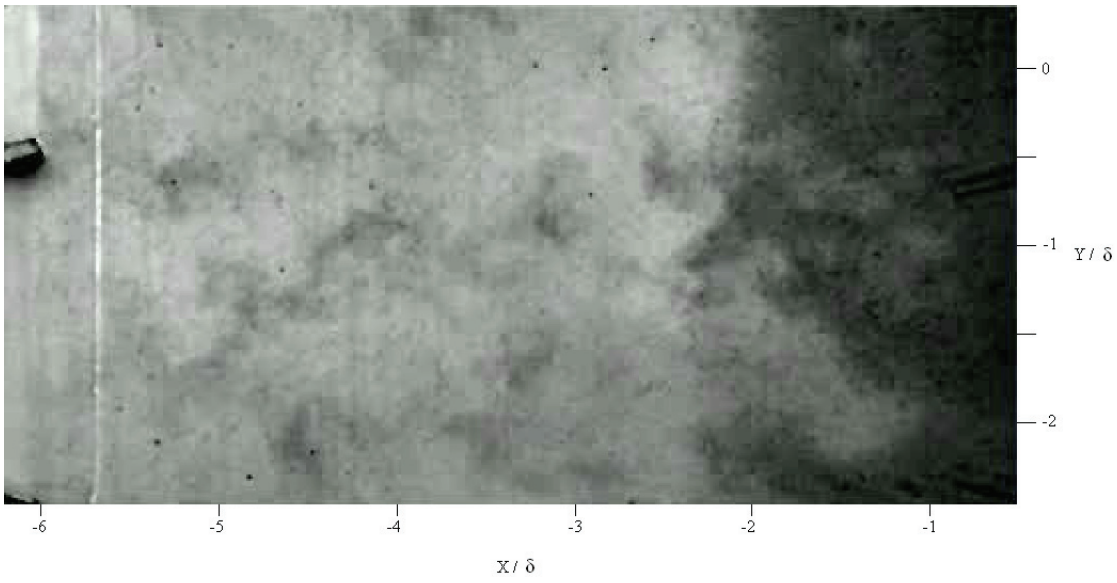

(a)

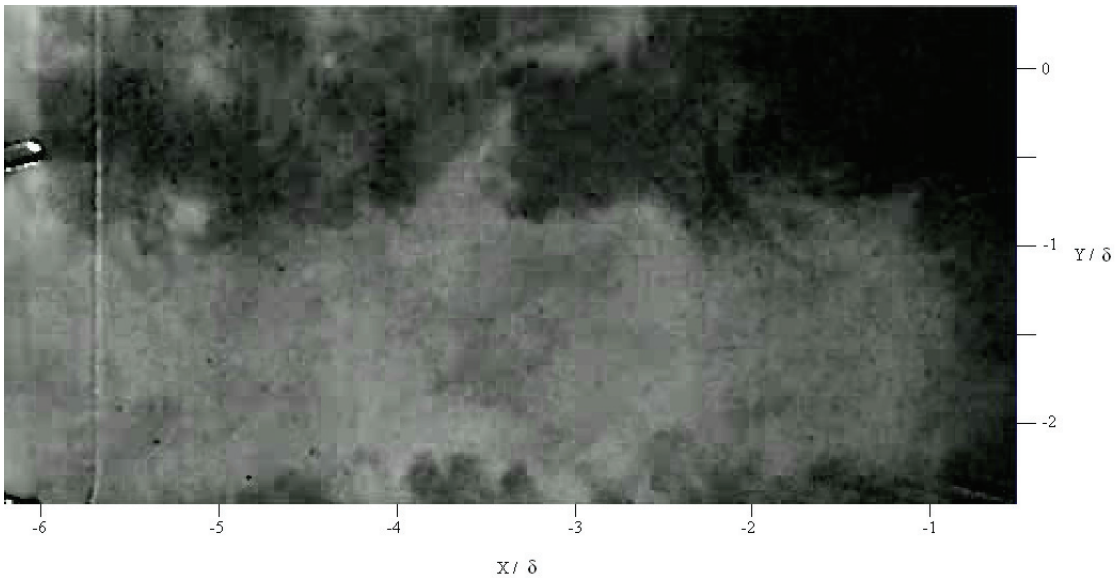

(b)

Figure 16. Instantaneous plan view PLS images at a height of 0.5δ showing the 3-D effect of the VGs on the Mach 2 separation region with VGs down (a) and VGs up at height of 0.48δ (b).

Figure 15 (a) shows that the separated flow region, which is the dark region at the right side of the image, is nominally 2-D, albeit with some large scale undulations. Note that there are signs of the strips seen by Ganapathisubramani et al. [2006b] corresponding to the undulations. When the VGs come to their full height their effect is clearly visible. The high speed flow created in the downwash region covers a large portion of the area downstream of the VGs. This seems to cause the separation region to move downstream by a considerable amount. Additionally, while the upstream extent of the separation region remains relatively constant in the upwash region, the scale of the separation region is greatly reduced. Figure 16, taken at a higher location in the boundary layer, also demonstrates the effects of the VGs. The upwash and downwash regions are represented by the low intensity and high intensity regions, respectively. The same effect is noticed in the separation region. The region is moved downstream in the downwash region and slightly upstream in the upwash region.

The structure of the separation region as it responded to the VGs was clearly 3-D. As was shown in the side view PLS, the separation region moved upstream in the upwash region and downstream in the downwash region.

The 3-D nature of the resulting shock was most likely caused because the VGs were placed so close to the ramp and the resulting SWTBLI. This creates a localized effect where the upwash and downwash regions exhibit completely different behavior. Optimal placement of the VGs at a further upstream location might allow the vortices to expand over a larger region and interact, causing the boundary layer as

a whole to become more energized resulting in a smaller separation region. Additionally, other types of VGs may produce more positive uniform results. In a previous study of passive VGs in this facility, Barter [1995] used Wheeler doublets to reduce the maximum upstream separation shock location, as measured with pressure transducers, by 60%. In that study, the author placed Wheeler doublets at 16δ upstream of the ramp compared to 6δ for the VGs of this study. The maximum Pitot pressure was observed to increase in the boundary layer from 28% at 6.6δ to 39% at 14.5δ. This increase in Pitot pressure with downstream distance demonstrated low profile VGs could continue to energize the boundary layer even as the resulting streamwise vortices lost strength. Ashill et al. [2002] showed evidence that counter-rotating vane VGs may create more decay resistant streamwise vortices, so the benefits of placing the VGs further upstream could be even more significant.

In the Mach 2 portion of this study, the VGs showed that in the downwash region there was a positive effect of moving the shock downstream and that the low-frequency oscillation was somewhat replaced by the frequency of the VGs. While the VGs were up, the scale of the intermittent region seemed to decrease in size and the shock seemed to remain in a relatively constant location. Additional work will be needed to determine if placement of the VGs at a further upstream location has a net positive effect of moving the shock downstream while also tending to remove the low-frequency oscillations.

4.2 EFFECTS OF UNSTEADY ACTUATION OF VGS ON MACH 5 SWTBLI

4.2.1 Undisturbed Mach 5 SWTBLI

A preliminary study of the undisturbed SWTBLI was also accomplished at Mach 5. In Mach 5 testing the shock seemed to have more jitter that at Mach 2, so 5-frame averages were used so that the shock would be more defined. This technique still acted as an effective low-pass filter removing the higher-frequency motion while still showing the location of the low-frequency oscillations. Figure 17 shows instantaneous PLS images with (a) showing the flowfield when the separation shock was at it furthest upstream location and (b) when the separation shock was at its furthest downstream location. The interface of the turbulent boundary layer and the freestream flow is visible upstream of the separation shock in both (a) and (b). Additionally, the 3-D structure of the separation shock is visible in both (a) and (b). Figure 18 shows 5-frame average PLS images with (a) showing the flowfield when the separation shock was at it furthest upstream location and (b) when the separation shock was at its furthest downstream location.

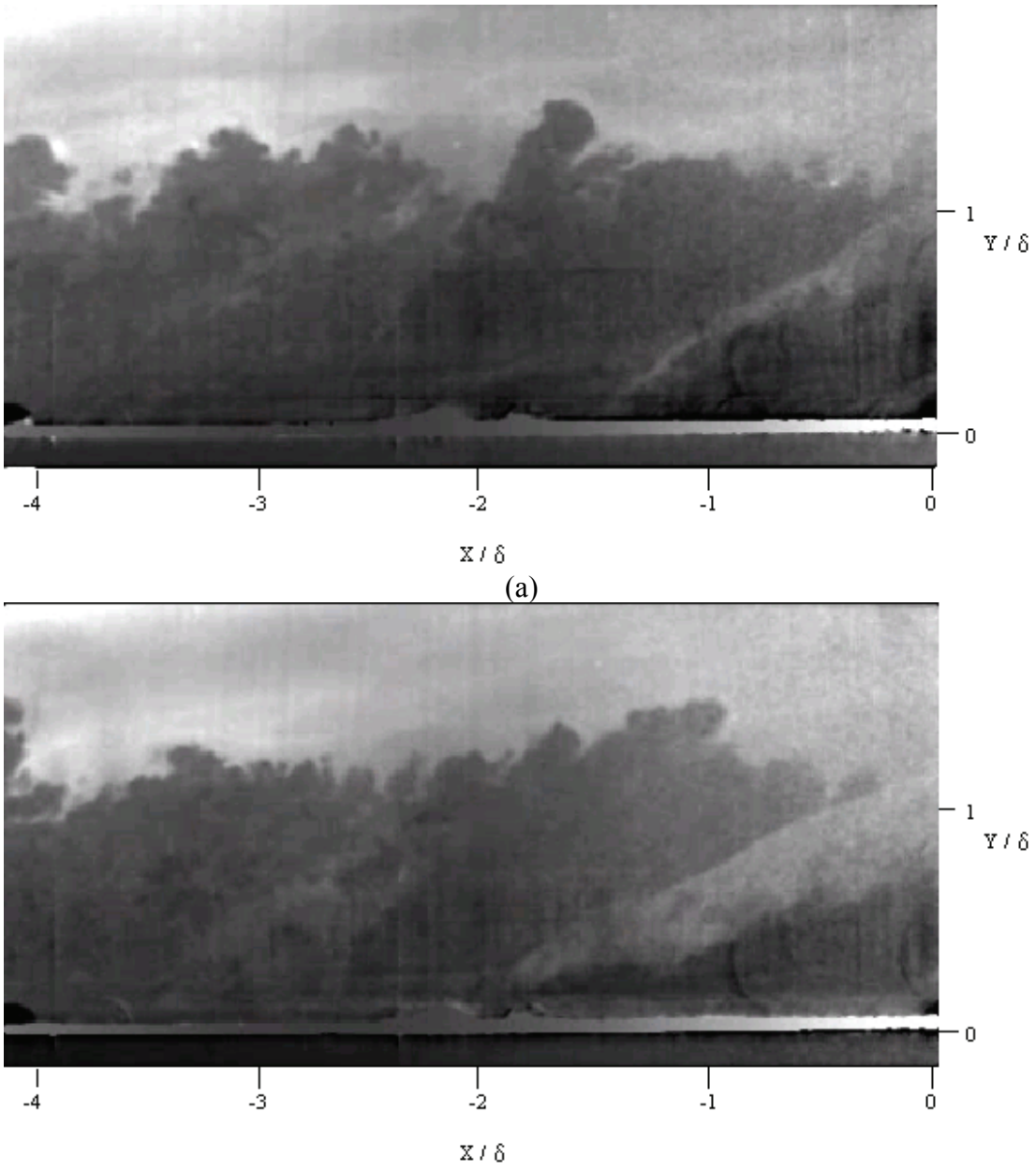

Figure 17. Instantaneous PLS images of undisturbed Mach 5 SWTBLI. Figure (a) shows the upstream location and (b) shows the downstream location.

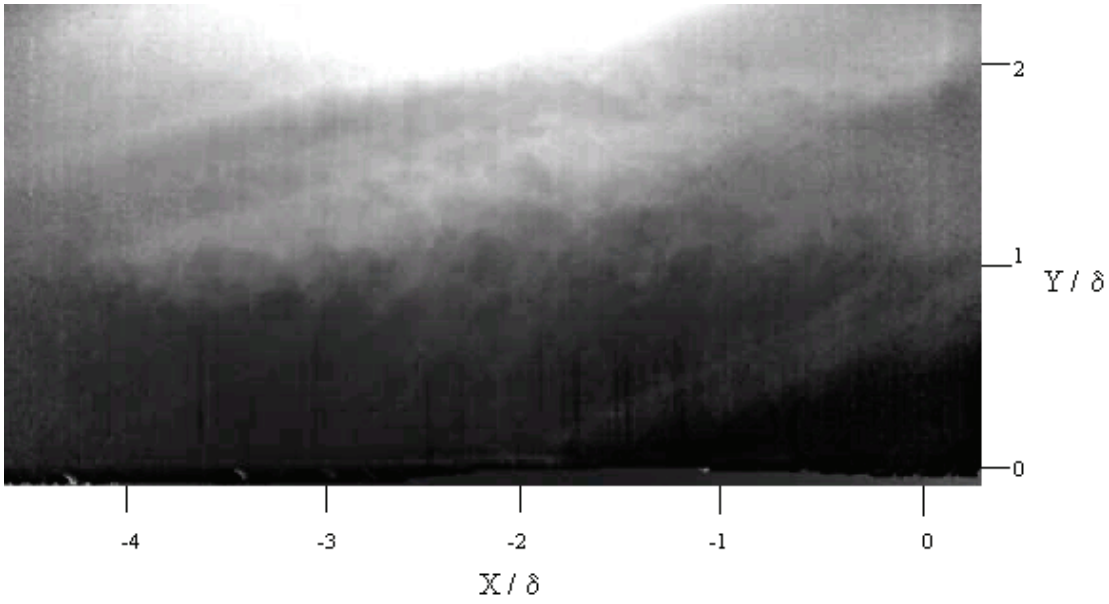

(a)

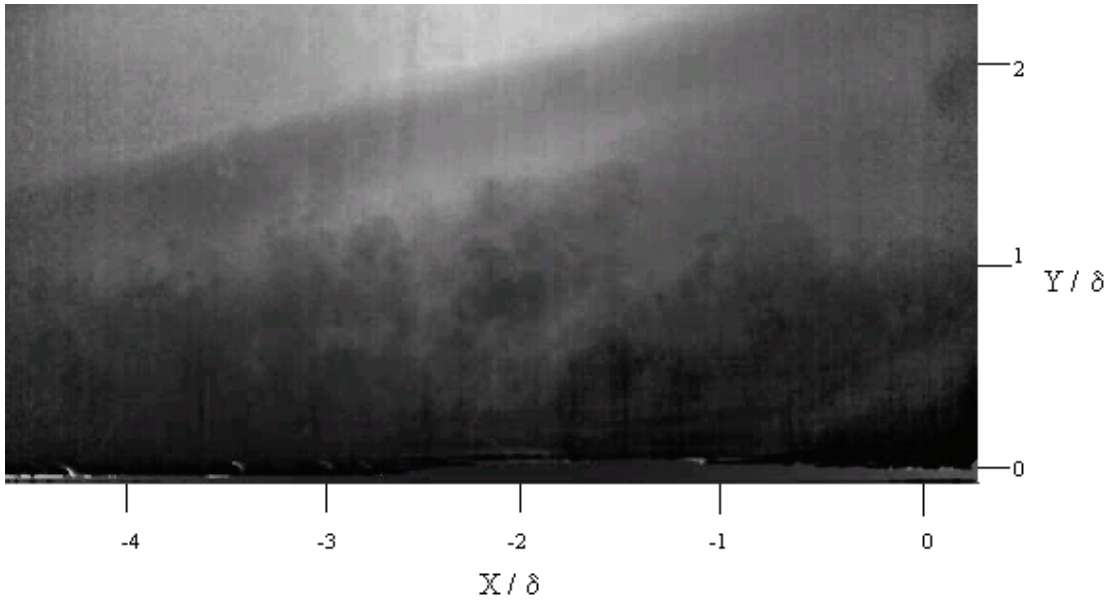

(b)

Figure 18. 5-frame averaged PLS images of undisturbed Mach 5 SWTBLI. Figure (a) shows the upstream location and (b) shows the downstream location.

The intermittent region was observed to extend from approximately -1δ to -2.5δ, which matches previous data. Note that in addition to the shock foot moving, the angle of the separation shock also changes. For the images in figure 18 the angle changes from approximately 24º in the upstream case to approximately 33º in the downstream case. This is an interesting observation because this trend was not apparent in the Mach 2 case, where the angle of the separation shock was 39º in both the upstream and downstream location.

4.2.2 PLS Imaging Results of Pulsed VGs on Mach 5 SWTBLI

4.2.2.1 PLS Imaging Results for Initial VG Height of 0.24 Inches

Once the baseline information was acquired, the effect of the VGs was then studied. Owing to ease of implementation and time constraints, as well as testing a consistent design, the VGs from the Mach 2 study were used at Mach 5. As discussed in section 3.2.1.1, there was a constraint on the maximum height of the VGs. The VGs used were approximately 0.24 *in* tall, and this was the height that the VGs were pulsed to for Mach 2 testing. This resulted in the VGs going to a scaled height of 0.48δ at Mach 2. This height of 0.48δ would have been matched for Mach 5 testing, but the VGs could not go to the required absolute height of 0.36 *in*. Instead the VGs were pulsed to the same absolute height of 0.24 *in* which was 0.32δ at Mach 5.

The first PLS images were taken in the downwash region. Figure 19 shows an instantaneous image of the flowfield structure when the VGs were at their full height of 0.32δ.

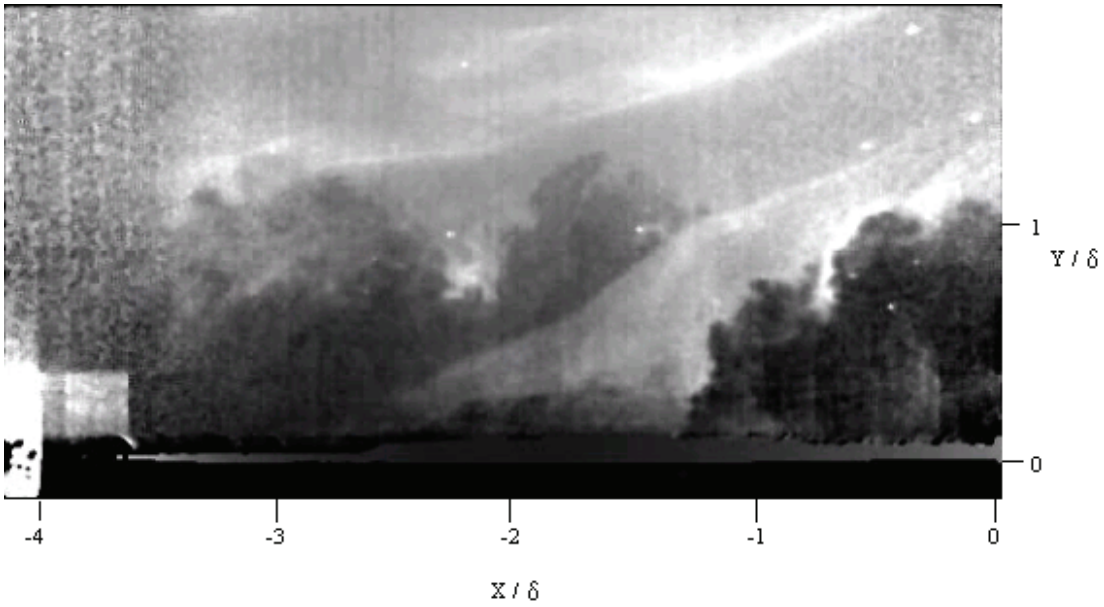

Figure 19. Instantaneous PLS image of interaction in downwash region of Mach 5 SWTBLI with VGs at full height of 0.32δ.

The turbulent structures are evident in the upstream boundary layer and the separation shock is seen to curve at approximately -2δ where a turbulent structure is directly above the shock. This demonstrates how the shock can respond to passing turbulent structures. Additionally, the separation region is observed downstream of the separation shock as the black region in the bottom right portion of the image.

Figure 20 shows 5-frame average PLS images of the interaction in the downwash region comparing when the VGs were down (a) and at the full height of 0.32δ (b).

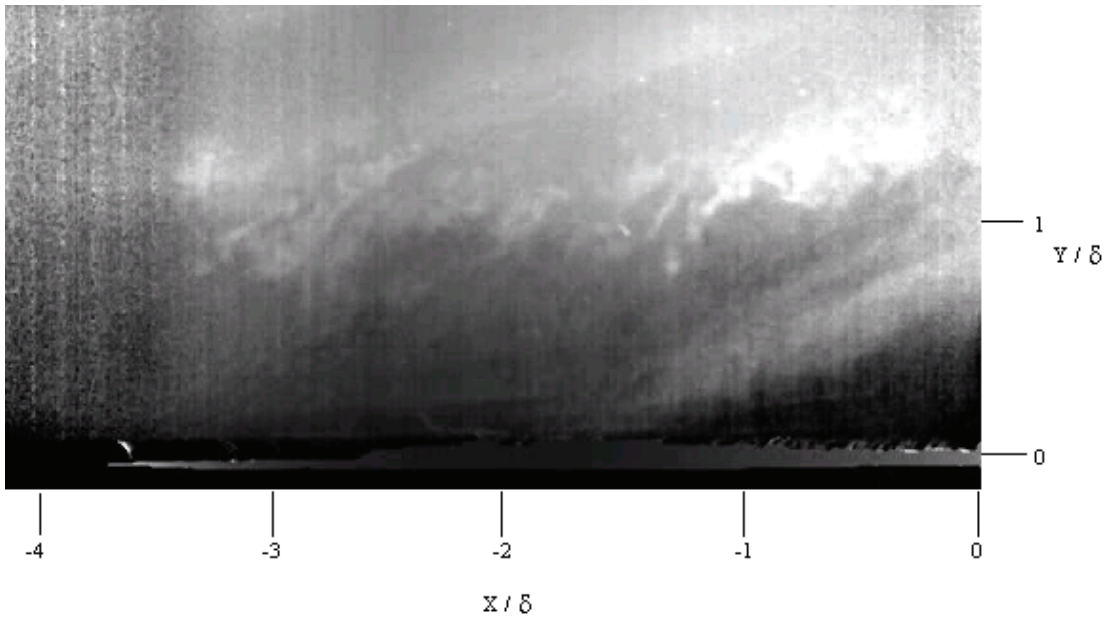

(a)

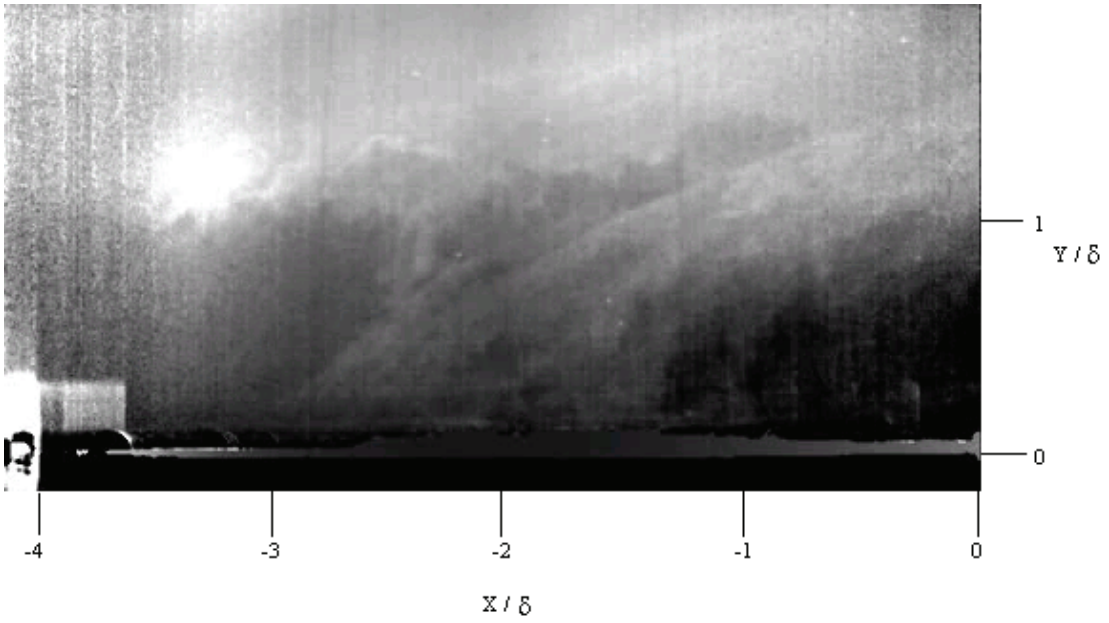

(b)

Figure 20. 5 frame averaged PLS images of interaction in downwash region of Mach 5 SWTLBI with VGs down (a) and with VGs at full height of 0.32δ (b).

Figure 20 shows that even in the downwash region the separation shock moved approximately 1δ further upstream than the furthest upstream location that was observed in the baseline case. This was surprising since the sheet location was in a downwash region and the VGs went to a lower scaled height than at Mach 2. The effect of the VGs in the upwash region at the same height of 0.32δ was then studied to gain insight into the flowfield. Figure 21 shows the effect of the VGs in the upwash region with (a) showing the interaction when the VGs were down and (b) showing the interaction when the VGs were at their full height of 0.32δ. The periodic lines of high intensity in the bottom right of figure 21 (b) are artifacts of the camera capturing the reflection of the laser sheet off of the VGs when they were up, and they are not caused by any phenomenon in the flowfield.

The separation shock foot was observed to move upstream beyond approximately -3.5δ. Additionally the separation region increased in scale by a large amount. The shock generated by the VGs was stronger at Mach 5 as compared to Mach 2, and most likely resulted in the boundary layer separating at a more upstream location.

Figure 22 shows two instantaneous images of the flowfield when the VGs were fully up. Note that the artifacts in the bottom right of the images are the stray reflections also found in figure 21 (b).

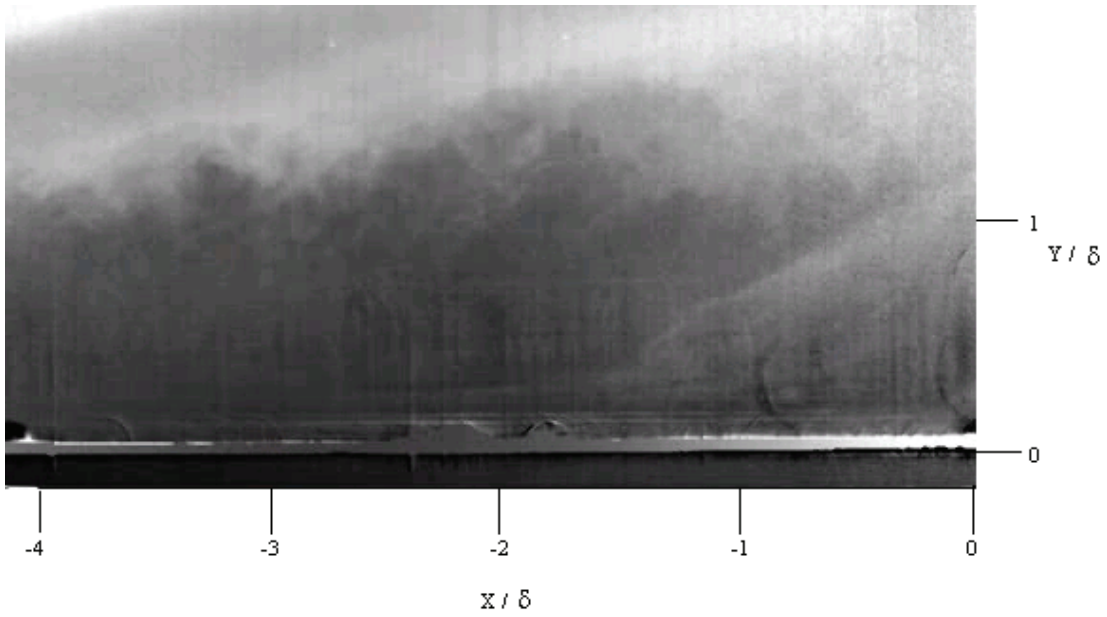

(a)

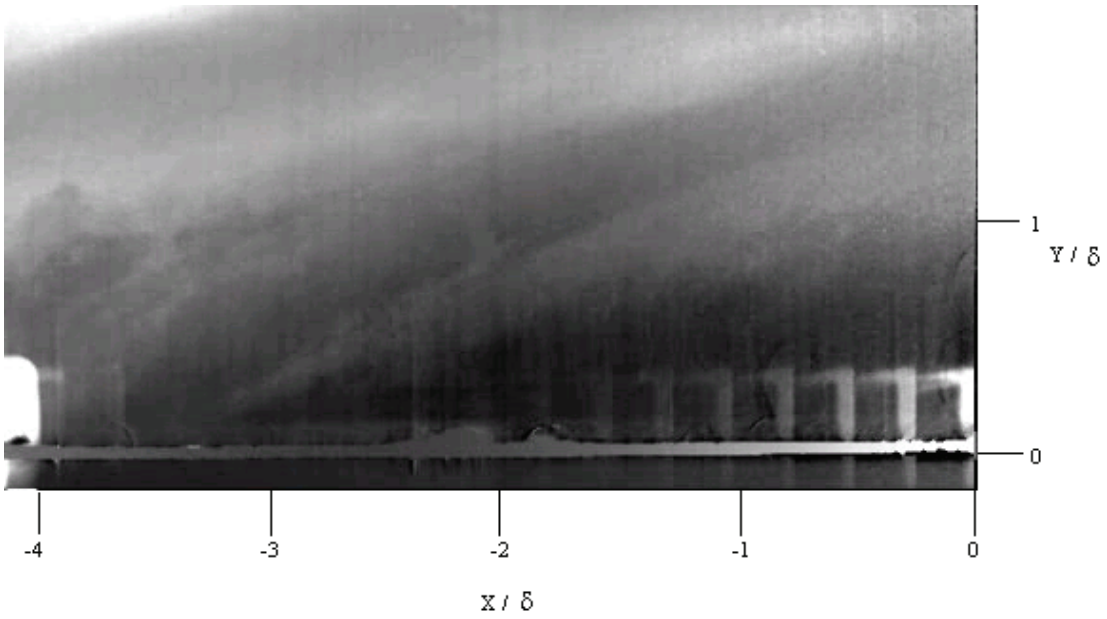

(b)

Figure 21. 5-frame averaged PLS images of interaction in upwash region of Mach 5 SWTBLI with VGs down (a) and with VGs at full height of 0.32δ (b).

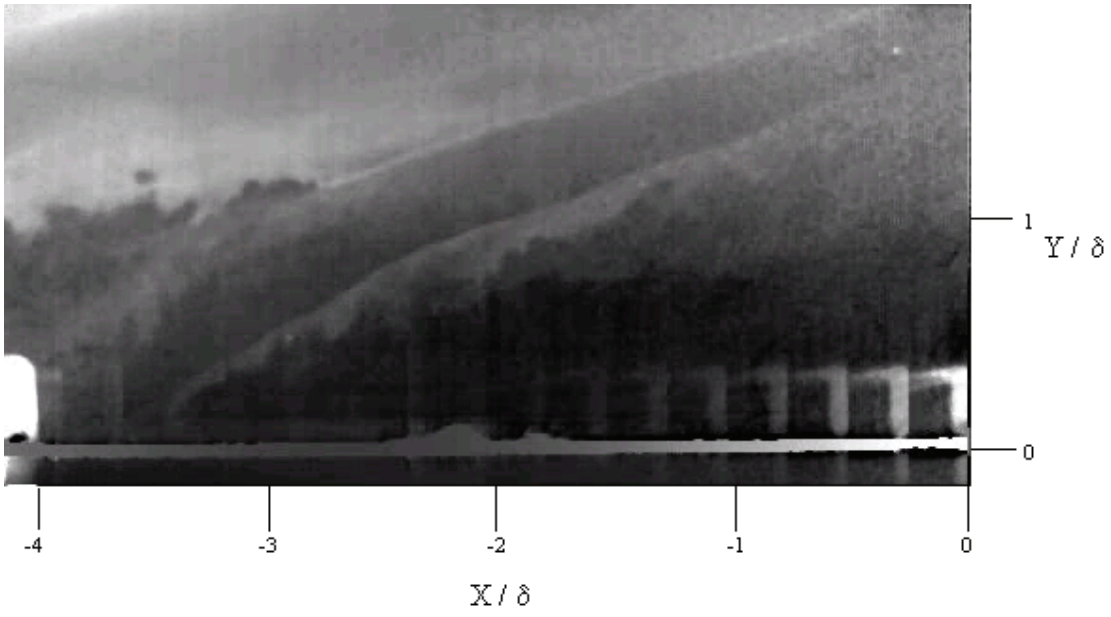

(a)

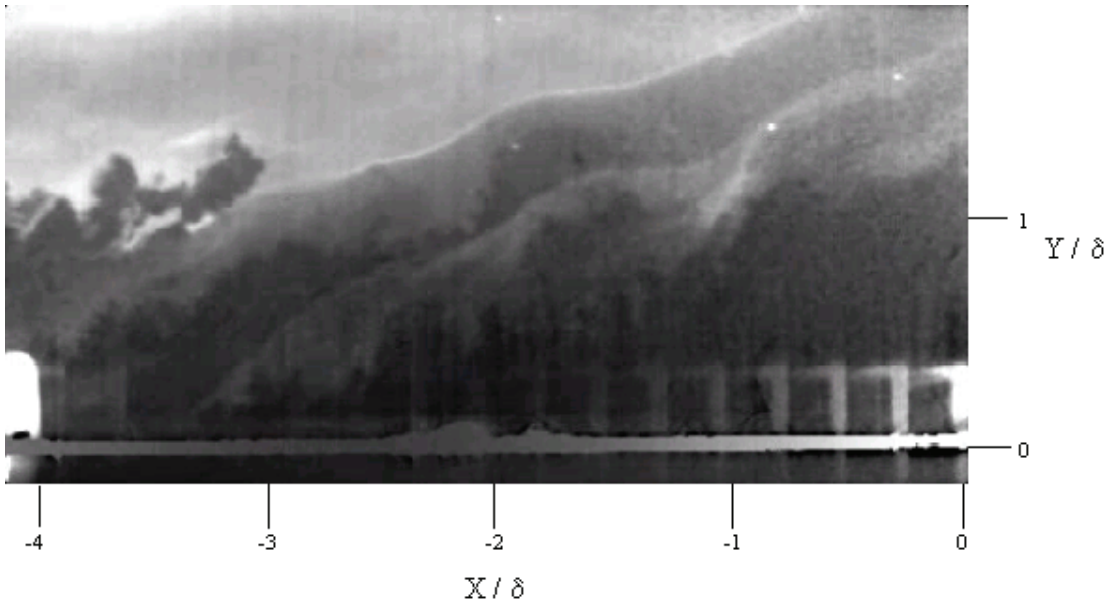

(b)

Figure 22. Instantaneous PLS images of shock location in upwash region of Mach 5 flow with VGs at full height of 0.32δ. Figure (a) shows a smooth shock while (b) shows a highly curved shock.

The shock generated by the VGs is clearly visible as the upper shock in figure 22 (a) and (b). The line has a higher intensity at the location of the shock due to the increased density behind the shock increasing the density of fog particles. The flow behind the shock then has lower intensity due to the evaporation of the fog particles caused by the increased temperature behind the shock. Additionally, the turbulent structures are visible upstream of the shock and appear smeared at the interface of the shock. The separation shock is also clearly visible as the flow downstream of the second shock has a higher intensity due to the increased density. Note that figure 22 (b) shows both the VG shock and the separation shock being highly 3-D as they respond to the turbulent structures. Also visible in both figure 22 (a) and (b) is the separation region, seen as the black region behind the separation shock. The scale of the separation region is very large and extends very far upstream. This images show that the VGs create a relatively strong shock, which results in the flow being more prone to separation, which in turn causes the separation shock to move upstream.

These images clearly show the effect of the VGs at 0.32δ in the Mach 5 SWTBLI was to move the shock upstream. In the image of the VGs fully up, there were two distinct shocks. The furthest left shock could be traced back to the beginning of the VGs, while the right shock still corresponded to the separation shock. The additional strong shock created by the VGs was most likely the cause of the separation shock moving so far upstream. Even though the VGs went to a lower scaled height at Mach 5, the flow deflection angle of the VGs themselves was high enough that they caused a much stronger shock at Mach 5. This shock may have

slightly separated the boundary layer or reduced the momentum of the boundary layer so that it was more prone to separation. The end result was that a strong shock was created off the leading edge of the VGs, which in turn caused the separation shock to move very far upstream in both the upwash and downwash region of the vortices.

The PLS movies were further examined and evidence was observed of the shock moving downstream during a portion of the VG insertion. During the initial upwards motion of the VGs before they were fully extended, the separation shock first moved downstream, and then moved upstream as the VGs completed their upward motion. This observation suggested that the VGs were extended too far into the flow, so the amplitude of actuation was reduced to one-half of the original value.

4.2.2.2 PLS Imaging Results for VG Height of 0.14 Inches

Because the initial rise of the VGs created a downstream motion of the shock, the VGs were recalibrated to achieve a final height of 0.14 *in* (0.19δ). When the VGs went to this height, the extreme upstream motion of the shock was no longer observed. The control was sporadic, however, and primarily depended upon the location of the shock before the VGs started coming up. Therefore, in the cycles of the VG motion when the shock started at a more upstream location, the VGs had the effect to move the shock to a more downstream location. In the case when the shock started further downstream, the shock remained at the same approximate location. Figure 23 shows the interaction in the downwash region for a case of positive control, while figure 24 shows the interaction when no control was obtained. In figures 23

and 24, image (a) corresponds to the VGs being down and image (b) when the VGs were at their full height of 0.19δ.

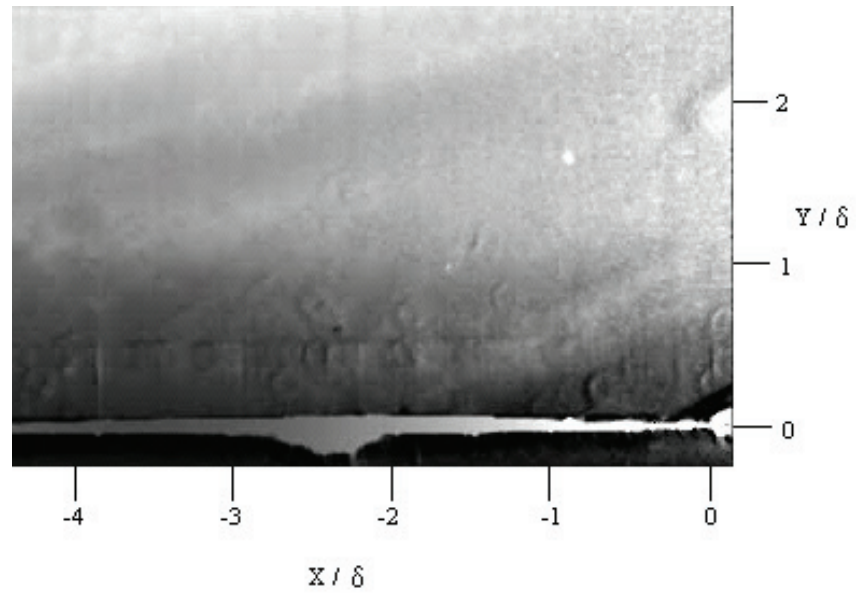

(a)

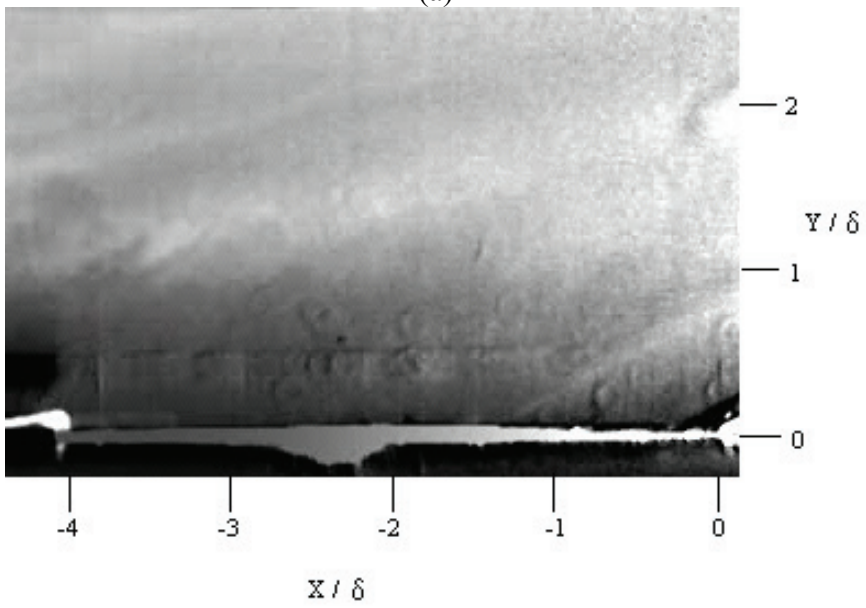

(b)

Figure 23. 5-frame averaged PLS images in downwash region of Mach 5 interaction showing control with VGs down (a) and with VGs up at 0.19δ (b).

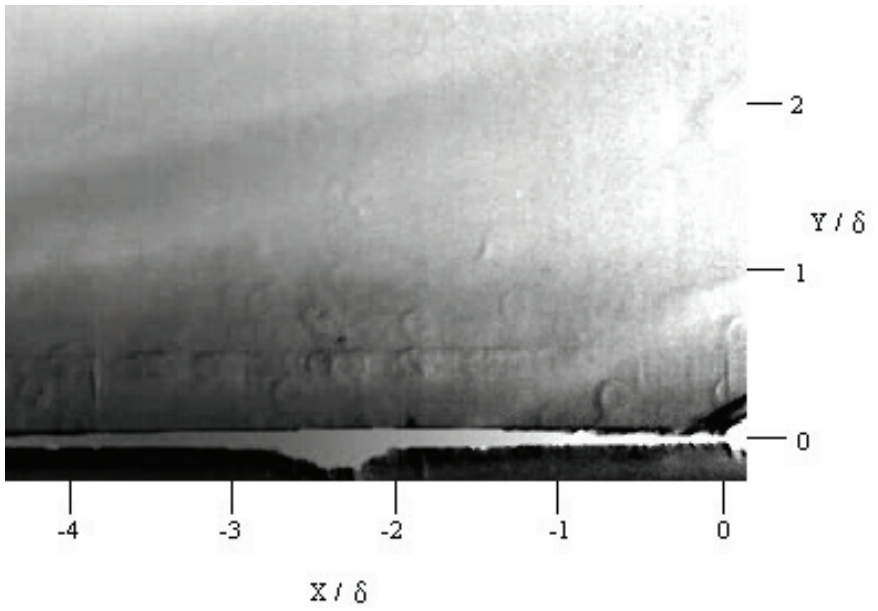

(a)

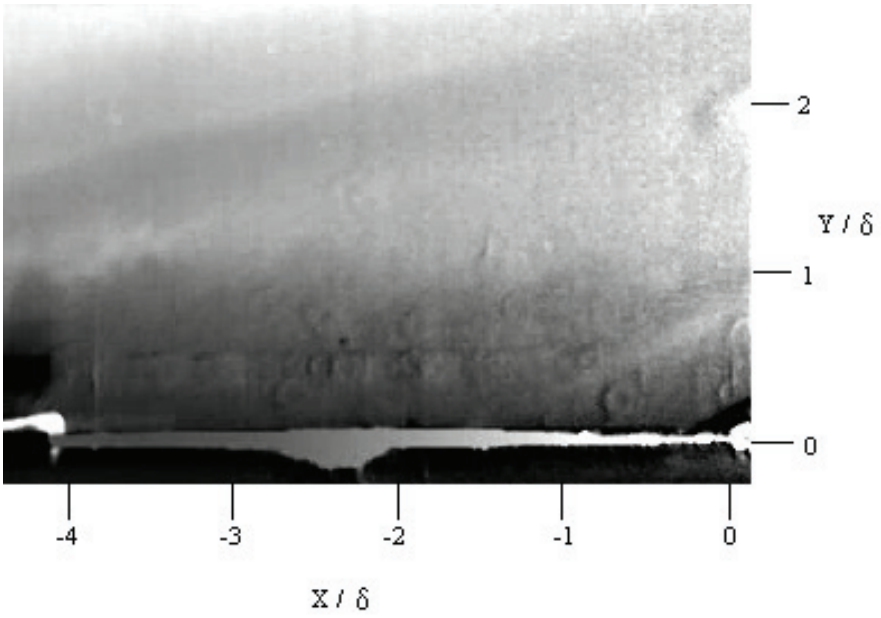

(b)

Figure 24. 5-frame averaged PLS images in downwash region of Mach 5 interaction showing no control with VGs down (a) and with VGs up at 0.19δ (b).

These images demonstrate that slight control was observed in the case when the shock began at a more upstream location. In figure 23 (a) the separation shock began at a location of -2.2δ and in (b) the separation shock was moved to approximately -1.5δ. This location, however, is still within the intermittent region of -1δ to -2.5δ observed in the baseline case. In figure 24 (a) the shock begins at a location of -1.5δ and that location is maintained in (b) when the VGs are at their full height. Additionally the shock was observed to become more swept, which was the opposite trend of what occurred at Mach 2.

The effect of the VGs at the lower height of 0.19δ was also studied in the upwash region. Figure 25 shows the location of the shock in the upwash region when the VGs were down (a) and when they were are their full height (b).

The shock still moved upstream in figure (b) when the VGs were inserted into the flow and there is still evidence of a shock being generated by the leading edge of the VGs. However, the shock from the VGs appears to be weaker and thus the separation shock does not move as far upstream as compared to when the VGs went to 0.32δ. For the case when the VGs went to 0.19δ, the motion of the separation shock in the upwash region was comparable to the Mach 2 case.

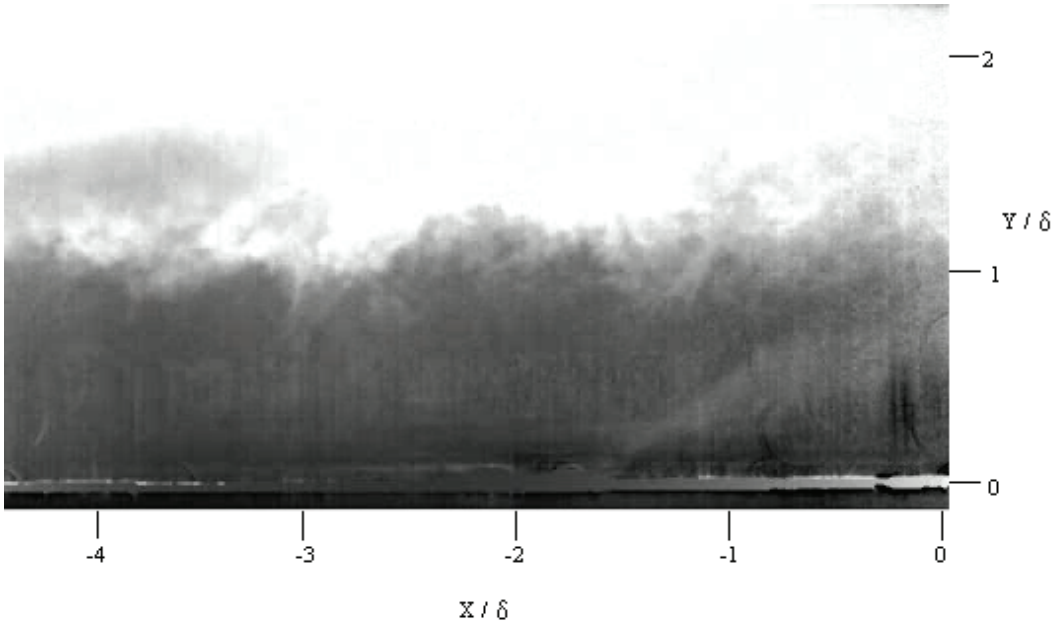

(a)

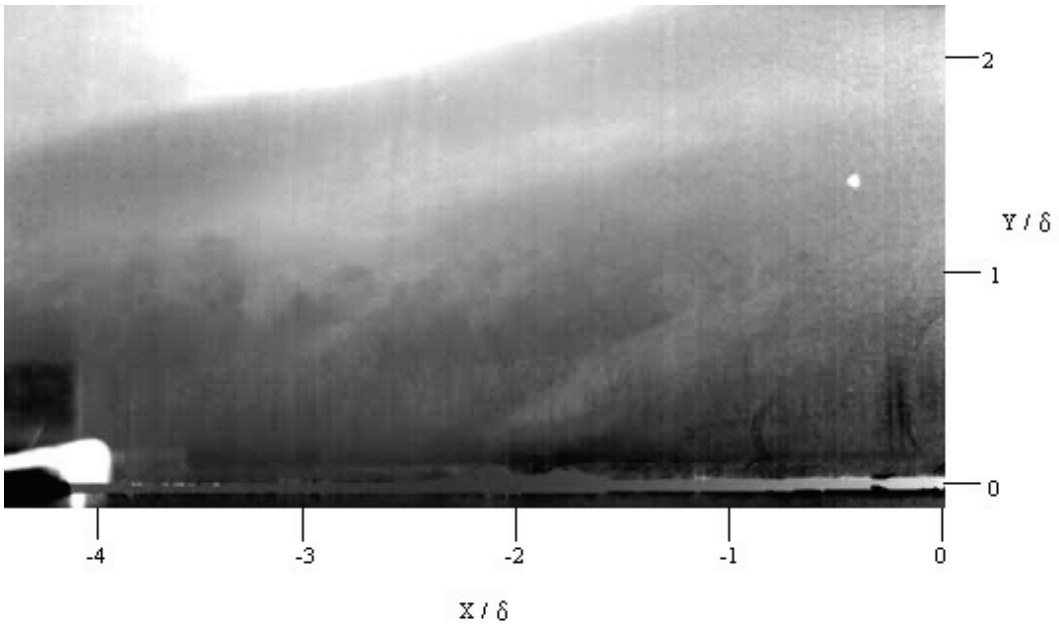

(b)

Figure 25. 5-frame averaged PLS images in upwash region of Mach 5 interaction with VGs down (a) and with VGs at full height of 0.19δ (b).

The VGs were not as effective at Mach 5 as they were at Mach 2. In the downwash region at Mach 2, the shock was consistently moved to a downstream location approximately 0.5δ outside the intermittent region. Slight control at Mach 5 was only observed when the shock was at a more upstream location when the VGs began their upwards motion. Additionally, for this case the shock was only moved to a downstream location that was still within the intermittent region. For the case when the shock began at a more downstream location the shock remained at a relatively constant location when the VGs came to their full height. Additionally, in both cases of the downwash region the shock was observed to become more swept, which was the opposite effect of what occurred at Mach 2. This result gives insight into a possible cause of the reduced effectiveness at Mach 5. Because the VGs generated a shock off their leading edge when they were raised to 0.32δ, they were only raised to 0.19δ to study their effectiveness. This has two important implications. First, because they did not come to their full mechanical height of 0.24 *in*, their projected streamwise area was greatly reduced, while the spanwise spacing between them was increased. This result most likely caused a reduced effectiveness of the VGs. The second implication is that the VGs may not have gone to a sufficiently large enough height to generate vortices that would reach into the high momentum region. If the vortices could not induce downwash high enough in the boundary layer, they would be less effective at increasing the momentum in the lower part of the boundary layer, and thus would not create the fuller velocity profile which would correspond to a downstream shock location. Evidence of these results may be apparent in the

resulting shock angle of the separation shock. As proposed in Mach 2 testing, if the shock becomes steeper because of the downwash inducing a velocity vector that is pointing slightly downwards, thus creating a larger effective deflection angle and a steeper shock, then at Mach 5 the VGs may not be creating a sufficient amount of downwash. If this is the case, then as previously mentioned, there may not be sufficient downwash to bring the high momentum fluid from the upper part of the boundary layer into the lower part of the boundary layer. This may be why the VGs do not cause the shock to move outside the intermittent region. Therefore, the geometry of the VGs should be redesigned to include a less steep deflection angle. This should result in the VGs generating a weaker shock when the VGs are at a higher height, allowing them to create vortices that reach to a higher point in the boundary layer resulting in a stronger downwash of higher momentum fluid.

4.2.2.3 Planview PLS Imaging Results of VGs in Mach 5 SWTBLI

Planview PLS imaging was also employed at Mach 5 to study the spanwise structure of the SWTBLI as it responded to the VGs. Figures 26 (a) and (b) show 10-frame average images of the SWTBLI acquired with the laser sheet at a wall normal height of 0.2δ. Figure 26 (a) shows the flowfield when the VGs were down. A similar structure to that observed in Mach 2 testing was observed with some large scale undulations in the separation region. Figure 26 (b) shows the structure of the separation region when the VGs were at their full height of 0.19δ.

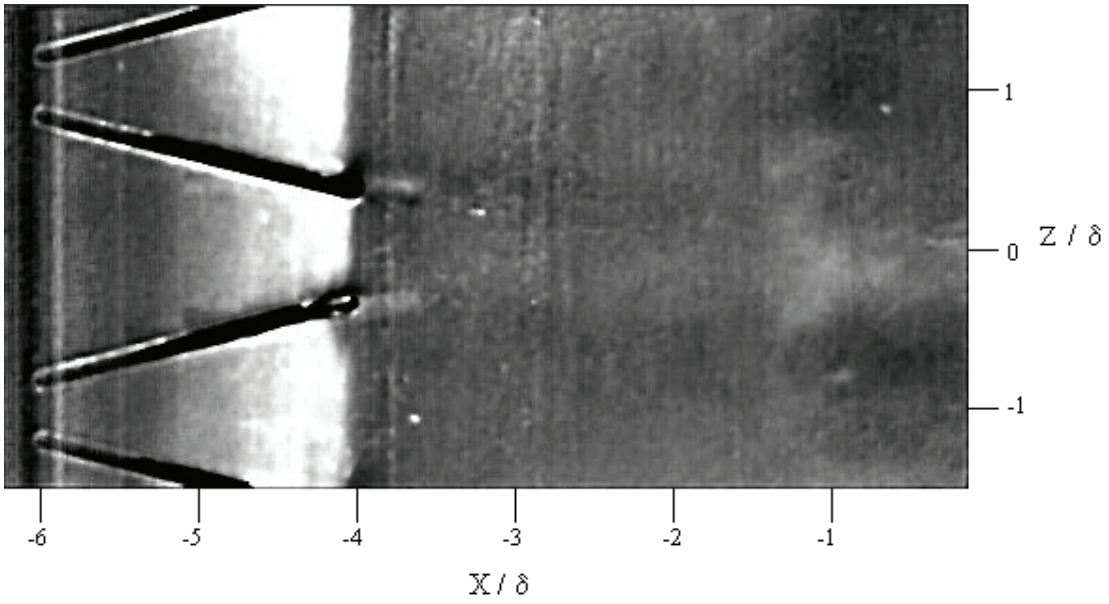

(a)

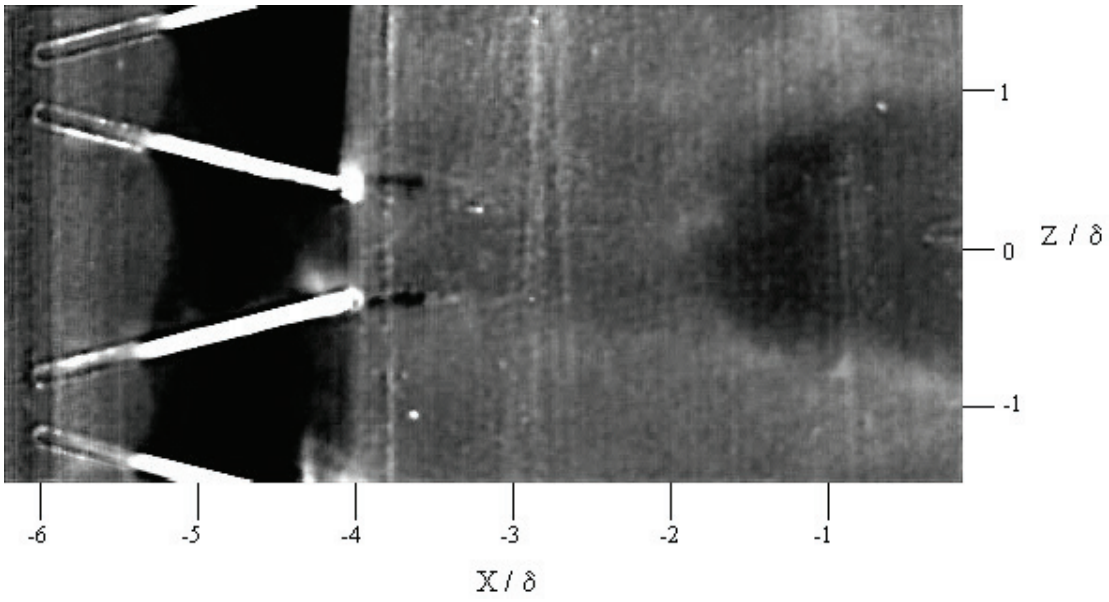

(b)

Figure 26. 10-frame average plan view PLS images of Mach 5 SWTBLI with laser sheet at wall-normal height of 0.2δ (a) when the VGs were down and (b) when the VGs were at their full height of 0.19δ.

Figure 26 (b) shows the resulting highly 3-D behavior of the separation region as it responds to the flow created by the VGs. At this sheet height of 0.2δ, the separation region in the upwash region, at a z-location of 0, is seen to extend upstream to approximately -2δ, while in the downwash region at a z-location of -1δ, the separation region appears to move out of the field of view. The separation region at this spanwise location may have decreased in scale enough that it does not reach vertically into this field of view at a wall-normal height of 0.2δ. These results are consistent with the corresponding side view PLS images, and demonstrate a shift of nearly 2δ in the separation region at a z-location only 1δ away. As mentioned in section 4.1.2.3, this is most likely a result of the VGs being placed too close to the ramp. In the Mach 5 study the VGs were located the same absolute distance away of 3 *in*, but this was only 4δ as compared to 6δ at Mach 2 due to the increased boundary layer thickness at Mach 5. A more optimal upstream placement may result in a less 3-D structure as it allows the vortices more time and space to interact.

While examining the plan view PLS movies for this study, another distinct phenomenon was observed that may be independent of the VGs. Several images, including figure 25, showed a 3-D shock structure even when the VGs were down. Figure 27 below shows another example image of this 3-D structure when the VGs were down. The undulations in the separation region vary in spanwise location between figures 25 and 27, suggesting that they are not an artifact of the VG slots, but may be related to the upstream boundary layer.

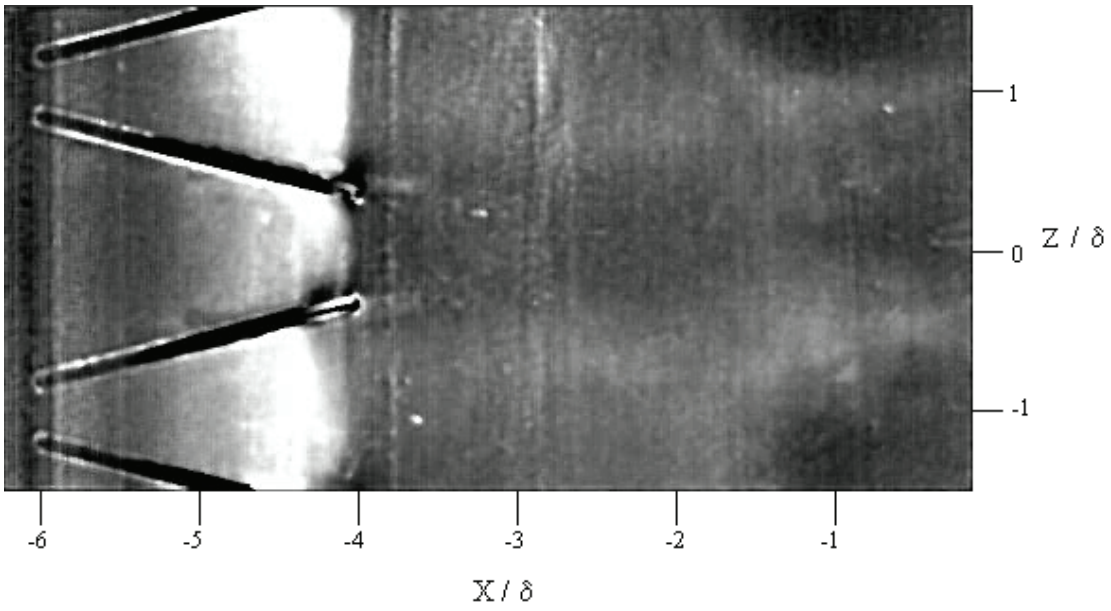

Figure 27. 10-frame average plan view PLS image of Mach 5 SWTBLI with laser sheet at wall-normal height of 0.2δ when the VGs were down, demonstrating a 3-D separation region.

Due to the low pulsing frequency of the VGs and high convection velocity of the tunnel, the flow when the VGs were down was effectively the undisturbed flow. This would suggest that the 3-D structure also exists in the baseline case for an undisturbed boundary layer. Additionally, recent studies by Ganapathisubramani et al. [2006b] at this same facility found similar results in a Mach 2 boundary layer. Since these PLS images showed an indication of similar structure in the Mach 5 boundary layer, a more in-depth study was completed.

4.3 LARGE-SCALE SPANWISE STRUCTURES IN MACH 5 BOUNDARY LAYER

Recent studies have shown the existence of large-scale structures in supersonic boundary layers. These structures were as long as 40δ and were shown to be correlated to the spanwise structure and location of the shock. A similar shock structure was observed in the Mach 5 VG study, so a more in-depth examination of the existence of these structures in a "hypersonic" boundary layer was examined. While the Mach number achieved constitutes the lower bound of the hypersonic regime this facility does not achieve flight hypersonic stagnation conditions. Therefore this study neglects some phenomena that influence hypersonic boundary layers, but nevertheless is somewhat indicative of hypersonic flow features. Additionally, these results at a minimum extend to the upper bound of the supersonic limit.

4.3.1 Plan View PLS Imaging of Undisturbed Mach 5 Boundary Layer

The first part of this study was to observe the undisturbed Mach 5 boundary layer. Therefore, the ramp was removed so that the SWTBLI was not present. In this manner the undisturbed boundary layer could be studied. As mentioned in Section 3.3, PLS imaging reveals the concentration of fog particles in the flow, therefore high and low signal intensity regions correspond to regions of high and low droplet concentration, respectively. The droplets tend to evaporate in regions with a relatively high static temperature (T) and so such regions exhibit low signal levels,

while the fog remains condensed in regions with low static temperature and so such regions exhibit high signal levels. If a constant stagnation temperature is assumed, then the energy equation ($C_pT_0 = C_pT + 0.5U^2$, where C_p is specific heat at constant pressure, T is the local static temperature and U is the local streamwise velocity), then regions of high static temperature are also regions of low velocity. Therefore, regions of low intensity tend to be regions of low velocity, and likewise regions of high intensity tend to be regions of high velocity. The reader should note that this technique is merely a qualitative approximation, as the finite times for evaporation and condensation will obviously affect the interpretation of the signal and thus the velocity. Nevertheless, this technique is very useful in the current situation as a tool to differentiate between high and low speed flow within a given field of view. Figure 28 shows a schematic of the interaction and the locations of the laser sheet used in this study.

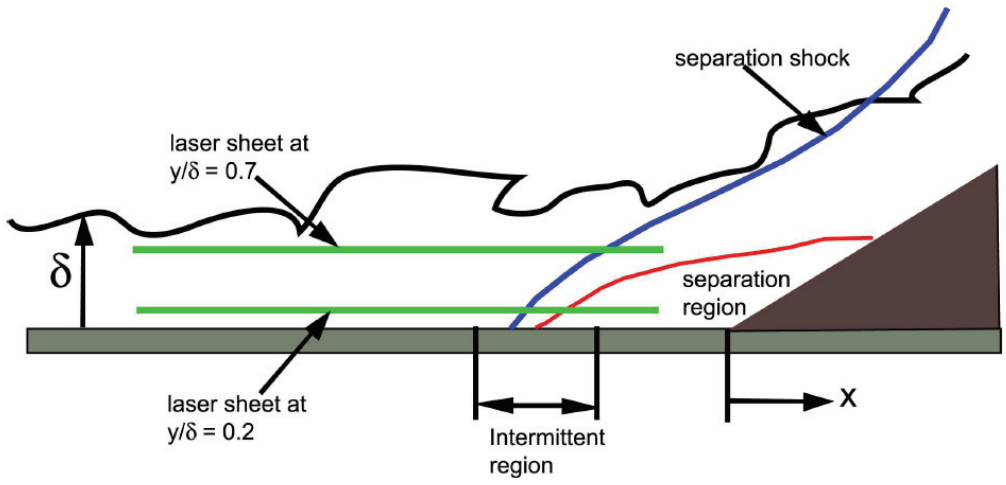

Figure 28. Schematic side view diagram of interaction and the locations of the laser sheet used in testing. Reproduced with permission from Ganapathisubramani, et al. [2006b]

4.3.1.1 Plan view PLS Image Results

Figure 29 presents a 10-frame average PLS image of the undisturbed boundary layer at a wall-normal height of 0.2δ.

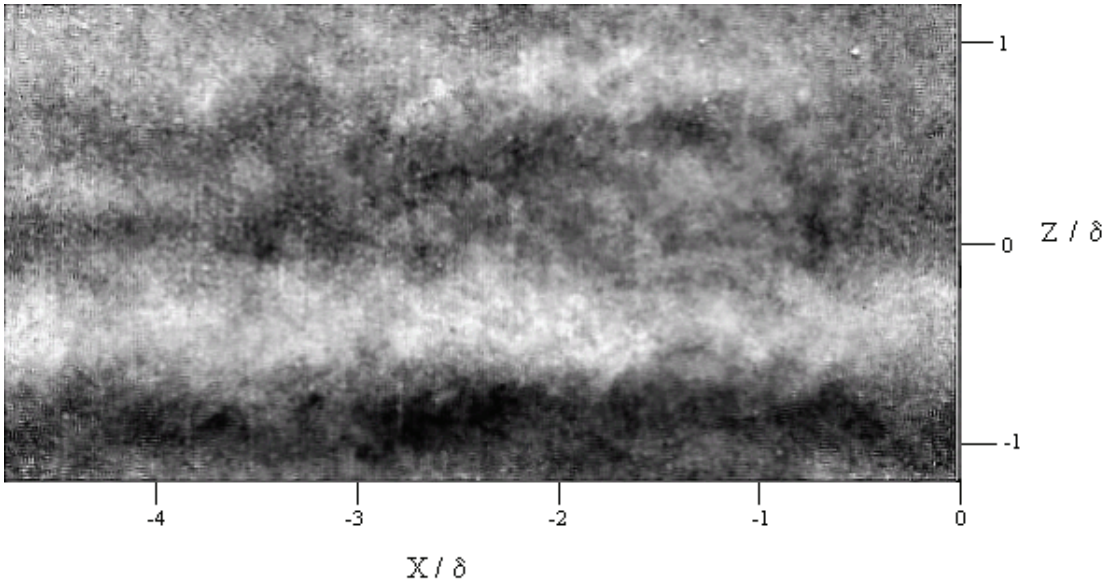

Figure 29. 10-frame averaged PLS image of Mach 5 undisturbed boundary layer at wall-normal height of 0.2δ illustrating the presence of uniform momentum strips.

This image clearly shows a high speed region from $-1 < z / \delta < 0$. A low speed strip is observed at $z = -1$. Note that these images are 10-frame average images, and with a field of view of approximately 5δ, that would suggest these strips may be up to 50δ long. While this estimate is high, it is consistent with results found in a Mach 2 boundary layer [Ganapathisubramani, et al. 2006b]. Figure 30 shows a sequence of 10 instantaneous plan view PLS images at a wall normal height of 0.2δ, with subsequent images separated by 100 μs, showing the strip structures in the flow.

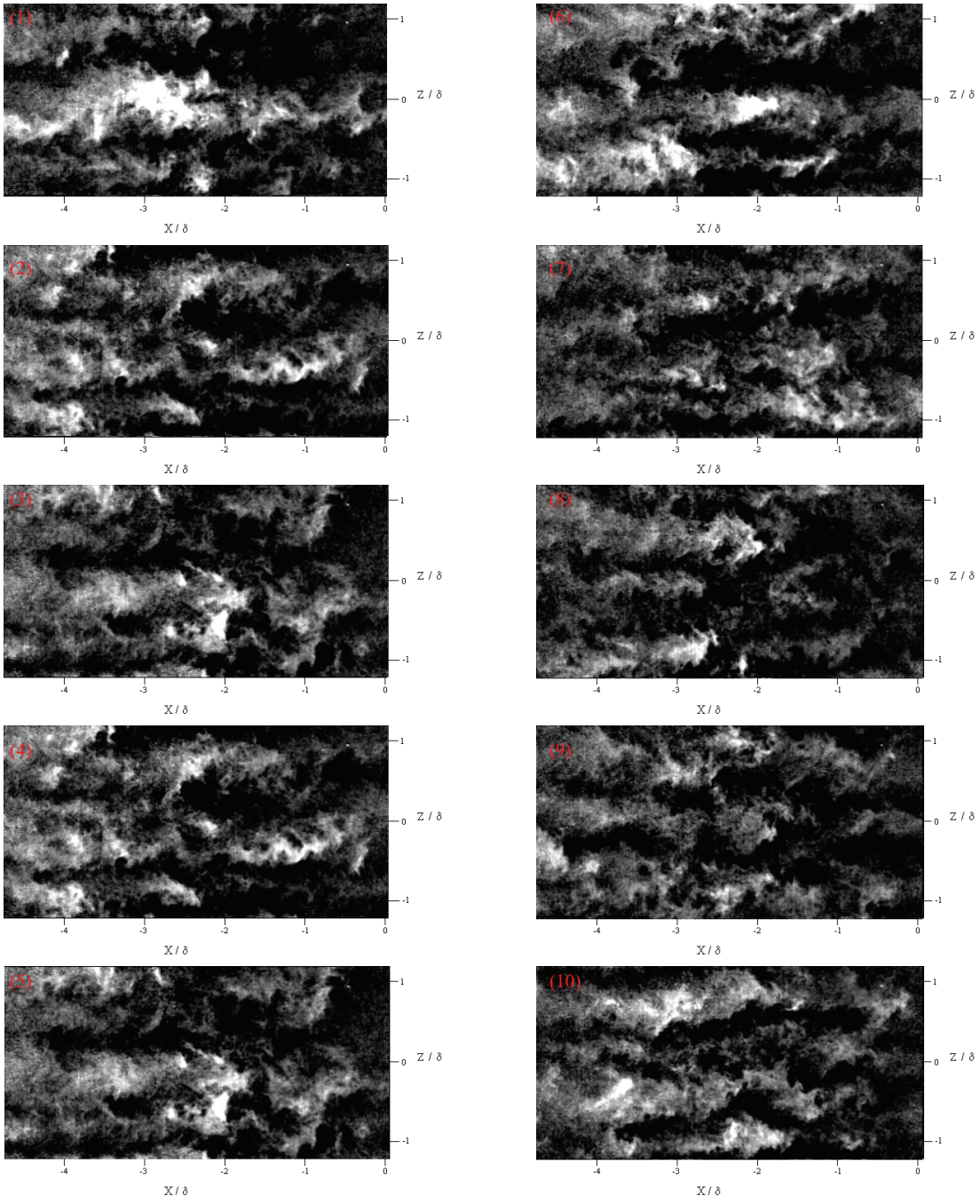

Figure 30. Sequence of 10 instantaneous PLS images of undisturbed Mach 5 boundary layer at wall-normal height of 0.2δ illustrating strips of uniform momentum fluid. Successive images are separated by 100 μs.

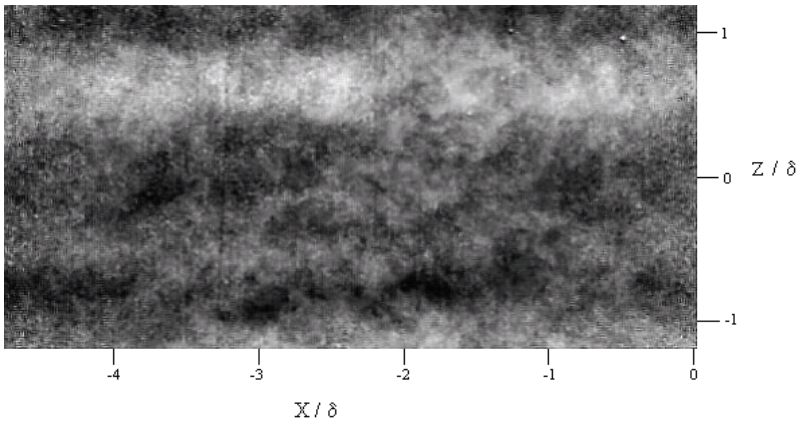

(a)

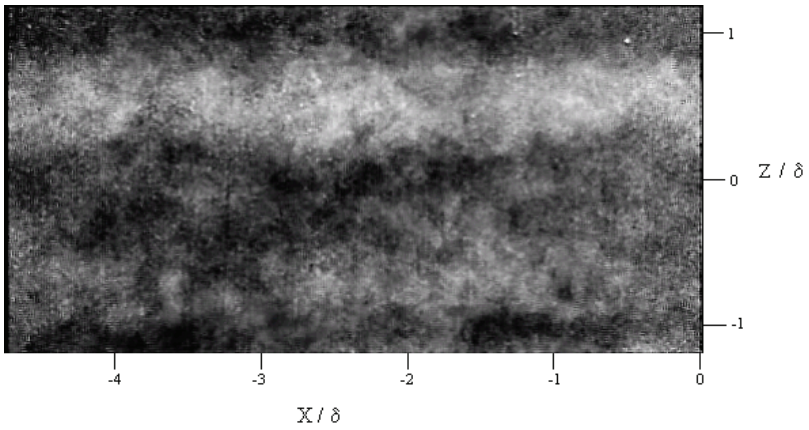

(b)

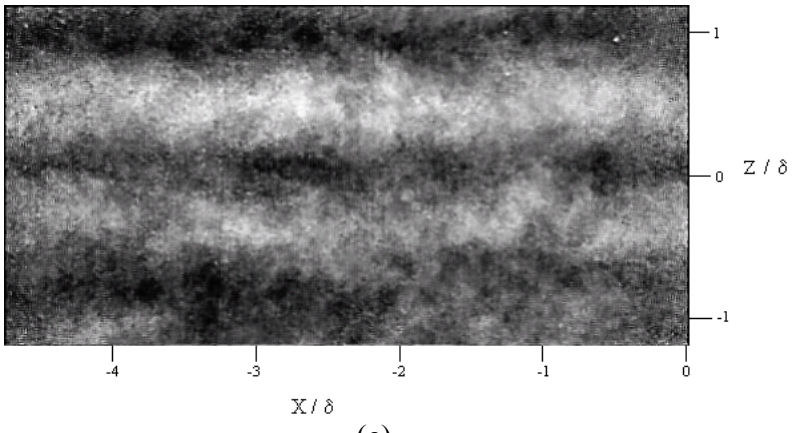

(c)

Figure 31. Three consecutive 10-frame average PLS images of undisturbed Mach 5 boundary layer with laser sheet at wall-normal height of 0.2δ.

Figure 31 shows three consecutive 10-frame average images which illustrate the possibility of longer structures. The effective time between locally averaged images is 1 ms. Figure 31 tracks a high-speed strip first seen in figure (a) as the high intensity region at the top of the image. This structure seems to remain in the same approximate spanwise location in figures (b) and (c), suggesting approximate lengths on the order of 150δ. This estimate appears extreme, and is most likely the artifact of two or more strips at the same spanwise location being in close succession to one another. This is likely not indicative of the length of a single strip.

Figure 31 (c) shows three low speed strips in series with two high speed strips. This suggests that over the approximately 2.5δ spanwise length, there are five distinct strips. This suggests a spanwise scale of 0.5δ for a single strip. The high speed strip illustrated in figure 29 above had a spanwise scale of 1δ. This would give a spanwise scale on the order of 0.5δ to 1δ, which is consistent with the recent findings of Ganapathisubramani, et al. [2006b] in a supersonic boundary layer and the results of Hutchins, et al. [2004] in incompressible boundary layers. This result is intriguing because it provides a result in the hypersonic regime, which taken in cohorts with the incompressible and supersonic results mentioned above suggests the spanwise scale of these strips is driven by outer scaling. As suggested by the incompressible VLSM model presented by Kim and Adrian [1999], these strips may be created by a series of hairpin vortex packets which coalesce and align end to end, creating pockets of uniform momentum fluid. These structures tend to originate within the inner part of

the boundary layer, and tend to follow inner scaling. However, the resulting uniform momentum strips investigated in the current study appear to follow outer scaling on the order of δ.

This study was extended to a wall-normal height of 0.7δ, as was accomplished in the Mach 2 study at this same facility. As was observed in that study, the strips were not consistently apparent at 0.7δ in the Mach 5 boundary layer. Figure 32 presents a 10-frame average PLS image which is indicative of the majority of the images observed at this wall-normal height.

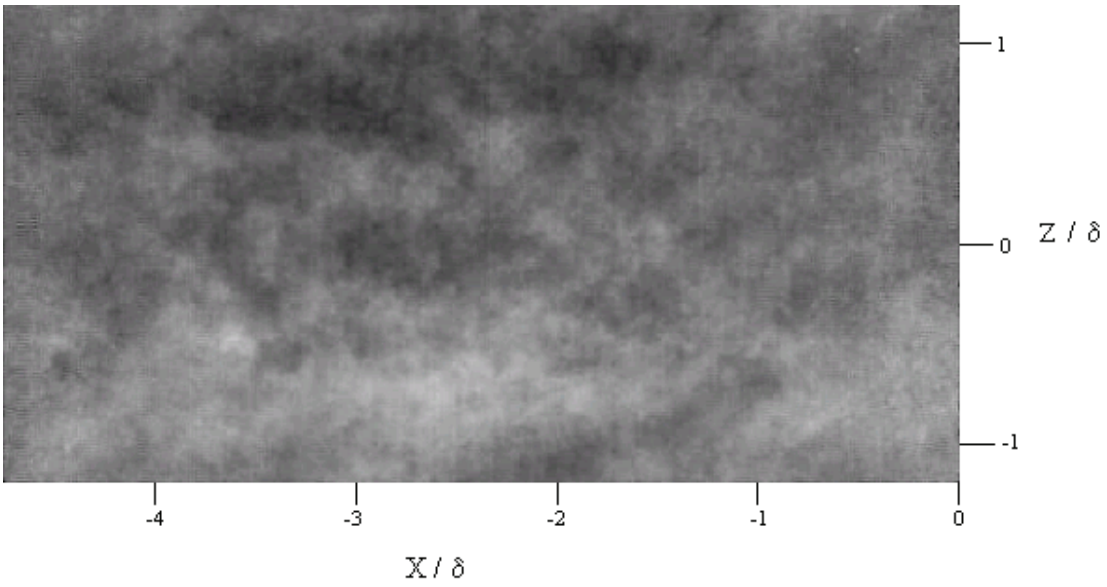

Figure 32. 10-frame average PLS image of undisturbed Mach 5 boundary layer with laser sheet at wall-normal height of 0.7δ illustrating the lack of strips.

Figure 33 shows a sequence of 10 instantaneous plan view PLS images at a wall-normal height of 0.7δ, with subsequent images separated by 100 μs. The strips are not readily apparent in these images.

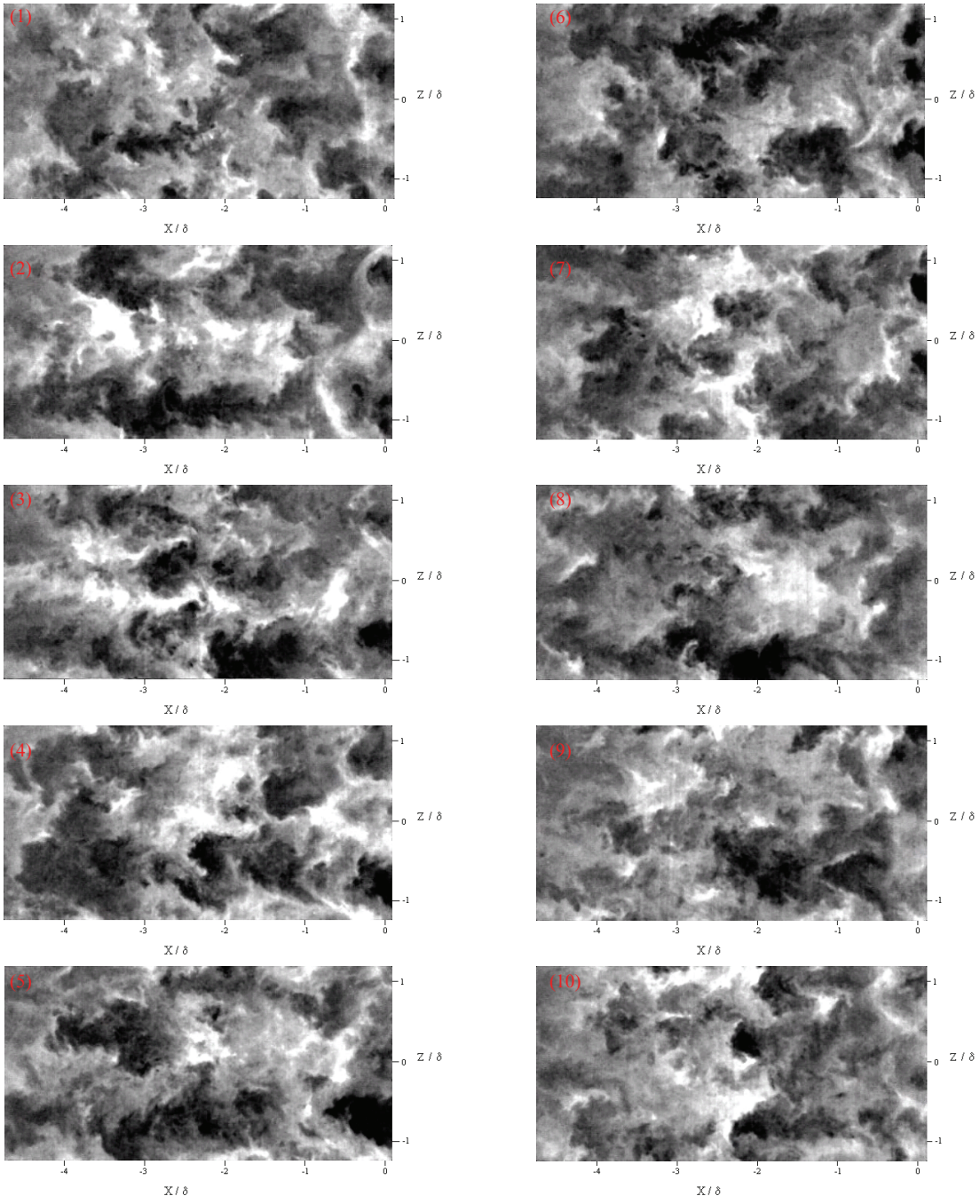

Figure 33. Sequence of 10 instantaneous PLS images of undisturbed Mach 5 boundary layer at wall-normal height of 0.7δ illustrating the lack of strips in the flow. Successive images are separated by 100 μs.

On average the strips observed at 0.2δ were not readily apparent at 0.7δ. There were a few cases when the strips were apparent, as seen in the 10-frame average PLS image in figure 34, but they were sporadic and were very subtle.

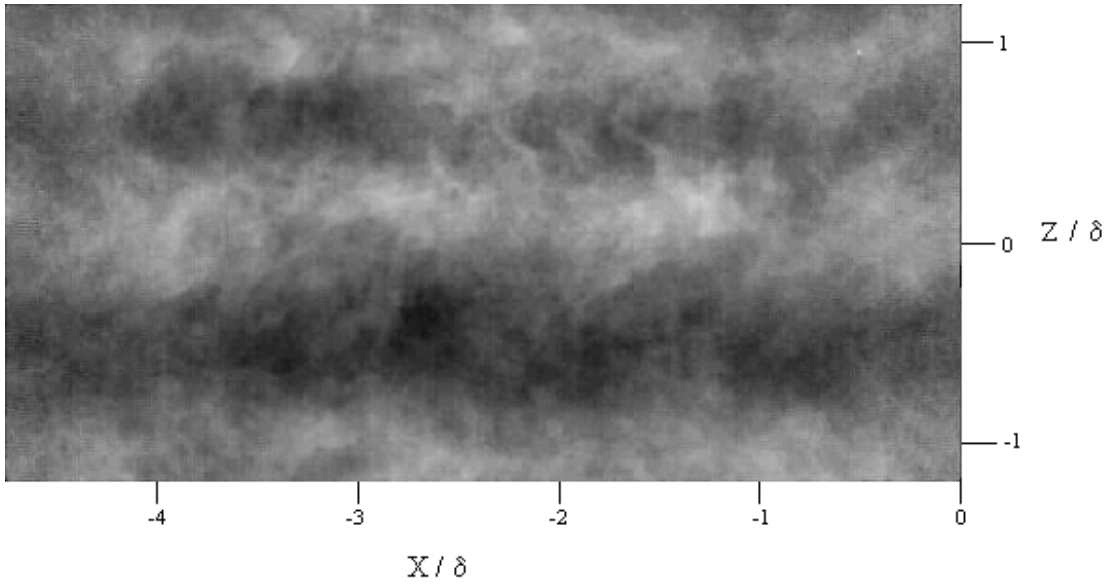

Figure 34. 10 frame averaged PLS image of Mach 5 undisturbed boundary layer at wall-normal height of 0.7δ illustrating the presence of uniform momentum strips.

These strips seem to be more subtle, but do coincide with the same spanwise scaling of 0.5δ to 1δ. These occurrences were not observed very often, with the majority of the images being similar to figure 32. In contrast, the strips were frequently observed on average at a wall-normal sheet height of 0.2δ. This could be a result of the velocity fluctuations being much smaller at a boundary layer height of 0.7δ; hence the static temperature variations are also smaller, causing the variation in fog concentration to be smaller, resulting in approximately the same signal.

Therefore these results do not infer that the strips are not always in the flowfield at this height, but rather they may be too subtle to detect with the PLS technique.

4.3.1.2 Upstream Boundary Layer Reconstruction Using Taylor's Frozen Flow Hypothesis

The next aspect of this study was to attempt to reconstruct a large scale of the upstream boundary layer. This was accomplished using Taylor's frozen flow hypothesis which suggests the turbulence is frozen as it convects past a given point. This allows a time history of data to be converted to a spatial distribution, thus giving insight into the structure of a much larger portion of the upstream boundary layer. This technique was employed in previous studies in this facility, which showed the existence of strips in a Mach 2 boundary layer. At 0.2δ, the convective velocity was taken to be $0.9U_\infty$, which was 693 m/s. Since the acquisition rate of the camera was 10 kHz, one image was taken every 100 μs. This resulted in the flow convecting approximately 69.3 mm per frame. The field of view of the camera was 91.4 mm (3.6 *in*) in the streamwise direction, which meant that a particle convected approximately 75% of the field of view per frame. Using this data, the middle 75% of successive images was placed end to end, with the first image forming the far right bound and the last image forming the left bound. In this manner, each new frame corresponded to 3.64δ in the streamwise direction. The spanwise scale was from approximately -0.9δ to 0.9δ. Figure 35 shows an example of the construction of the instantaneous spatial structure in the upstream boundary layer.

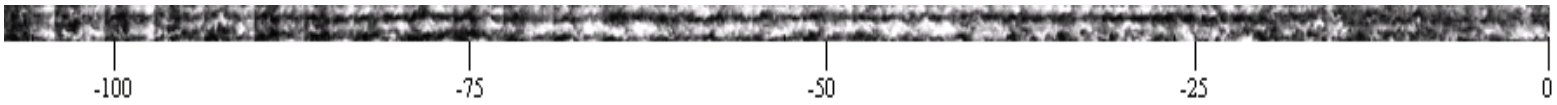

X / δ

(a)

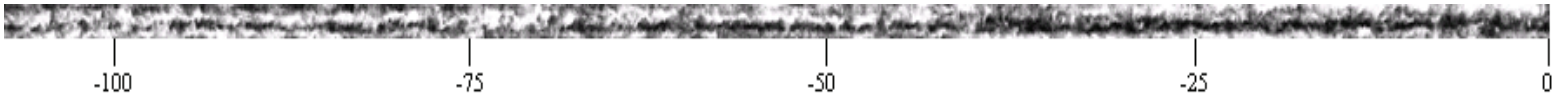

X / δ

(b)

X / δ

(c)

Figure 35. Images of upstream boundary layer created using Taylor's Hypothesis. Image (c) is an expanded section of image (b) with the boxes showing the approximate extent of two individual high speed strips.

Figure 35 (a) is an example showing three distinct strips as they propagate downstream. Figure 35 (b) shows another example, more indicative of the average strips that were observed. Figure 35 (c) is an enlarged section of figure 35 (b) which shows two complete strips. The strip marked by the red box extends from approximately -75δ to -90δ. The strip marked by the blue box extends from approximately -40δ to -75δ. Note that while there appears to be a distinct separation between these two strips, they are separated by perhaps only one delta. Given that they are in the same approximate spanwise location, they essentially combine to form a strip over 50δ in length.

These results show the existence of similar "strip" like structures to those seen in previous studies of a Mach 2 turbulent boundary layer [Ganapathisubramani, et al. 2006b]. The results illustrate the length scale that these strips can achieve, on the order of 40δ on average, as well as the spanwise scale, on the order of 0.5δ to 1δ. Previous studies [Erengil and Dolling 1991] used a simple relation of the freestream velocity divided by the scale of turbulent structures on the order of 1δ to determine a frequency of oscillation upwards of 40 kHz. While this range of frequencies was observed in SWTBLI, a dominant frequency range of 0.4 – 2 kHz was also found [Dolling and Brusniak 1989]. This low-frequency oscillation has been the motivation of much work over the past few years, and indeed was the motivation for this study. The results found here of structures that are 40δ long are significant, in that they provide a turbulent mechanism that is capable of reducing the frequency of SWTBLIs

by an order of magnitude to approximately match the dominant large-scale oscillation frequencies of the separated flow. Using the same relation as above, structures of 40δ would lower the frequency to 1 kHz, while the structures that were found to be even longer would lower the frequency even further. To examine if these structures do play an integral role in SWTBLIs, a more in-depth study was completed using the same experimental setup with the addition of the ramp to generate a SWTBLI.

4.3.2 Plan View PLS Imaging of Undisturbed Mach 5 SWTBLI

As mentioned above, large scale coherent structures on the order of 40δ were found in the Mach 5 turbulent boundary layer. These structures may provide the mechanism responsible for the low-frequency oscillation observed in SWTBLIs. To examine this possibility, plan view PLS imaging of a Mach 5 SWTBLI was accomplished to determine if the coherent structures influenced the location of the separation region. Figure 36 shows a series of images that illustrate the full evolution of an upstream burst in the separation region as it responds to the strips in the upstream boundary layer. This image sequence contains six 10-frame average PLS images and the effective time between each locally averaged image is 1 ms. This series is 6ms of data, and illustrates the low-frequency oscillation of the separation region.

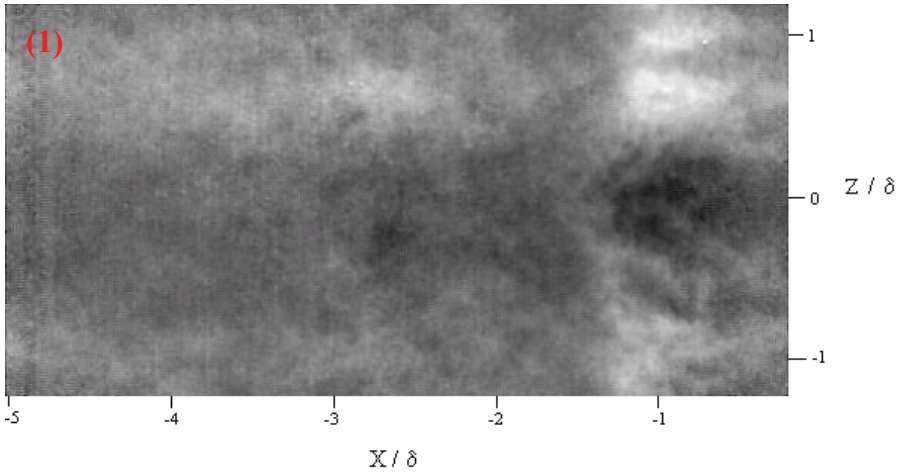
(1)
1
0
-1
Z / δ
-5
-4
-3
-2
-1
X / δ

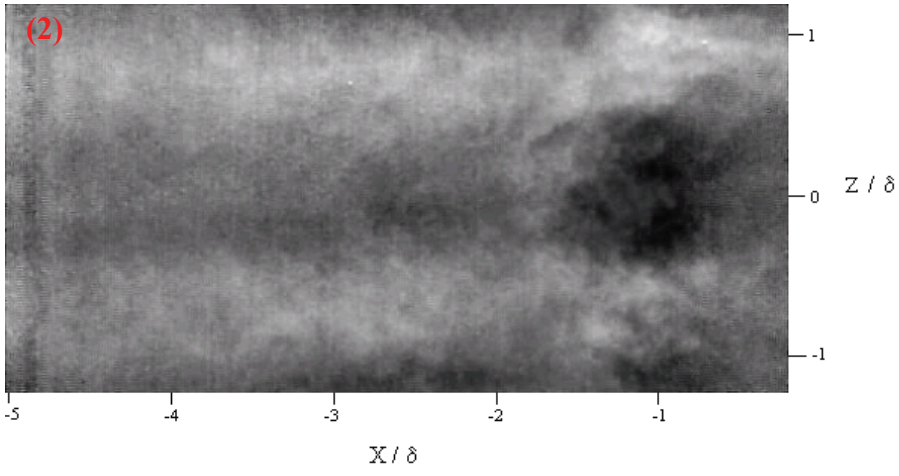
(2)
1
0
-1
Z / δ
-5
-4
-3
-2
-1
X / δ

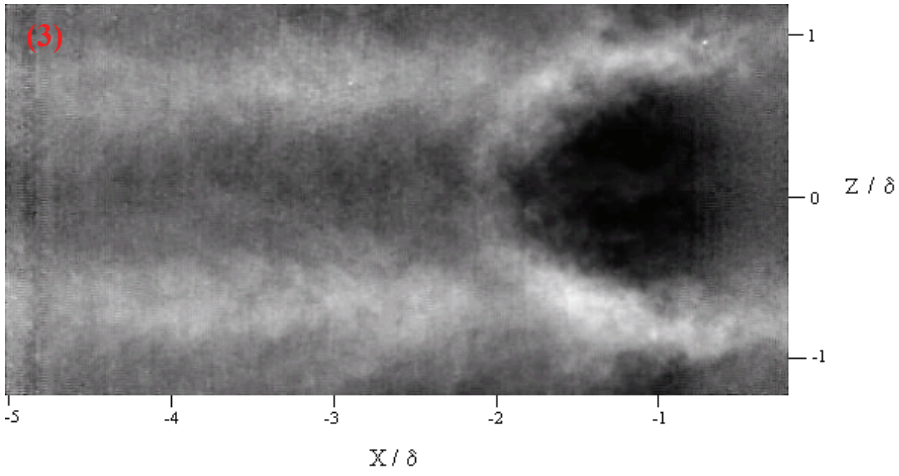
(3)
1
0
-1
Z / δ
-5
-4
-3
-2
-1
X / δ

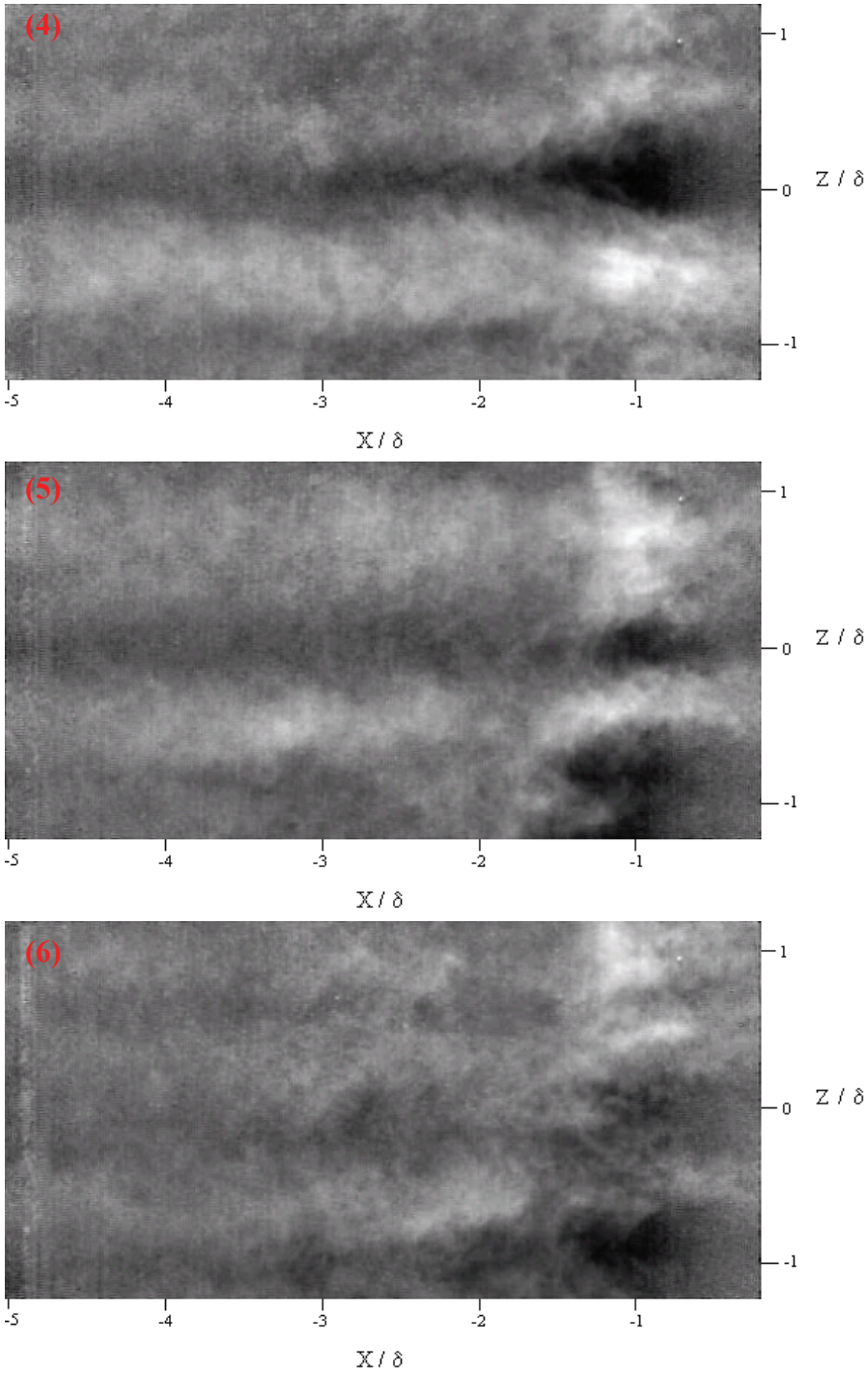

Figure 36. Series of six consecutive 10-frame average PLS images showing the evolution of a low-frequency oscillation of the separation region and corresponding strips.

Figure 36 shows the strips in the upstream boundary layer and an undulated separation region corresponding particularly to the low-speed strips. There are also regions of high intensity behind the separation shock corresponding to high-speed strips. This would indicate that the effect of the high-speed strip is to cause the boundary layer to be less prone to separation. These results would appear to coincide with the results of Beresh et al. [2002], where PIV data in a Mach 5 SWTBLI in the same facility showed that positive velocity fluctuations in the lower part of the boundary layer tend to cause the shock to move downstream, while negative velocity fluctuations tend to cause the shock to move upstream. We can presume that these low-speed and high-speed strips are, in effect, creating a less-full or more-full velocity profile at this height of 0.2δ.

Additionally, figure 36 shows six consecutive average images which capture the low-frequency motion of the separation region. Image (1) of figure 36 shows a nominally 2-D shock structure, with an undulated separation region corresponding to the upstream strips. Image (2) shows an upstream motion of the separation region in the middle of the image and the formation of a low-speed strip directly upstream. Image (3) shows this separation region and the corresponding low-speed strip expanding to a large scale. The separation region and the strip are still visible in image (4), but have decreased in scale and have started to move downstream. Image (5) shows that the separation region remains, but that it moves to a further downstream location. Additionally it shows another separation region evolving in the bottom of the image, resulting from the corresponding low-speed strip in the

upstream boundary layer. Image (6) shows the separation region in the middle of the image being consistent with image (1) before the low-speed strip appeared. Additionally, this image shows the upstream evolution of the separation region in the lower part of the image as the corresponding low-speed strip becomes even more noticeable.

In figure 36 the separation region in the center of the flowfield extends upstream and contracts back downstream over images (2) and (3). This would suggest that the oscillation occurred over approximately 20 images, which using the relation from the Taylor's hypothesis data corresponds to a structure approximately 70δ in length. This results in a frequency on the order of 0.5 – 0.6 kHz, within the region of low frequency oscillations observed by Erengil and Dolling [1991].

Figure 37 presents 50 of the instantaneous images used to compute the average images in figure 36. The time between these images was 100 μs. Note that the images in figure 37 were processed to illustrate the location of the shock and separation region, rather than the strips in the upstream boundary layer. If the signal measured in the upstream boundary layer was contrast stretched to illustrate the strips, the shock and separation region would not be as clear as there would be mainly very bright and dark spots. The strips are emphasized in the average images in figure 36, and can still be noticed in the instantaneous images in figure 37. As previously mentioned, the instantaneous images are best viewed as a movie rather than a set of images.

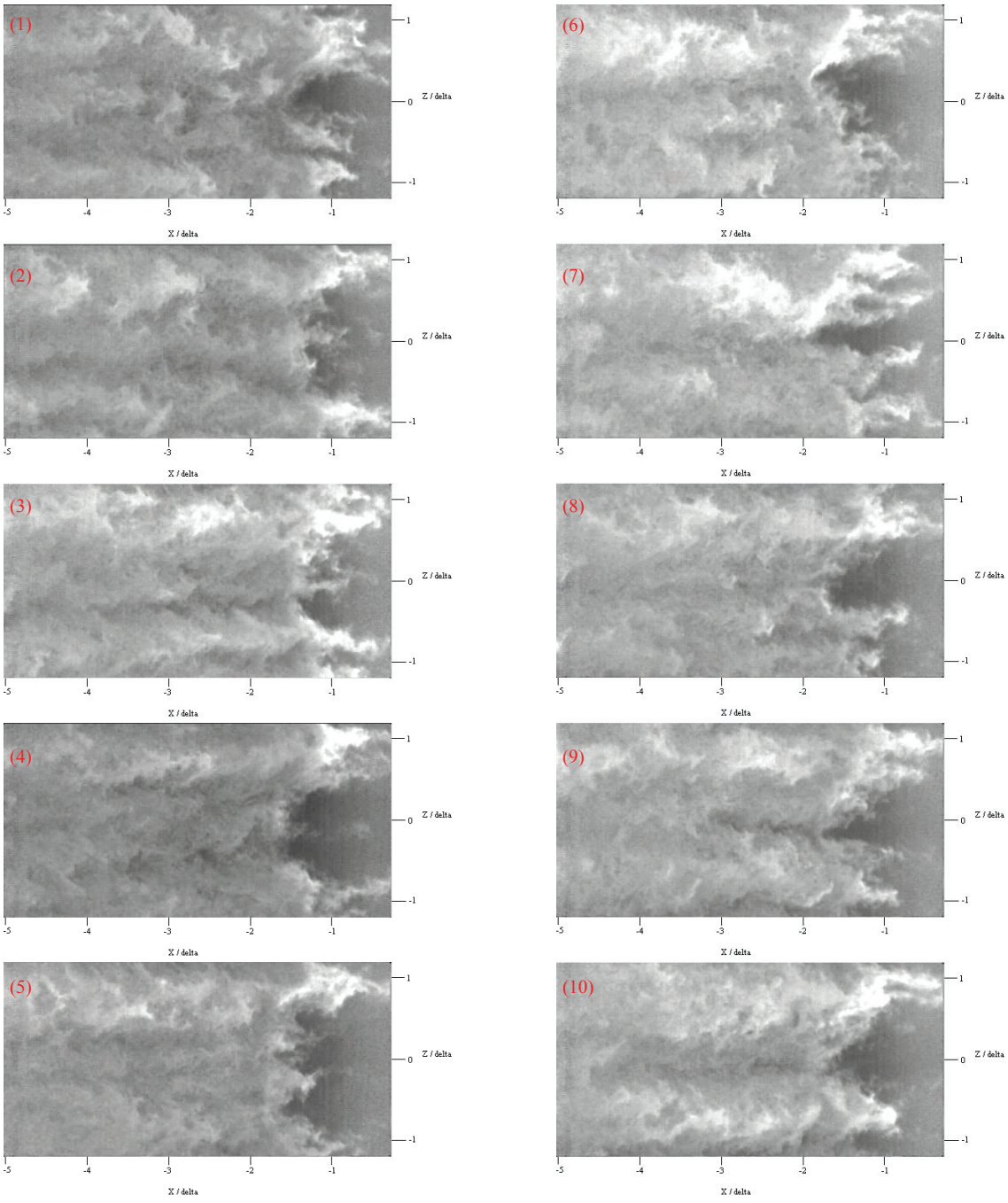
(1)
(2)
(3)
(4)
(5)
(6)
(7)
(8)
(9)
(10)
Z / delta
X / delta
1
0
-1
-5
-4
-3
-2
-1

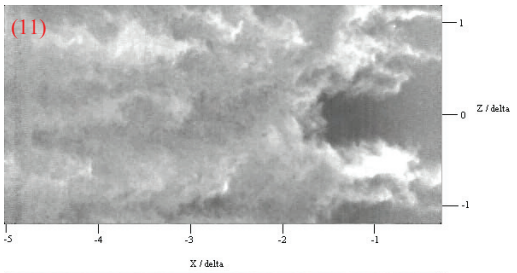
(11)
1
0
-1
Z / delta
-5
-4
-3
-2
-1
X / delta

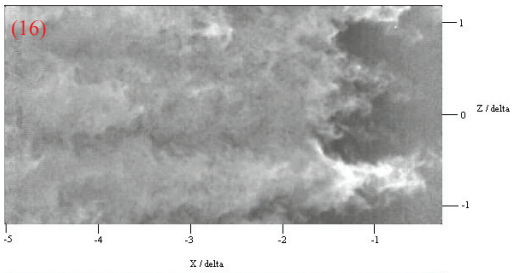
(16)
1
0
-1
Z / delta
-5
-4
-3
-2
-1
X / delta

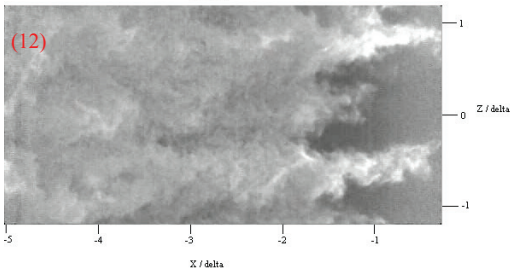
(12)
1
0
-1
Z / delta
-5
-4
-3
-2
-1
X / delta

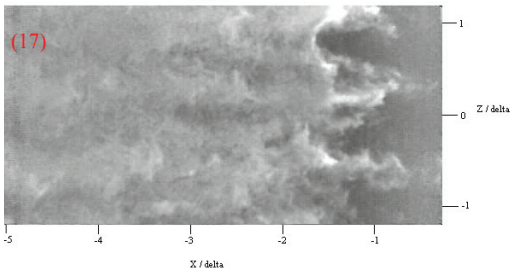
(17)
1
0
-1
Z / delta
-5
-4
-3
-2
-1
X / delta

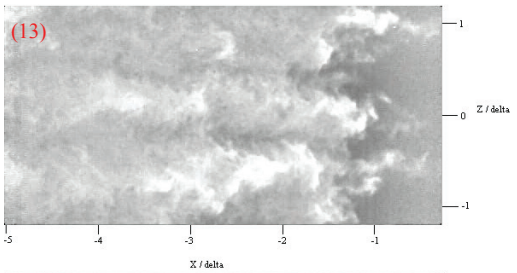
(13)
1
0
-1
Z / delta
-5
-4
-3
-2
-1
X / delta

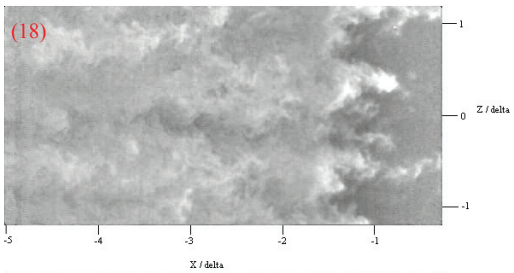
(18)
1
0
-1
Z / delta
-5
-4
-3
-2
-1
X / delta

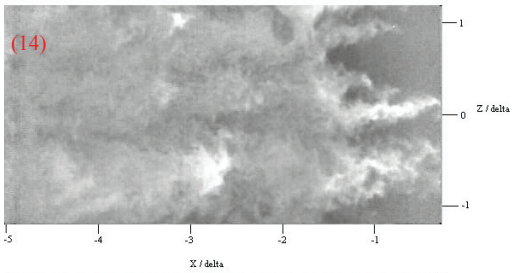
(14)
1
0
-1
Z / delta
-5
-4
-3
-2
-1
X / delta

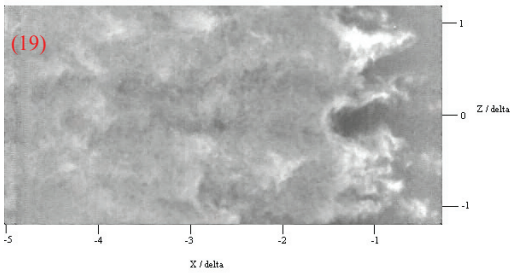
(19)
1
0
-1
Z / delta
-5
-4
-3
-2
-1
X / delta

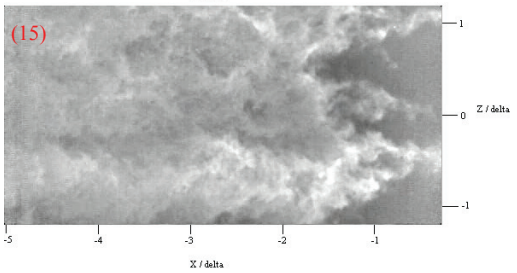
(15)
1
0
-1
Z / delta
-5
-4
-3
-2
-1
X / delta

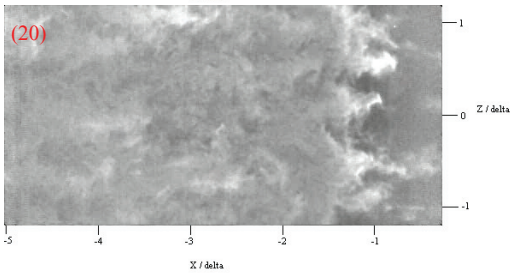
(20)
1
0
-1
Z / delta
-5
-4
-3
-2
-1
X / delta

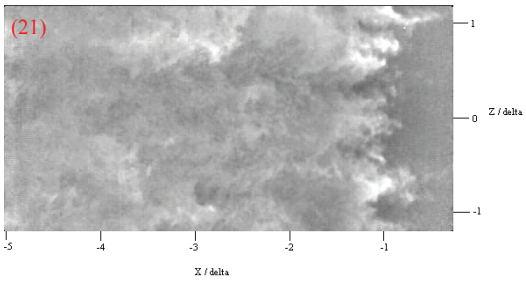
(21)
1
0
-1
Z / delta
-5
-4
-3
-2
-1
X / delta

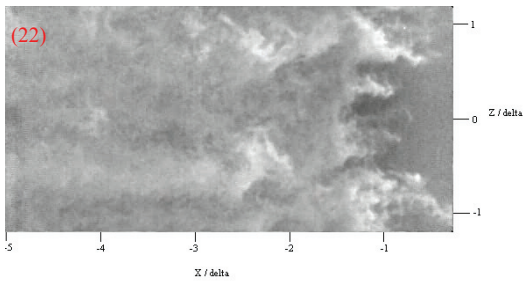
(22)
1
0
-1
Z / delta
-5
-4
-3
-2
-1
X / delta

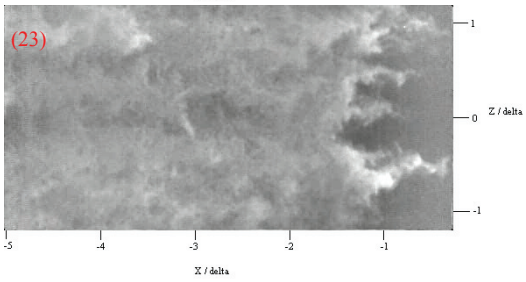
(23)
1
0
-1
Z / delta
-5
-4
-3
-2
-1
X / delta

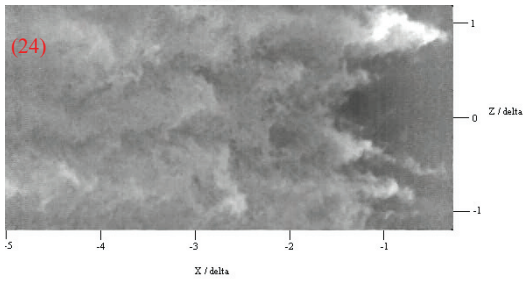
(24)
1
0
-1
Z / delta
-5
-4
-3
-2
-1
X / delta

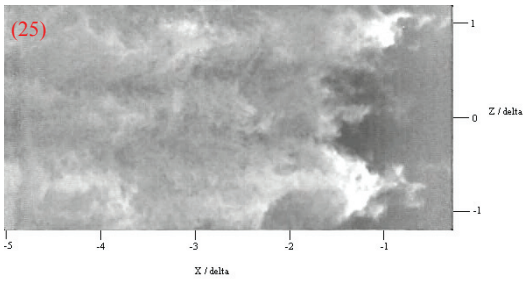
(25)
1
0
-1
Z / delta
-5
-4
-3
-2
-1
X / delta

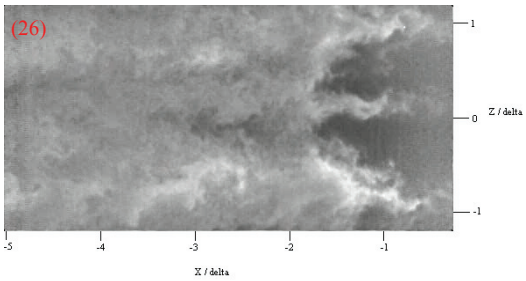
(26)
1
0
-1
Z / delta
-5
-4
-3
-2
-1
X / delta

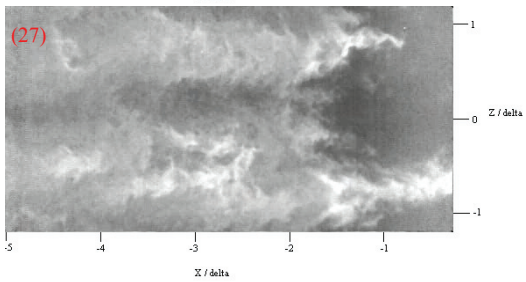
(27)
1
0
-1
Z / delta
-5
-4
-3
-2
-1
X / delta

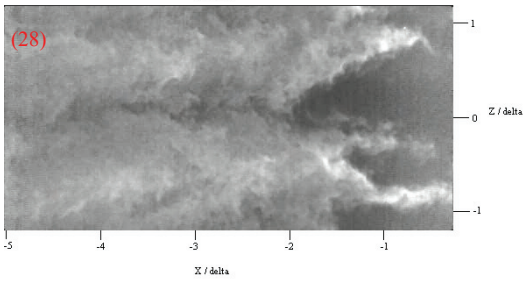
(28)
1
0
-1
Z / delta
-5
-4
-3
-2
-1
X / delta

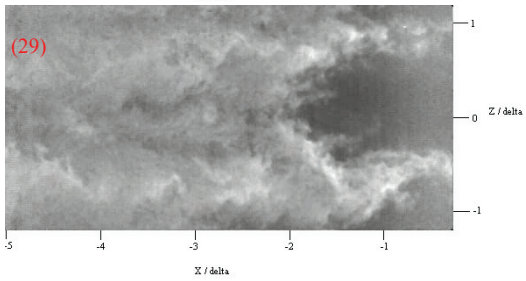
(29)
1
0
-1
Z / delta
-5
-4
-3
-2
-1
X / delta

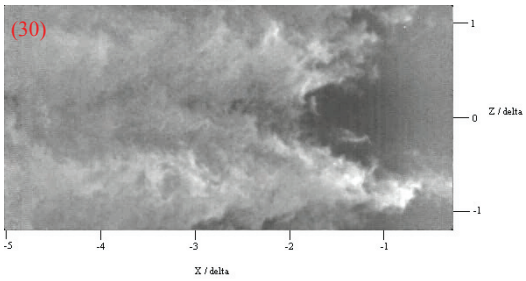
(30)
1
0
-1
Z / delta
-5
-4
-3
-2
-1
X / delta

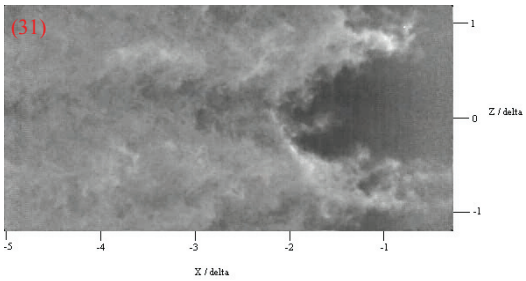
(31)
1
0
-1
Z / delta
-5
-4
-3
-2
-1
X / delta

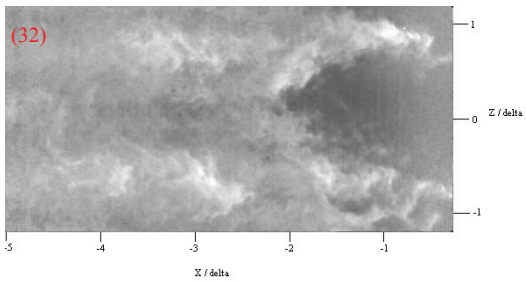
(32)
1
0
-1
Z / delta
-5
-4
-3
-2
-1
X / delta

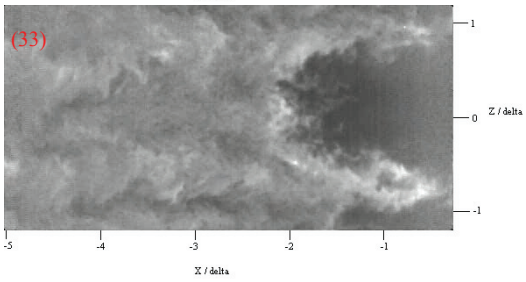
(33)
1
0
-1
Z / delta
-5
-4
-3
-2
-1
X / delta

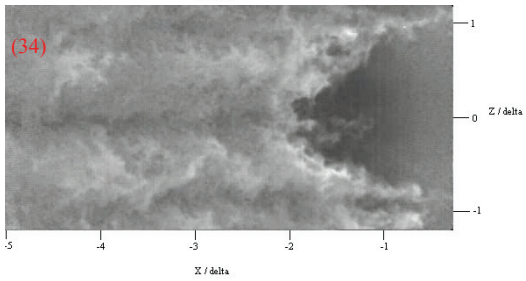
(34)
1
0
-1
Z / delta
-5
-4
-3
-2
-1
X / delta

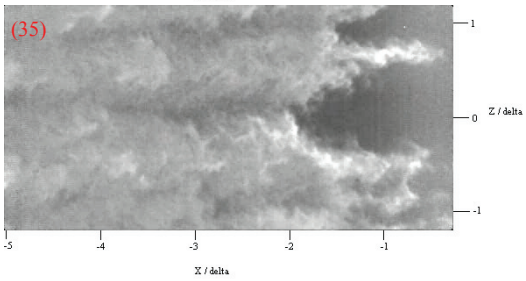
(35)
1
0
-1
Z / delta
-5
-4
-3
-2
-1
X / delta

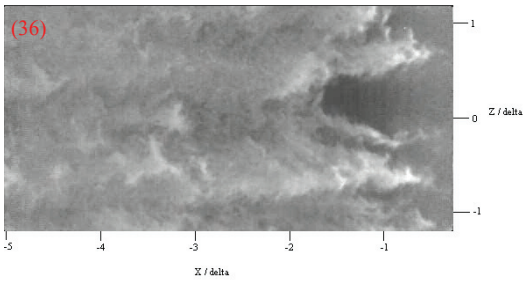
(36)
1
0
-1
Z / delta
-5
-4
-3
-2
-1
X / delta

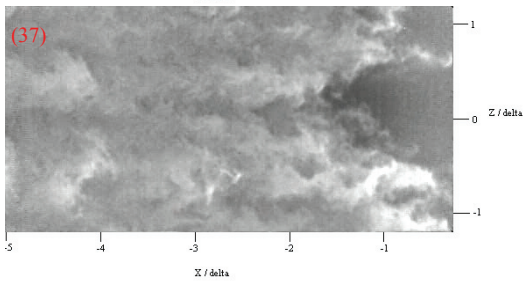
(37)
1
0
-1
Z / delta
-5
-4
-3
-2
-1
X / delta

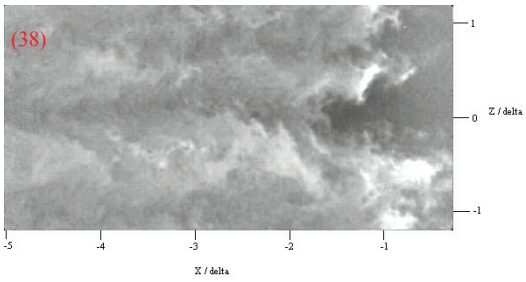
(38)
1
0
-1
Z / delta
-5
-4
-3
-2
-1
X / delta

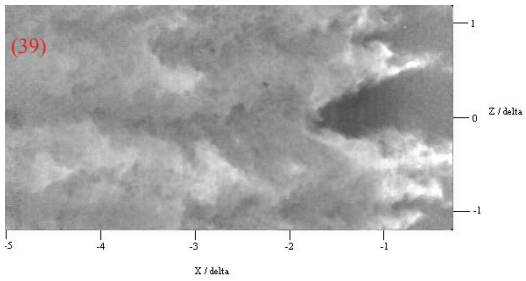
(39)
1
0
-1
Z / delta
-5
-4
-3
-2
-1
X / delta

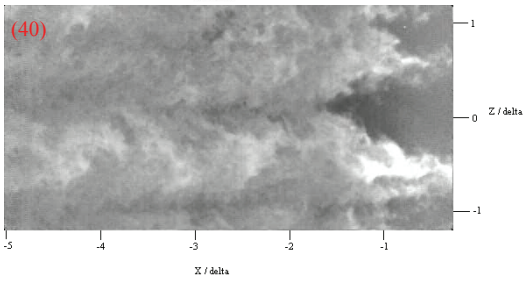
(40)
1
0
-1
Z / delta
-5
-4
-3
-2
-1
X / delta

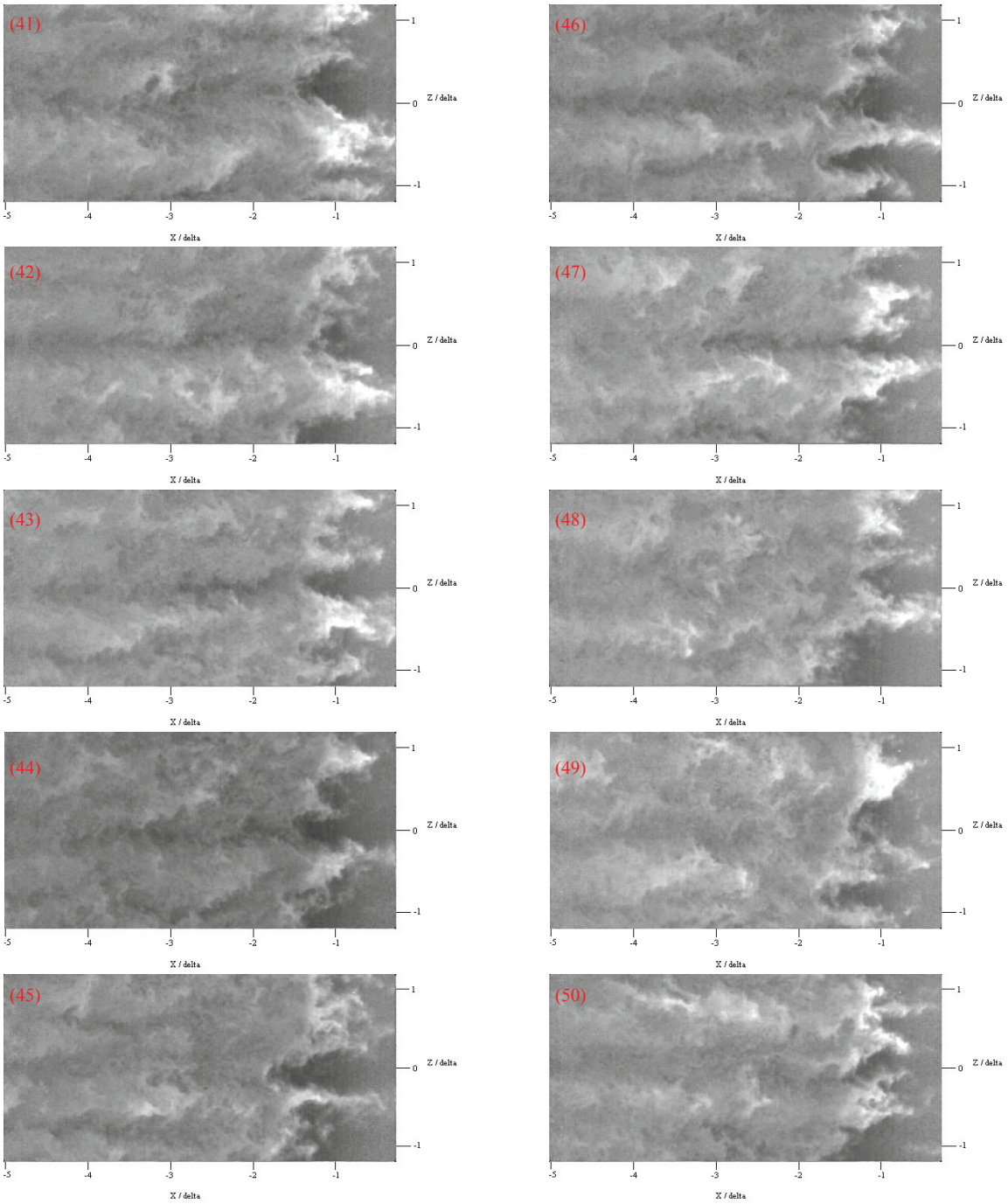

Figure 37. A time-sequence of 50 instantaneous PLS images demonstrating low frequency motion of the separation region and the corresponding strips in the upstream boundary layer. Time between successive images is 100 μs.

Figures 36 and 37 show the evolution of the interaction structure as it adapts to the strips in the incoming upstream boundary layer. This appears similar to the evolution of the shock as it responded to the VGs. In essence, these strips are like the upwash and downwash regions created by the VGs, and the shock structure changes based on the incoming boundary layer.

Similar plan view images were taken with the same field of view with the laser sheet at a wall-normal height of 0.7δ; however, due to the swept nature of the separation shock and the scale of the separation region, these structures were not visible at this height. The reader is referred to figure 28 in section 4.3.1 for an illustration relating the separation region and the laser sheet location. As previously mentioned, a recent investigation by Beresh et al. [2002] used PIV to study the Mach 5 upstream boundary layer and found a correlation between the velocity profile of the lower part of the upstream boundary layer and the shock foot motion. They found that the maximum conditionally-averaged velocity fluctuations occurred over a range of heights of 0.15δ to 0.37δ, with little difference being observed in the velocity profile above 0.5δ. In the current study the strips were observed at 0.2δ, which suggests that the strips may be the mechanism which causes the velocity fluctuations in this region. There were little, if any, variations at 0.7δ between the velocity profiles in the results of Beresh et al. [2002]. The results of that study and the current study suggest that the strips may not be strong enough to detect at 0.7δ. There may be slight velocity fluctuations as a result of the strips, but the PLS technique may not

be sensitive enough to detect them. The smaller change in velocities may not cause a temperature change large enough to cause evaporation of the fog, and a noticeable change in signal in the PLS image.

It is not clear whether the strips themselves cause the shock to move, or if the strips make the flow more or less-prone to separation, and the resulting change in the separation region causes the shock to move. Previous studies by Erengil and Dolling [1993] showed that the shock velocity, determined by differentiating the shock location, was correlated to fluctuations in the ratio of static pressures across the shock. They also showed that the fluctuations in the pressure ratio preceded the fluctuations in the shock velocity, indicating that the changes in the pressure ratio produced changes in the shock velocity. They also found a correlation between upstream pressure fluctuations and the shock velocity, possibly consistent with the presence of strips, but this correlation was much weaker than that of the pressure ratio. This would seem to indicate that while the upstream boundary layer plays a role in the shock velocity, the change in pressure in the separation region downstream of the shock is more important.

It is of note that a previous study by Gramman and Dolling [1992] showed that a characteristic pressure signal was found to convect downstream and coincide with the shock foot shifting its direction. The duration of the signal corresponded to the time required for the passage of a structure with a length scale of about 2.5δ to 3δ, with a convective velocity of 0.75 of the freestream velocity. They found these characteristic pressure signals as far as 10-12 boundary layer thicknesses upstream of

the interaction. Based on these results, Erengil and Dolling [1991b] suggested that large-scale turbulent structures may be responsible for the shift in direction of the shock. Barter [1999] suggested that these large-scale structures may account for the small-scale shock motions, but they did not suitably account for the large-scale motions. With the presence of strips that are 40δ long, it may indeed be that these large-scale structures are responsible for the large-scale motions as well. Combining the results of the current study with those mentioned above, it seems to indicate that this change in the velocity of the upstream boundary layer causes the pressure fluctuations upstream of the shock. The strips could then result in increased or decreased momentum and hence a fuller or less-full velocity profile, resulting in the boundary layer being less-prone or more-prone to separation, respectively. This could potentially change the scale of the separation region, which coupled with the upstream fluctuations causes the shock to change velocity and hence location.

Chapter 5

Summary and Conclusions

5.1 Summary of Results

This study used PLS imaging to examine several different aspects of SWTBLIs. The first objective was to study the effects of VGs on a Mach 2 SWTBLI. Two pairs of counter-rotating vane type VGs were actuated at 50 Hz to a height of 0.48δ, and were placed such that their trailing edge was 6δ upstream of a 20º compression ramp. Side-view PLS was used to image at two spanwise locations corresponding to the upwash and downwash regions created by the counter-rotating vortices. In the upwash region, the VGs most likely caused a reduction in momentum in the boundary layer by bringing low-momentum fluid from the lower part of the boundary layer into the upper part of the boundary layer. This may have caused the boundary layer to become more prone to separation, which resulted in the observed effect of the separation shock moving upstream when the VGs came to their full height.

The opposite effect was observed in the downwash region, where the VGs caused the separated flow region to reduce in scale. When the VGs were at their full height, they moved the shock to approximately -1.5δ, which was 0.7δ further than the downstream extent of the intermittent region and was 1.5δ further than the upstream

extent of the intermittent region. Additionally, when the VGs were fully up, not only did the shock move downstream but the angle of the shock increased as well. This was most likely a result of the downwash inducing a downward component of velocity, resulting in the deflection angle of the ramp and separation region effectively increasing. The results show that at this spanwise location where the VGs induced downwash, the separation shock was moved downstream beyond the extent of the intermittent region by a relatively large margin.

The next aspect of this study was to examine the effect of the same VGs in a SWTBLI generated by a 28º compression ramp in a Mach 5 flow. The same mechanical VG setup from Mach 2 testing was used, which resulted in the trailing edge of the VGs being 4δ upstream of the ramp, owing to the increased boundary layer thickness at Mach 5. Initially the VGs were inserted to a height of 0.32δ, which was their mechanical limit, instead of the 0.48δ as in Mach 2. The downwash region was imaged first, and the VGs had the opposite effect compared to the Mach 2 results. When the VGs were at their full height the shock moved further upstream. PLS images in the upwash region gave some insight into the cause of this. A strong shock generated by the leading edge of the VGs was observed and most likely caused the boundary layer to become even more prone to separation regardless of the influence of the upwash region. This resulted in the separation shock moving very far upstream beyond the extent of the intermittent region. The VGs had the opposite effect of what was desired.

The VGs were inserted to a lower height of 0.19δ, and some sporadic control of the shock was observed. The separation shock was moved downstream only when the shock started at the upstream edge of the intermittent region when the insertion of the VGs started. In this case the VGs had the effect of moving the shock slightly downstream, but the shock still remained in the intermittent region. In the case when the shock starts at a more downstream location, the shock remains at approximately the same location and there is not much of an effect from the VGs.

For both Mach 2 and Mach 5, the resulting spanwise structure of the interaction was observed to be highly 3-D. The side view PLS images showed the separation shock tended to be in a downstream location when a downwash region existed upstream, whereas the separation shock was in an upstream location when an upwash region existed upstream. The upwash and downwash regions were separated by approximately only 1δ in the spanwise direction. Plan view PLS was used to study this 3-D behavior and confirmed that the VGs created a highly 3-D shock structure. Although this 3-D behavior may be a result of the VGs being too close to the ramp, the resulting 3-D effects of the VGs may be inherent in the counter-rotating vortex setup. Because the vortices are counter-rotating, they will always create upwash and downwash regions, which will induce negative and positive velocity fluctuations, causing the shock to move upstream and downstream, respectively.

The final aspect of this study was to examine a Mach 5 turbulent boundary layer for the presence of large-scale streamwise structures, referred to as “strips”, which have recently been found by Ganapathisubramani, et. al [2006a], in a Mach 2

turbulent boundary layer. The authors of that study identified long strips of uniform momentum fluid using wide-field PIV that extended to lengths of 8δ. The authors of that study speculated that these low frequency events could explain the low frequency unsteadiness observed in the shock and separation region. Ganapathisubramani, et. al [2006b] also studied the effect of these strips on a Mach 2 SWTBLI and found that the strips could extend up to 40δ in length, and that the strips did have an influence on the separation region. A correlation was found between the separation point at a given spanwise location and the average upstream velocity over a range of 9δ upstream at the same spanwise location. This correlation was found using plan view PIV data taken in the Mach 2 facility. These studies served as motivation for the last aspect of testing in the current study.

Plan view PLS images did show similar low-speed and high-speed strips in the Mach 5 undisturbed turbulent boundary layer. Taylor's hypothesis was used to create a spatial reconstruction of the upstream boundary layer and strips were observed of order 40δ long. Additionally, successive strips at the same spanwise location were observed to be separated by only a few boundary layer thicknesses, which could suggest extremely long regions of coherent streamwise velocity fluctuations. This result appears to match well with the Mach 2 investigation of Ganapathisubramani [2006b], and supports speculation that these structures may cause the low frequency unsteadiness of SWTBLIs.

Plan view PLS images of the Mach 5 SWTBLI were also taken. When 10-frame average PLS images were created, they showed that an upstream shock

location and a large separation region were coincident with corresponding upstream low-speed strips. Likewise, a downstream shock location and a region less prone to separation corresponded to high-speed strips. These results, though qualitative in nature, agree with the correlation found by Ganapathisubramani, and support speculation that these strips cause the low frequency oscillation in SWTBLIs.

5.2 CONCLUSIONS AND FUTURE WORK

The counter-rotating vane type VGs used in this study moved the separation shock downstream in both Mach 2 and Mach 5 testing; however, at Mach 5 the effect was sporadic and the shock did not move beyond the extent of the intermittent region. The reduced effectiveness at Mach 5 may be a result of the VGs being pulsed to a significantly lower scaled height and being placed at a closer scaled location to the ramp. The same VG deflection angle produced a much stronger shock at Mach 5. If the VGs were made more swept in the streamwise direction, they may be able to be injected to a higher height without causing the strong shock, thus inducing more downwash and becoming more effective. Further work is needed to study the effectiveness of redesigned VGs at Mach 5.

Additionally, the resulting 3-D shock structure of both the Mach 2 and Mach 5 studies may be the result of the VGs being placed too close to the interaction, as previous studies showed that a location two to three times further upstream may be optimal. This may be an inherent effect of the counter-rotating VGs, however, as they should always create distinct upwash and downwash regions. Future work is

suggested to study the effectiveness of counter-rotating VGs placed at a more optimal upstream location. Additionally, other types of VGs that do not induce counter-rotating vortices, perhaps co-rotating VGs which can still be easily pulsed through slots in the floor, should be studied to determine if the 3-D shock structure can be alleviated.

Qualitative PLS results show the existence of large-scale low-speed and high-speed regions in the Mach 5 boundary layer. These results seem to agree with the quantitative results found at Mach 2 by Ganapathisubramani [2006b]. A similar investigation at Mach 5 using PIV is suggested to provide quantitative data and confirm the existence of the strips. This will allow more direct comparisons to the Mach 2 study as well as incompressible studies.

5.3 EXTENSION OF "STRIP" MODEL ON SWTBLIS

A study at Mach 2 by Hou [2003] showed that thickening and thinning of the upstream boundary layer correlates to upstream and downstream shock locations. This behavior has been suggested as a possible mechanism responsible for the low frequency oscillations of the separation shock foot and separation region. However, studies by Chan [1996], Comninos [1997] and Beresh [1999] showed this correlation was not evident at Mach 5, suggesting some other unknown mechanism was responsible for the low frequency oscillation. The thickening and thinning of the boundary layer at Mach 2 may merely be a marker of the strips found by Ganapathisubramani et al. [2006b]. The strips may cause the boundary layer to

become locally thick or thin, due to the velocity fluctuations that are induced within the boundary layer. It may be the strips and not the thickening and thinning of the boundary layer that causes the separation shock to oscillate and become 3-D. The shock may not move as a result of the boundary layer becoming thick or thin, rather the shock may move because the strips change the momentum in the lower part of the boundary layer.

In the case of the Mach 5 SWTBLI, the low frequency oscillation was still apparent even though there was not a thickening and thinning of the boundary layer. If a similar mechanism is responsible for the low frequency oscillation in both the Mach 2 and Mach 5 cases, the thickening and thinning of the BL is not that mechanism, as has been previously suggested. The mechanism may be the strips and this is why there is not a discernable thickening and thinning of the boundary layer corresponding to an upstream or downstream movement of the separation shock at Mach 5. Rather, as evidenced in the PLS at Mach 5, the existence of the strips may cause the shock to move, and the marker of the strips at Mach 2, the thickening and thinning of the BL, is merely not evident at Mach 5. This may be caused by additional compressibility effects at Mach 5, where the height of the boundary layer remains constant and does not need to become thick or thin to adjust to the strips' large velocity fluctuations within the boundary layer. Additionally, the effect of the strips may not be as strong at Mach 5, in that the velocity may not fluctuate by the same relative magnitude as at Mach 2. This may cause less pronounced fluctuations in the velocity profile, which could result in the height not needing to change to

accommodate the velocity fluctuation. Future PIV studies at Mach 5 would help determine the range of velocity fluctuations within the boundary layer.

Finally, a previous study by Chan [1996] employed the PLS technique to capture end-view images in the spanwise, wall-normal plane. Due to limitations in the laser and the camera at that time, that study was restricted to a 3 Hz image acquisition rate. The results of that study did show spanwise fluctuations in the boundary layer height up to 2δ. With the improvements in technology of the current setup, future work is suggested to examine end-view images taken at an acquisition rate of 20 kHz, which would allow for more closely time-resolved data. This can be accomplished by combining two of the Coherent Evolution-90 lasers operating at 10 kHz and shifting the pulse of one laser by half of one period so that an effective 20 kHz repetition rate is achieved. The APX cameras used in this study are capable of 20 kHz image acquisition, albeit at half the spatial resolution. Therefore, two cameras could be employed to achieve a larger field of view, capable of a sufficient spanwise scale. In this manner, the spanwise evolution of the boundary layer could be observed. This may provide more insight into the thickening and thinning of the boundary layer at Mach 2. The evolution of the boundary layer may demonstrate that the thick and thin portions of the boundary layer correspond to the presence of strips. This may provide information regarding the scale of the structures in this spanwise plane.

Appendix A – Moving Flap Design

The author also completed design and fabrication of a moveable flap for use in future inlet unstart studies. Preliminary PLS results of the flap as a SWTBLI generator demonstrated that the flap assembly was operational. The leading edge of the flap was slightly raised above the floor and was blunted. This created a stronger shock than a conventional compression ramp, which along with the small cavity in front of the flap (necessitated by the rotating motion) caused a larger separation region than expected.

The flap was driven by an Oriental Motor model BX6200AM-30. This motor was ¼ HP (200 W) Brushless DC motor that was rated at 125 lb-in of torque. A 30:1 gear ratio was used to allow the higher torque capacity, which resulted in a variable speed from 0.1 – 100 revolutions per minute. The Oriental Motor OPX-1A programmable controller was used to program specific motion regiments for the motor. The output shaft of the motor was fitted with a pinion gear, which moved a rack up and down. Linear motion bearings were used to ensure only vertical motion of the rack assembly. A shaft with a ball bearing fit on the end was attached to the end of the rack and fit inside an open linear ball bearing attached to the flap. This design allowed the single ball bearing on the shaft to move freely within the track provided by the open bearing when the flap was rotated. This translation was necessary because a single attachment point of the shaft to the flap assembly was not possible because the shaft was locked in one horizontal location. This design allowed

the shaft to push on different locations on the flap assembly when it was rotated. The flap was designed to rotate to a deflection angle of 30º.

Figures A1 through A7 illustrate modeling schematics of the flap and VG assemblies as well as photographs of the actual test models.

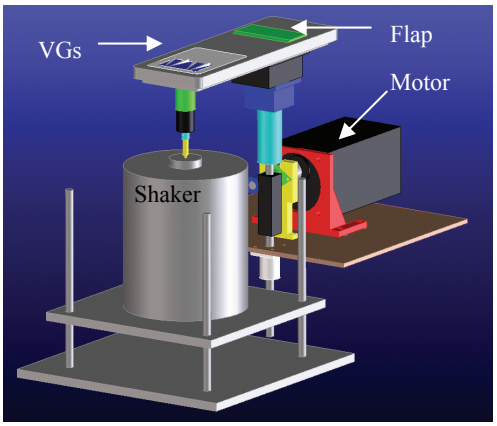

Figure A1. Schematic of flap and VG assembly with flap in down position.

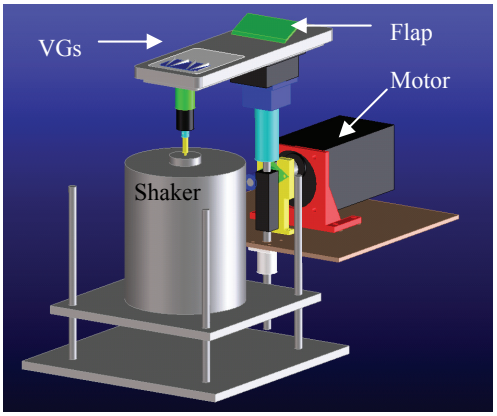

Figure A2. Schematic of flap and VG assembly with flap in up position.

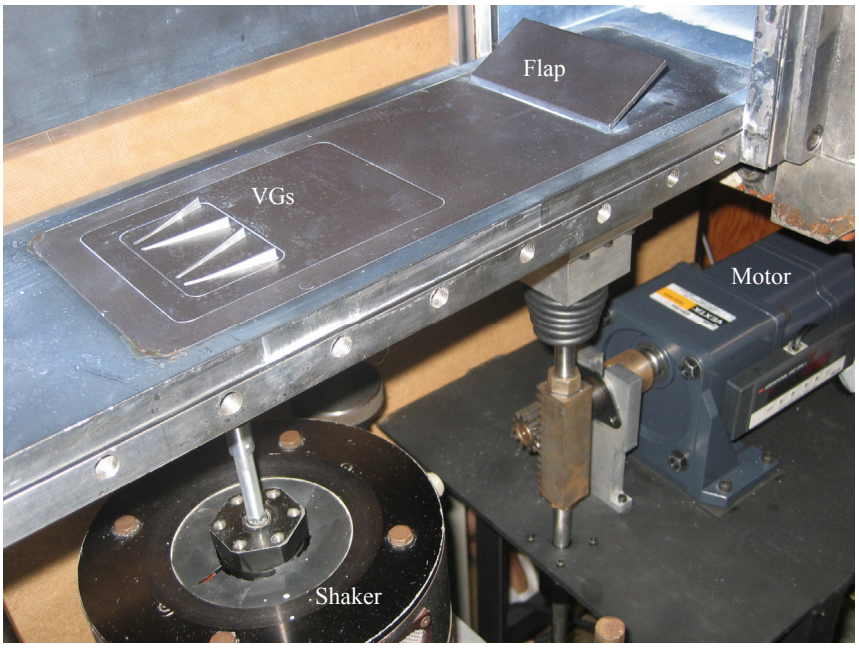

Figure A3. Photograph of flap and VG assembly with flap in up position.

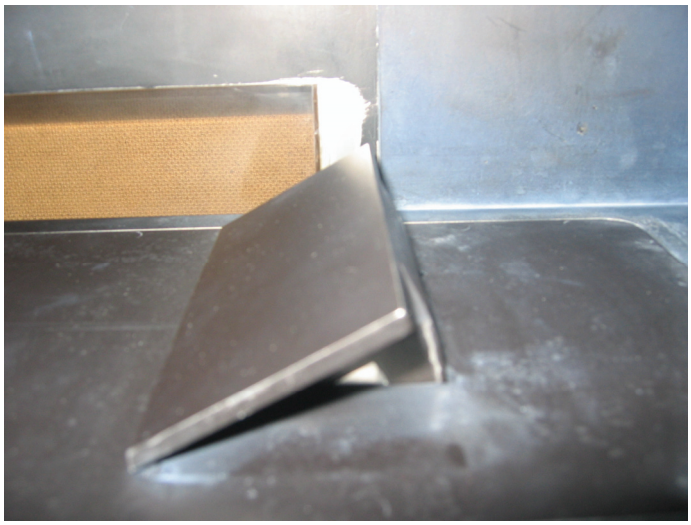

Figure A4. Photograph of flap in an up position mounted in the wind tunnel.

Figure A5. Photograph showing entire flap and VG assembly with flap in up position.

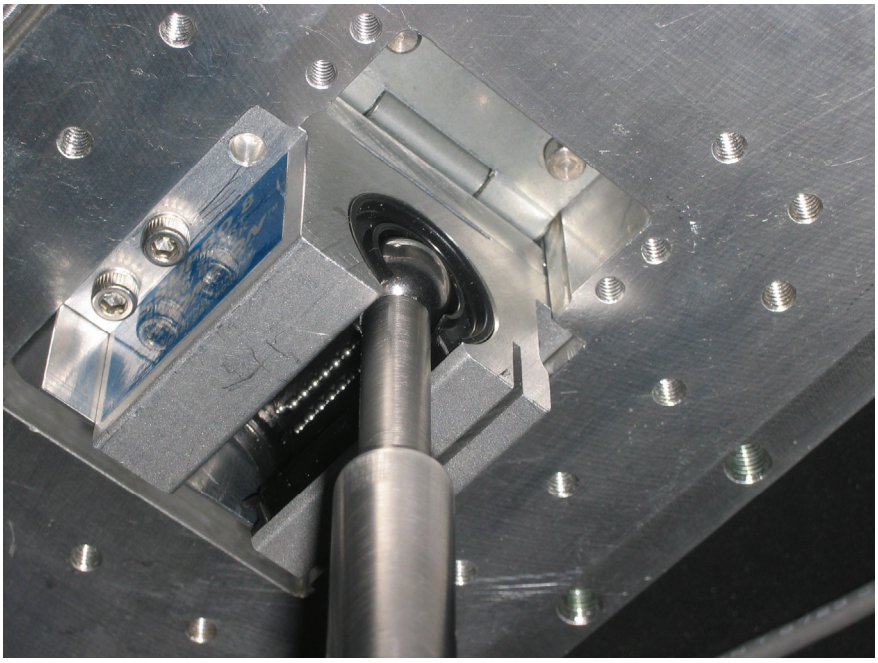

Figure A6. Ball bearing and shaft mounted inside open linear ball bearing.

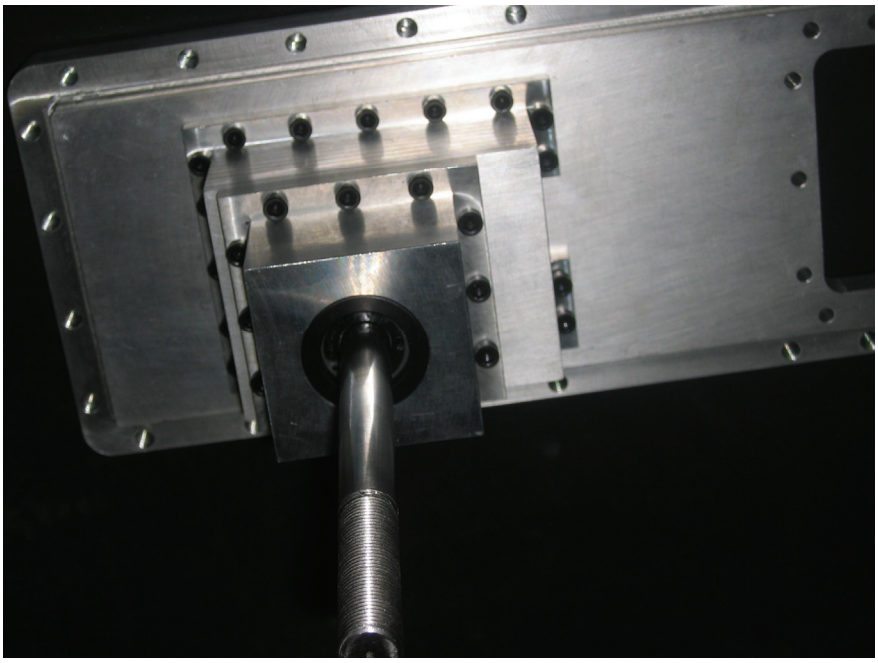

Figure A7. Similar view of shaft mounted inside linear motion ball bearing.

References

Adrian, R. J., Meinhart, C. D., and Tomkins, C. D. (2000), "Vortex Organization in the Outer Region of the Turbulent Boundary Layer," Journal of Fluid Mechanics, Vol. 422, 2000, pp. 1-53.

Ashill, P.R., Fulker, J. L., and Hackett, K. C. (2001), "Research at DERA on Sub Boundary Layer Vortex Generators (SBVGs)," AIAA Paper 2001-0887.

Ashill, P.R., Fulker, J. L., and Hackett, K. C. (2002), "Studies of Flows Induced by Sub Boundary Layer Vortex Generators (SBVGs)," AIAA Paper 2002-0968.

Barter, J. W. (1995), "Prediction and Passive Control of Fluctuating Pressure Loads Produced by Shock-Induced Turbulent Boundary Layer Separation," Ph.D. Dissertation, Department of Aerospace Engineering and Engineering Mechanics, The University of Texas, Austin, TX, 1995.

Beresh, S. J. (1999), "The Effect of the Incoming Turbulent Boundary Layer on a Shock-Induced Separated Flow Using Particle Image Velocimetry," Ph.D. Dissertation, Department of Aerospace Engineering and Engineering Mechanics, The University of Texas, Austin, TX, August 1999.

Beresh, S. J., Clemens, N. T., and Dolling, D. S. (2002), "Relationship between Upstream Boundary-Layer Velocity Fluctuations and Separation Shock Unsteadiness," *AIAA Journal*, Vol. 40, No. 12, December 2002, pp. 2412-2422.

Bueno, P. C., Hou, Y. X., Clemens, N. T., Dolling, D. S. (2004), "Wide- Field PIV Study of Pulsed Jet Injection Upstream of Mach 2 Shock Wave/Boundary Layer Interaction," AIAA Paper 2004-0707.

Bueno, P. C., Ganapathisubramani, B., Clemens, N. T., and Dolling, D. S. (2005), "Cinematographic Planar Imaging of a Mach 2 Shock Wave / Turbulent Boundary Layer Interaction," AIAA Paper 2005-0441.

Bueno, P. C., Wagner, J. L., Searcy, J.A., Ganapathisubramani, B., Clemens, N. T., Dolling, D. S. (2006), "Experiments in Unsteady Forcing of Mach 2 Shock Wave/Boundary Layer Interactions," AIAA Paper 2006-0878.

Chan, S. C. (1996), "Planar Laser Scattering Imaging of Shock Wave Turbulent Boundary Layer Interactions," M.S. Thesis, Department of Aerospace Engineering and Engineering Mechanics, The University of Texas at Austin, Austin, TX, 1996.

Clemens, N. T., and Mungal, M. G. (1991), "A Planar Mie Scattering Technique for Visualizing Supersonic Mixing Flows," Experiments in Fluids, Vol. 11, pp. 175-185, 1991.

Comninos, M. (1997), "Investigation into the Cause of Unsteadiness of Shock Wave / Turbulent Boundary Layer Interaction using Planar Laser Scattering," M. S. Thesis, Department of Aerospace Engineering and Engineering Mechanics, The University of Texas at Austin, Austin, Texas, December 1997.

Dolling, D. S. and Brusniak, L. (1989), "Separation Shock Motion in Fin, Cylinder, and Compression Ramp Induced Turbulent Interactions," *AIAA Journal*, Vol. 27, No. 6, June 1989, pp. 734-742.

Dolling, D. S. and Murphy, M. T. (1983), "Unsteadiness of the Separation Shock Wave Structure in a Supersonic Compression Ramp Flowfield," AIAA Journal, Vol. 21, No. 12, pp. 1628-1634, December 1983.

Dolling, D. S. (1993), "Fluctuating Loads in Shock Wave/Turbulent Boundary Layer Interaction: Tutorial and Update," AIAA Paper 93-0284, January 1993.

Erengil, M. E., and Dolling, D. S. (1991), "Unsteady Wave Structure near Separation in a Mach 5 Compression Ramp Interaction," *AIAA Journal*, Vol. 29, No. 5, May 1991, pp. 728-735

Ganapathisubramani, B., Longmire, E. K., and Marusic, I. (2003a), "Characteristics of Vortex Packets in Turbulent Boundary Layers," *Journal of Fluid Mechanics*, Vol. 478, 2003, pp. 35-46.

Ganapathisubramani, B., Hutchins, N., Hambleton, W.T., Longmire, E. K., and Marusic, I. (2003b), "Investigation of Large-Scale Coherence in a Turbulent Boundary Layer Using Two-Point Correlations," *Journal of Fluid Mechanics*, Vol. 524, 2003, pp. 57-80.

Ganapathisubramani, B., Clemens, N. T., and Dolling, D. S. (2006a), "Large-Scale Motions in a Supersonic Turbulent Boundary Layer," *Journal of Fluid Mechanics,* Vol. 556, 2006, pp. 271-282.

Ganapathisubramani, B., Clemens, N. T., and Dolling, D. S. (2006b), "Planar Imaging Measurements to Study the Effect of Spanwise Structure of Upstream Turbulent Boundary Layer on Shock Induced Separation," AIAA Paper 2006-324.

Hou, Y. X. (2003), "Particle Image Velocimetry Study of Shock Induced Turbulent Boundary Layer Separation", Ph.D. Dissertation, Department of Aerospace Engineering and Engineering Mechanics, The University of Texas at Austin, Austin, TX, 2003.

Hou, Y. X., Ünalmis, Ö. H., Bueno, P. C., Clemens, N. T., and Dolling, D. S. (2004), "Effects of Boundary-Layer Fluctuations on Unsteadiness of 5 Blunt-Fin Interactions", *AIAA Journal*, Vol. 42, No. 12, December 2004, pp 2615-2619.

Hutchins, N., Ganapathisubramani, B., Marusic, I. (2004), "Dominant Spanwise Fourier Modes and Existence of Very Large Scale Coherence in Turbulent Boundary Layers," *15th Australasian Fluid Mechanics Conference, December 13-17, Sydney, Australia*, 2004.

Kim, K. C., and Adrian, R. J. (1999), "Very Large-Scale Motion in the Outer Layer," *Physics of Fluids*, Vol. 11(2), 1999, pp. 417-422.

Lin, J. C. (2002), "Review of Research on Low-Profile Vortex Generators to Control Boundary-Layer Separation," *Progress in Aerospace Sciences*, Vol. 38, No. 4, 2002, pp. 389-420.

Lin, J. C. (1999), "Control of Turbulent Boundary-Layer Separation Using Micro-Vortex Generators," AIAA Paper 99-3404, 1999.

McClure, W. B. (1992), "An Experimental Study of the Driving Mechanism and Control of the Unsteady Shock Induced Turbulent Separation in a Mach 5 Compression Corner Flow," Ph.D. Dissertation, Department of Aerospace Engineering and Engineering Mechanics, The University of Texas at Austin, Austin, TX, August 1992.

Müller, Jürgen; Mümmler, Rainer and Staudacher, Werner, (2001), "Comparison of Some Measurement Techniques for Shock-Induced Boundary Layer Separation", Aerospace Science and Technology, Vol. 5, 2001, pp. 383-395.

Samimy, M., Arnette, S. A., and Elliot, G. S. (1994), "Streamwise Structures in a Supersonic Turbulent Boundary Layer," Physics of Fluids, Vol. 6(3), 1994, pp. 1081-1083.

Tomkins, C. D., and Adrian, R. J. (2003), "Spanwise Structure and Scale Growth in Turbulent Boundary Layers," *Journal of Fluid Mechanics*, Vol. 490, 2003, pp. 37-74.

Ünalmis, O. H., and Dolling, D. S. (1994), "Decay of Wall Pressure Field and Structure of a Mach 5 Adiabatic Turbulent Boundary Layer," AIAA Paper 94-2363.

Ünalmis, O. H., and Dolling, D. S. (1998), "Experimental Study of Causes of Unsteadiness of Shock Induced Turbulent Separation," AIAA *Journal*, Vol. 36-3, 1998, pp. 371-378.

Vita

Jeffrey Alan Searcy was born in Seguin, Texas. Following graduation from Samuel Clemens High School in Schertz, Texas, in 2000, he was accepted to the United States Air Force Academy in Colorado Springs, Colorado. He completed his Bachelor of Science degree in Aeronautical Engineering and was a distinguished graduate of the Class of 2004, June 2004. He received his reserve commission as a 2nd Lieutenant in the United States Air Force in June 2004. That September he began graduate school at the University of Texas at Austin to pursue his Master's degree.

This thesis was typed by the author.